POLITECNICO DI TORINO
Repository ISTITUZIONALE

Unscented Kalman Filter and Control in TSE(3) with Applications to Spacecraft Dynamics

Original
Unscented Kalman Filter and Control in TSE(3) with Applications to Spacecraft Dynamics / Michael Wittal, M., Mangiacapra, G., Nazari, M., Capello, E.. - In: NONLINEAR DYNAMICS. - ISSN 0924-090X. - (2022).

Availability:
This version is available at: 11583/2950934 since: 2022-01-18T12:28:49Z

Publisher:
Springer

Published
DOI:

Terms of use:

This article is made available under terms and conditions as specified in the corresponding bibliographic description in the repository

Publisher copyright
Springer postprint/Author's Accepted Manuscript

(Article begins on next page)

26 June 2026

Nonlinear Dynamics

Unscented Kalman Filter and Control in TSE(3) with Applications to Spacecraft Dynamics

--Manuscript Draft--

Manuscript Number:	NODY-D-21-01189R1
Full Title:	Unscented Kalman Filter and Control in TSE(3) with Applications to Spacecraft Dynamics
Article Type:	Original Research
Keywords:	UKF; Unscented; Kalman; Filter; spacecraft; dynamics; Lie; Groups; SE(3); TSE(3); stochastic ; control; Navigation; Guidance; Backstepping; Controller; Sigma points; rigid; body; motion; attitude; determination; tangent; bundle; sensors; GN&C
Corresponding Author:	Matthew Michael Wittal, M.S. NASA John F Kennedy Space Center Merritt Island, FL UNITED STATES
Corresponding Author Secondary Information:	
Corresponding Author's Institution:	NASA John F Kennedy Space Center
Corresponding Author's Secondary Institution:	
First Author:	Gennaro Mangiacapra, MS
First Author Secondary Information:	
Order of Authors:	Gennaro Mangiacapra, MS
	Matthew Michael Wittal, M.S.
	Elisa Capello, Ph.D
	Morad Nazari, Ph.D
Order of Authors Secondary Information:	
Funding Information:	Faculty Innovative Research in Science and Technology (FIRST) — Dr. Morad Nazari
Abstract:	This paper presents a novel rigid-body navigation and control architecture within the framework of special Euclidean group SE(3) and its tangent bundle TSE(3) while considering stochastic processes in the system. The proposed framework combines the orbit-attitude motions of the rigid body into a single, compact set. The stochastic state filter is designed based on the unscented Kalman filter (UKF) which uses a special retraction function to encode the sigma points onto the manifold. The navigation system is then integrated and evaluated with two different control techniques on TSE(3): An almost globally asymptotically stabilizing Morse-Lyapunov-based control system with backstepping and a robust sliding mode-based control system. Also, the performance of the UKF in TSE(3) proposed here is compared with similar filters in the literature to demonstrate the robustness and accuracy of the proposed filter in a realistic setting. Numerical simulations are conducted to demonstrate the effectiveness of the proposed navigation filter for the full state estimation. In addition, the navigation and control systems are tested in the nonlinear gravity field of a small celestial body with an irregular shape. In particular, the performance of the closed-loop systems are studied in a tracking problem of spacecraft motion near the asteroid Bennu based on OSIRIS-REx mission data.
Response to Reviewers:	The revised manuscript and rebuttal have been submitted for the reviewer's consideration. The authors recommend reviewing the rebuttal first as a guide to changes made in the manuscript at the reviewers' recommendation. Thank you again for your time and consideration!

Powered by Editorial Manager® and ProduXion Manager® from Aries Systems Corporation

Order of Authors (with Contributor Roles):	Gennaro Mangiacapra, MS (Conceptualization: Supporting; Formal analysis: Equal; Methodology: Equal; Visualization: Lead; Writing – original draft: Equal)
	Matthew Michael Wittal, M.S. (Conceptualization: Lead; Formal analysis: Equal; Methodology: Equal; Visualization: Supporting; Writing – original draft: Equal; Writing – review & editing: Supporting)
	Elisa Capello, Ph.D (Conceptualization: Supporting; Supervision: Supporting; Writing – original draft: Supporting; Writing – review & editing: Supporting)
	Morad Nazari, Ph.D (Conceptualization: Supporting; Supervision: Lead; Validation: Supporting; Writing – review & editing: Supporting)

Powered by Editorial Manager® and ProduXion Manager® from Aries Systems Corporation

Revised Manuscript "Unscented Kalman Filter and Control in TSE(3) with Applications to Spacecraft Dynamics"
Click here to view linked References
Click here to access/download;Manuscript;MaWiCaNa21NoDy_submission_

Noname manuscript No.
(will be inserted by the editor)

Unscented Kalman Filter and Control on TSE(3) with Application to Spacecraft Dynamics

Gennaro Mangiacapra · Matthew Wittal · Elisa Capello · Morad Nazari

Abstract This paper presents a novel rigid-body navigation and control architecture within the framework of special Euclidean group SE(3) and its tangent bundle TSE(3) while considering stochastic processes in the system. The proposed framework combines the orbit-attitude motions of the rigid body into a single, compact set. The stochastic state filter is designed based on the unscented Kalman filter (UKF) which uses a special retraction function to encode the sigma points onto the manifold. The navigation system is then integrated and evaluated with two different control techniques on TSE(3): An almost globally asymptotically stabilizing Morse-Lyapunov-based control system with backstepping and a robust sliding mode-based control system. Also, the performance of the UKF in TSE(3) proposed here is compared with similar filters in the literature to demonstrate the robustness and accuracy of the proposed filter in a realistic setting. Numerical simulations are conducted to demonstrate the effectiveness of the proposed navigation filter for the full state estimation. In addition, the navigation and control systems are tested in the nonlinear gravity field of a small celestial body with an irregular shape. In particular, the performance of the closed-loop systems are studied in a tracking problem of spacecraft motion near the asteroid Bennu based on OSIRIS-REx mission data.

G. Mangiacapra
Politecnico di Torino, Torino 10129, Italy & Navigation System Engineer, Northrop Grumman Italia, Pomezia (RM), 00040, Italy; Email: gennaro.mangiacapra@outlook.it

M.M. Wittal
Embry-Riddle Aeronautical University, 1 Aerospace Blvd., Daytona Beach, FL 32114, USA; NASA Kennedy Space Center, FL 32899, USA; Email: wittalm@my.erau.edu

E. Capello
Politecnico di Torino, CNR-IEIIT, Corso Duca degli Abruzzi 24, Torino, 10129, Italy; Email: elisa.capello@polito.it

M. Nazari
Embry-Riddle Aeronautical University, 1 Aerospace Blvd., Daytona Beach, FL 32114, USA; Email: nazarim@erau.edu

1 Introduction

Rigid body translational motion can be formulated and propagated using several types of formulation such as Cowell, Encke, Clohessy-Wilthsire, equinoctial elements, or a unified state model [1–3]. Rotational kinematics are often modeled using attitude parameterization sets. Minimal parameterization sets (such as principal rotation angles, Euler angles, and classical and modified Rodrigues parameters) are defined in 3-dimensional Euclidean space $\mathbb{R}^3$ and can exhibit singularities. Quaternions are redundant and are defined on the 3-sphere S^3 [4,5] and hence they do not have the singularity issue. However, due to their non-uniqueness, they can result in an undesired phenomenon called unwinding [6] for large rotations such as rigid body initial tumbling, although this can be avoided by using discontinuous feedback or nonlinear control laws [7].

Attitude estimation has been performed using quaternions and a three-parameter set for the local error representation in the literature, including [8,9]. Alternatively, rigid body attitude can be expressed using the rotation or direction cosine matrix defined on the special orthogonal group SO(3). Formalism of the attitude using rotation matrices helps to avoid the problems of singularity and non-uniqueness [10–13].

Conventionally, the analysis of rigid body translational and rotational dynamics are conducted separately, resulting in separate control laws for each. However, as clearly discussed in several references such as [14–16], there are good reasons that the

coupling between the translational and rotational dynamics of a rigid body should be considered in dynamics analysis and control design. In the case of spacecraft navigation and control, the simultaneous modeling of orbital-attitude dynamics using special Euclidean group $\mathsf{SE}(3)$ and their tangent bundle $\mathsf{TSE}(3)$ is especially advantageous due to its consideration of that coupling. Such coupling can be due to several effects such as nonlinear gravity fields or attitude-dependent forces due to drag and solar radiation pressure, and it occurs in missions such as spacecraft rendezvous, proximity operations, and docking, or in spacecraft hovering around small bodies. The consideration of this coupling results in accurate dynamic analysis and control design of rigid bodies, as shown in [17–21].

When considering real-world applications, the inclusion of stochastic processes is a crucial part of any navigation and control system. The navigation system includes the sensors and the filter, while the control system is composed of the control algorithm and the actuators. The navigation filter enables the correct estimation of the states based on the sensor measurements. The on-board instruments, such as the inertial measurement unit, gyroscopes, accelerometers, and star trackers, have limited accuracy and are usually characterized by a degree of uncertainty. These uncertainties can arise not only due to the noise in the instruments, but also from electrical components, communication systems, or external disturbances, and result in inaccuracies and loss of precision. In addition, some states might not be observable, as is the case when considering gyroscope biases. For the reasons mentioned above, there is a need for using state filters, such as the Kalman filters, that are capable of handling stochastic processes and can fuse the measurements from different sources optimally to estimate unobservable states [13, 22, 23].

Although the control problem on $\mathsf{TSE}(3)$ for space applications has been extensively studied [24–26], the navigation problem on $\mathsf{TSE}(3)$ still requires further research. State filter design on $\mathsf{SE}(3)$, with application to robotics, has been of growing interest in the literature. Extended Kalman filter (EKF) on $\mathsf{SE}(3)$ [27,28], discrete-EKF (D-EKF) on $\mathsf{SE}(3)$ [29,30], and unscented Kalman filter (UKF) on $\mathsf{SE}(3)$ [31–33] are some examples. According to the literature, these estimators are more accurate than their counterparts designed in Euclidean space, although formulation development of the filter design on $\mathsf{SE}(3)$ is more complex than that in Euclidean space. The aforementioned publications exploit the geometrical mechanics framework by using the associated maps and operators in the state update step, where the measurements are defined in the Lie algebra but the filter is designed on the Lie group $\mathsf{SE}(3)$.

In this paper, a novel rigid body navigation and control system on Lie groups $\mathsf{SE}(3)$ and their tangent bundles $\mathsf{TSE}(3)$ is developed. The navigation filter is designed by advancing the unscented transform (UT) based UKF introduced in [34] using retraction to address the fact that the system states are on $\mathsf{TSE}(3)$. The stochasticity is treated on $\mathsf{SE}(3)$ and its tangent bundle $\mathsf{TSE}(3)$ as discussed in [27, 31, 35] and a retraction function between the manifold and the Euclidean space [36, 37], the inverse of which is used to encode the UT sigma points onto the manifold and decode them from the manifold, respectively. The performance of the proposed filter is compared in terms of robustness and accuracy with three other Kalman filters on $\mathsf{SE}(3)$ in the literature. Furthermore, the regulation controller in [18] is extended to the case of tracking problem to design an almost globally asymptotically stable Morse-Lyapunov backstepping (MLBS) tracking control on $\mathsf{TSE}(3)$. In addition, a tracking sliding mode control (SMC) is designed on $\mathsf{TSE}(3)$ to verify the results of the MLBS tracking control. The integrated stochastic estimation and tracking control on Lie groups and their tangent bundles proposed in this paper results in a precise, asymptotically stable navigation and control system that considers the orbit-attitude coupling in the presence of stochasticity. The efficacy of this navigation and control system is demonstrated in the problem of spacecraft motion around a small irregular central body which can be considered as a pre-landing phase that focuses on navigating to a specific point of interest. The properties of asteroid Bennu are used for the central body and the gravitational interaction between the spacecraft and Bennu is modeled according to that in [38]. The accuracy of the estimator in the presence of stochasticity and stability and convergence of the closed loop are validated in the numerical simulation results. Note that the extensive contribution and revisions made in this paper as compared to the authors' previous work [39] including, but certainly not limited to, the tracking SMC and comparison of the filters provided here, makes this work distinct from the previous work.

2 Preliminaries and Problem Statement

2.1 Lie group $\mathsf{SE}(3)$ and its Lie algebra $\mathfrak{se}(3)$

The rigid body configuration may be defined by six degrees of freedom, three of which are related to the location of its center of mass and the other

three are related to its rotation. The pose (configuration) of a rigid body, also known as the Denavit-Hartenberg representation within the robotics community, can be expressed as

$$g = \begin{bmatrix} R & r \\ 0_{1\times 3} & 1 \end{bmatrix} \in \mathsf{SE}(3) \tag{1}$$

where $\mathsf{SE}(3)$ is defined as the semi-direct product of $\mathbb{R}^3$ and $\mathsf{SO}(3)$, i.e. $\mathsf{SE}(3) = \mathbb{R}^3 \ltimes \mathsf{SO}(3)$, $R \in \mathsf{SO}(3)$ is the rotation matrix from the body frame to the inertial frame such that $\det(R) = 1$ and $R^T R = I_3$ (I_3 is the 3×3 identity matrix), and $r \in \mathbb{R}^3$ is the position vector from the origin of the inertial frame to the center of mass of the rigid body expressed in the inertial frame. According to [40, 41], the Lie group $\mathsf{SE}(3)$ is a smooth manifold obeying group properties (closure under multiplication, identity, associativity, and invertability) and its associated group operations are differentiable. The smoothness of the matrix Lie group implies the existence of a single tangent space at each point. The tangent space at the identity element of the group, i.e. $g = I_4$ (when $R = I_3$ and $r = [0, 0, 0]^T$), is referred to as Lie algebra [42] and is denoted as

$$\mathfrak{se}(3) = \left\{ \bar{\mathcal{V}}^\vee = \begin{bmatrix} \varpi^\times & \bar{v} \\ 0_{1\times 3} & 0 \end{bmatrix}, \ \varpi^\times \in \mathfrak{so}(3), \ \bar{v} \in \mathbb{R}^3 \right\} \tag{2}$$

where $(\cdot)^\vee$ denotes the wedge map $(\cdot)^\vee : \mathbb{R}^6 \to \mathfrak{se}(3)$, $\bar{\mathcal{V}} = [\varpi^T, \bar{v}^T]^T \in \mathbb{R}^6$ is a vector comprised of $\bar{v} \in \mathbb{R}^3$ and $\varpi \in \mathbb{R}^3$, $\mathfrak{so}(3)$ is the set of 3×3 skew symmetric matrices such that for the vector $\varpi = [\varpi_1, \varpi_2, \varpi_3]^T \in \mathbb{R}^3$, the cross map $(\cdot)^\times : \mathbb{R}^3 \to \mathfrak{so}(3)$ is defined as

$$\varpi^\times = \begin{bmatrix} 0 & -\varpi_3 & \varpi_2 \\ \varpi_3 & 0 & -\varpi_1 \\ -\varpi_2 & \varpi_1 & 0 \end{bmatrix} \in \mathfrak{so}(3) \tag{3}$$

From the definitions of Lie group $\mathsf{SE}(3)$ and its Lie algebra $\mathfrak{se}(3)$ above, the geometric link between the two formulations can be understood. The Lie algebra can be considered a linearization of the Lie group, near the identity element [43]. Due to the complexity of the nonlinear structure of the Lie group, it is difficult to study with conventional mathematical tools. The important feature of the Lie algebra is that it is a linear vector space and thus it can be studied using the tools developed in linear algebra.

The exponential map $\exp : \mathfrak{se}(3) \to \mathsf{SE}(3)$ allows the transfer of Lie algebra elements to the Lie group which can intuitively be interpreted as a wrapping operation from the tangent plane onto the manifold. Formally, it is a local diffeomorphism from a neighborhood of zero in $\mathfrak{se}(3)$ onto a neighborhood of the identity element in $\mathsf{SE}(3)$ [44]. The exponential coordinates are defined as

$$\xi = \begin{bmatrix} \Theta \\ \bar{p} \end{bmatrix} \in \mathbb{R}^6 \tag{4}$$

where $\Theta \in \mathbb{R}^3$ represents the principal rotation vector. This is the product of eigenaxis (principal axis) and eigenangle (principal angle) of rotation, i.e. $\Theta = \theta e$, $\theta = \|\Theta\|$, $\bar{p} \in \mathbb{R}^3$ represents the translational vector. Hence, the configuration g is obtained via exponential map as

$$g = \exp(\xi^\vee) = \sum_{n=0}^{\infty} \frac{1}{n!} (\xi^\vee)^n \tag{5}$$

which can be written as [45]

$$g = \begin{bmatrix} R(\Theta) & S(\Theta)\bar{p} \\ 0 & 1 \end{bmatrix} \in \mathsf{SE}(3) \tag{6}$$

where $R(\Theta) \in \mathsf{SO}(3)$ is the rotation matrix from body frame to the inertial frame. The rotation matrix is obtained via the Rodrigues formula as

$$R(\Theta) = \exp(\Theta^\times) = I + \frac{\sin\theta}{\theta}\Theta^\times + \frac{1-\cos\theta}{\theta^2}(\Theta^\times)^2 \tag{7}$$

and

$$S(\Theta) = I + \frac{1-\cos\theta}{\theta^2}\Theta^\times + \frac{\theta - \sin\theta}{\theta^3}(\Theta^\times)^2 \tag{8}$$

Note that the inverse of the exponential map is the logarithmic map $\log : \mathsf{SE}(3) \to \mathfrak{se}(3)$ which can be interpreted as an unwrapping operation. The exponential coordinates can be obtained via logarithmic map as

$$\xi^\vee = \log_{\mathsf{SE}(3)}(g) \in \mathfrak{se}(3) \tag{9}$$

2.2 Rigid body motion formulation on $\mathsf{SE}(3)$

The rigid body kinematic and kinetic equations of motion are given as

$$\begin{aligned} \dot{g} &= g\mathbb{V}^\vee \\ \dot{\mathbb{V}} &= \mathbb{I}^{-1}\mathrm{ad}^*_{\mathbb{V}}\mathbb{I}\mathbb{V} + \mathbb{I}^{-1}u \end{aligned} \tag{10}$$

where $g \in \mathsf{SE}(3)$ represents the rigid body configuration as defined in Eq. (1), $\mathbb{V} = [\omega^T, v^T]^T \in \mathbb{R}^6$ is the augmented velocity vector comprised of the angular velocity vector $\omega \in \mathbb{R}^3$ of the body and the translational velocity $v \in \mathbb{R}^3$ of the center of mass with respect to the inertial frame, expressed in the body frame. In Eq. (10), $u = u_e + u_c \in \mathbb{R}^6$ is the input, $u_e \in \mathbb{R}^6$ denotes the total external inputs (consisting of the external moments and external forces) and $u_c \in \mathbb{R}^6$ is the control input produced

by the control system (consisting of the control moment and control force). Also, in Eq. (10), the inertia tensor is given as

$$\mathbb{I} = \begin{bmatrix} J & 0_{3\times3} \\ 0_{3\times3} & mI_3 \end{bmatrix} \in \mathbb{R}^{6\times6} \tag{11}$$

where $J \in \mathbb{R}^{3\times3}$ is the moment of inertia about the center of mass, and m is the mass of the body. Moreover, the co-adjoint operator is defined as

$$\mathrm{ad}^*_{\mathbb{V}} = \mathrm{ad}^T_{\mathbb{V}} = \begin{bmatrix} -\omega^\times & -v^\times \\ 0_{3\times3} & -\omega^\times \end{bmatrix} \in \mathbb{R}^{6\times6} \tag{12}$$

where the adjoint operator $\mathrm{ad}_{\mathbb{V}}$ is

$$\mathrm{ad}_{\mathbb{V}} = \begin{bmatrix} \omega^\times & 0_{3\times3} \\ -v^\times & -\omega^\times \end{bmatrix} \in \mathbb{R}^{6\times6} \tag{13}$$

This operator allows the transformation of a tangent vector from the tangent space around one element to the tangent space around another. The states are thus represented by $x = (g, \mathbb{V}) \in \mathsf{SE}(3) \times \mathbb{R}^6 = \mathsf{TSE}(3)$, the tangent bundle of $\mathsf{SE}(3)$. In this framework, both the attitude and the translational displacement are considered simultaneously. This allows to design an estimation algorithm and a control system in $\mathsf{TSE}(3)$, which is more versatile and more accurate than the standard decoupled procedures.

3 Stochastic Processes, Filter, and Control Design on Lie Group and its Tangent Bundle

3.1 Stochastic processes on Lie groups and system formulation

The mathematical model employed for the control and state estimation is usually developed in Euclidean space, which is an affine space and, by definition, is a geometric structure based on the vectorial space [42]. When the mathematical modeling is performed in Euclidean space, it is common to deal with uncertainties simply by using an additive approach. Basically, an additive white Gaussian noise can be considered as representative of the many random processes that occur in nature. However, when the model is developed in $\mathsf{SE}(3)$ and its tangent bundle $\mathsf{TSE}(3)$, uncertainties and stochastic processes cannot be formulated using the conventional mathematical models that are commonly used in the Euclidean space. This is due to the fact that $\mathsf{SE}(3)$ is a nonlinear manifold and not a vectorial space [35]. In this paper, the formulation covered in [27,31] is used to accommodate a stochastic process in the model. Since the source of noise is assumed to be in vector space, the exponential map $\exp(\cdot)$ is used to map it into $\mathsf{SE}(3)$ as

$$\hat{g} = g\exp(\eta_g^\vee) \quad \eta_g \sim \mathcal{N}(0_{p\times1}, Q_g) \tag{14}$$

where $\hat{g} \in \mathsf{SE}(3)$ is the noisy, estimated pose, $g \in \mathsf{SE}(3)$ is the true pose, and $\eta_g \in \mathbb{R}^p$ $(p = 6)$ denotes the pose process noise in Euclidean space with a zero mean Gaussian distribution and covariance matrix $Q_g \in \mathbb{R}^{p\times p}$. Note that the exponential mapping of η_g onto the estimated pose $\hat{g}$ is multiplicative, as shown in Eq. (14). Also note that calculation of the maximum likelihood estimate (MLE) should be performed within the Euclidean space in which the noise is defined, not in the Lie group or Lie algebra. The calculation of MLE is outside the scope of this paper, and thus the relationships among the MLE of group elements versus those of the algebra are not discussed here. For a generalized approach to determine the maximum likelihood estimates on manifolds, the reader is referred to [46]. Also, specific approaches to Lie groups and the exponential-logarithm mappings of Gaussian distributions can be found in [47] and [48].

The conventional stochastic system formulation which best accommodates the application of Kalman filter theory considers an additive approach for both process and measurement noise. The process noise is added to the state derivative equation and the measurement noise is added to the system output equation. In this work, the aforementioned approach cannot be adopted, since the state of the system $x = (g, \mathbb{V})$ is on $\mathsf{TSE}(3)$. Although the velocity, expressed in $\mathbb{R}^6$, allows the simple addition of the noise, the pose requires the notation given in Eq. (14), since it is defined on $\mathsf{SE}(3)$. Despite the fact that different estimation techniques can be found in the literature, none of them account for a state vector that is defined on $\mathsf{TSE}(3)$. Therefore a novel, augmented formulation is introduced.

It is assumed that the rigid body pose and augmented velocity are measurable and the output of the system, $z \in \mathbb{R}^{2q}$ $(q = 6)$ consists of the principal angles of rotation Θ, the translational vector components r, the angular velocity ω, and the translational velocity v. It must be emphasized that principal rotation angles are only used to represent the attitude in the simulation results, while they are obtained based on the rotation matrix. In addition, using the principal angle of rotation allows one to take advantage of the maps and operators defined in Section 2, thus producing a compact, stochastic system formulation on $\mathsf{TSE}(3)$ as

$$\dot{\hat{x}} : \begin{cases} \dot{\hat{g}} = g\mathbb{V}^\vee \exp(\eta_g^\vee) \\ \dot{\hat{\mathbb{V}}} = \mathbb{I}^{-1}\mathrm{ad}^*_{\mathbb{V}+\eta_{\mathbb{V}}}\mathbb{I}(\mathbb{V}+\eta_{\mathbb{V}}) + \mathbb{I}^{-1}u \end{cases} \tag{15}$$

$$z = [(\log_{\mathsf{SE}(3)}(\exp(\zeta_g)g)^{\vee})^T,\ \mathbb{V}^T + \zeta_{\mathbb{V}}^T]^T \in \mathbb{R}^{2q} \quad (16)$$

where $(\cdot)^{\vee}$ is the inverse of the wedge map. The dependence on time is omitted for the readability of the equations. The state process noise $\eta = [\eta_g^T, \eta_{\mathbb{V}}^T]^T \in \mathbb{R}^{2p}$ is assumed to be a Gaussian white noise with zero mean and covariance matrix $Q \in \mathbb{R}^{2p\times 2p}$, i.e. $\eta \sim \mathcal{N}(0_{2p\times 1}, Q)$, and the measurement noise $\zeta = [\zeta_g^T, \zeta_{\mathbb{V}}^T]^T \in \mathbb{R}^{2q}$ is assumed to be a Gaussian white noise with zero mean and covariance matrix $T \in \mathbb{R}^{2q\times 2q}$, i.e. $\zeta \sim \mathcal{N}(0_{2q\times 1}, T)$. Furthermore, the process noise and measurement noise are assumed to be uncorrelated. The process noise given in Eq. (14) includes components for both $\dot{\hat{g}}$ and $\dot{\hat{\mathbb{V}}}$ in the form of the process noise η. The stochastic system formulation in Eqs. (15) and (16) is written in the following compact form, which will be employed in the description of the UKF steps described in the subsequent section:

$$\begin{aligned} \dot{\hat{x}} &= f(x, u, \eta) \\ z &= h(x, \zeta) \end{aligned} \quad (17)$$

where $f(\cdot) \in \mathsf{TSE}(3)$ represents the nonlinear state function that depends on the state, input, process noise, and time and $h(\cdot) \in \mathbb{R}^{2q}$ represents the measurement function that depends on the state, the measurement noise, and time. Note that the time dependence is omitted.

3.2 Unscented Kalman filter design on Lie groups and their tangent bundles

Starting from the stochastic system formulation introduced in Eq. (15) and (16), the state estimation is performed using a UKF. This type of filter belongs to a family of sigma-point Kalman filters called linear regression Kalman filters, which use a statistical linearization technique. In the EKF-based approaches, the state distribution is generally propagated analytically through the first-order linearization of the nonlinear system. Due to the linearization used in EKF, it is only capable of achieving first-order accuracy [34]. This procedure can lead to large errors or corrupted estimates [33]. The UKF instead handles the problem with a deterministic sampling approach. The Gaussian state distribution is represented by a set of sample points that completely capture the mean and covariance of the distribution. These points are known as sigma points and are propagated through the nonlinear dynamics with the purpose of capturing the *a posteriori* mean and covariance with high accuracy [37]. The UKF is based on the leading intuition that it is harder to approximate an arbitrary nonlinear function than to approximate a probability distribution [49]. This idea results in a filter which is able to achieve good performance even with pronounced nonlinearities or non-Gaussian distributions [50]. However, this algorithm has a higher computational cost than conventional EKF filters, even if the computation of the Jacobian is spared [51].

Generally, Kalman filter techniques consists of two main steps: 1) The prediction step where the state and its error covariance are predicted on the basis of the filter's dynamical model. Usually, this phase is called the *a priori* estimate of the system and leads to the estimated states $\hat{x}_{k+1|k}$ and state error covariance $P_{k+1|k}$, where the integer k denotes the current time step. 2) The measurement update step is where the *a priori* state is corrected with an external measure. This procedure allows one to improve the state estimate and is called the the *a posteriori* estimate of the system, leading to $\hat{x}_{k+1|k+1}$ and $P_{k+1|k+1}$. The UKF has an additional preliminary step consisting of the UT during which the sigma points are computed.

3.2.1 Sigma points selection step

The number of the sigma points depends on the number of dimensions in the system. Given the current error covariance matrix $P_{k|k} \in \mathbb{R}^{2q\times 2q}$ and process noise matrix $Q_k \in \mathbb{R}^{2p\times 2p}$, two different sets of sigma points are computed. The UT requires $4p+1$ points for the first set and $4q+1$ for the second one, where the additional point in each set refers to the mean of the corresponding distribution. Therefore, the matrix $\chi_p \in \mathbb{R}^{2p\times(4p+1)}$ is related to the error covariance matrix and is constructed from $2p$ rows of $4p+1$ sigma points, and the matrix $\chi_q \in \mathbb{R}^{2q\times(4q+1)}$ is related to the process noise and is constructed of $2q$ rows of $4q+1$ sigma points. The matrix $\chi_p \in \mathbb{R}^{2p\times(4p+1)}$ of $4p+1$ sigma column vectors $\chi_{p,i}$ is formed according to

$$\begin{aligned} \chi_{p,0} &= 0 \in \mathbb{R}^{2p} \\ \chi_{p,i} &= \chi_{p,0} + \left(\sqrt{(p+\lambda_p)P_{k|k}}\right)_i \in \mathbb{R}^{2p} \\ &\quad (i = 1, \cdots, 2p) \\ \chi_{p,i} &= \chi_{p,0} - \left(\sqrt{(p+\lambda_p)P_{k|k}}\right)_{i-p} \in \mathbb{R}^{2p} \\ &\quad (i = 2p+1, \cdots, 4p) \end{aligned} \quad (18)$$

where $\chi_{p,0}$ represents the mean of the distribution at time step k, the other $4p$ points (i.e. $\chi_{p,i}$, $i = 1, 2, \cdots, 4p$) denote the dispersion around $\chi_{p,0}$, and $\lambda_p = (\alpha^2 - 1)p \in \mathbb{R}$ is a scaling parameter. The constant α determines the spread of the sigma points around their mean and is usually set to a small, positive value, e.g. $10^{-4} \leq \alpha \leq 1$. $(\sqrt{(p+\lambda_p)P_{k|k}})_i$

is the ith column of the matrix square root (i.e. lower triangular Cholesky factorization). Moreover the sigma points are defined along with their weights as follows

$$W_{p,0}^{(m)} = \frac{\lambda_p}{\lambda_p + p}, \quad W_{p,0}^{(c)} = \frac{\lambda_p}{\lambda_p + p} + (1 - \alpha^2 + \beta)$$
$$W_{p,i}^{(m)} = W_{p,i}^{(c)} = \frac{1}{2(\lambda_p + p)} \quad (i = 1, \cdots, 4p) \quad (19)$$

where the superscripts (c) and (m) refer to the covariance and the mean, respectively. The first ones will be used to compute the sigma points mean after they are passed through the nonlinear system, while the latter ones are used for the computation of the sigma points covariances. In addition, the subscript zero refers to the mean of the distribution. The constant β is used to incorporate prior knowledge of the distribution of the state. The value β is optimal for Gaussian distribution and is commonly selected as $\beta = 2$. In other words, the weights are constructed as

$$W_p^{(m)} = [W_{p,0}^{(m)}, W_{p,1}^{(m)}, \cdots, W_{p,4p}^{(m)}]$$
$$W_p^{(c)} = [W_{p,0}^{(c)}, W_{p,1}^{(c)}, \cdots, W_{p,4p}^{(c)}] \quad (20)$$

The same procedure applies to the set χ_q related to the process noise matrix. In particular, the matrix $\chi_q \in \mathbb{R}^{2q \times (4q+1)}$ of $4q + 1$ sigma column vectors $\chi_{q,i}$ is formed according to

$$\chi_{q,0} = 0 \in \mathbb{R}^{2q}$$
$$\chi_{q,i} = \chi_{q,0} + \left(\sqrt{(q + \lambda_q)Q}\right)_i \in \mathbb{R}^{2q}$$
$$(i = 1, \ldots, 2q)$$
$$\chi_{q,i} = \chi_{q,0} - \left(\sqrt{(q + \lambda_q)Q}\right)_{i-q} \in \mathbb{R}^{2q}$$
$$(i = 2q + 1, \ldots, 4q) \quad (21)$$

and their weights

$$W_{q,0}^{(m)} = \frac{\lambda_q}{\lambda_q + q} \quad W_{q,0}^{(c)} = \frac{\lambda_q}{\lambda_q + q} + (1 - \alpha^2 + \beta)$$
$$W_{q,i}^{(m)} = W_{q,i}^{(c)} = \frac{1}{2(\lambda_q + q)} \quad (i = 1, \cdots, 4q) \quad (22)$$

That is, the matrix χ_q and the weights $W_q^{(m)}$ and $W_q^{(c)}$ can be defined via methodology identical to that defined in Eqs. (19) and (20) where p is replaced by q. In the update step, a third set of sigma points χ_u will be generated with the one-step-ahead state prediction $\hat{x}_{k+1|k}$. In principle, a third set of weights may be defined, however in this case we choose to use the same of the χ_p set.

3.2.2 Prediction step

The *a priori* state estimate $x_{k+1|k}$ and the state error state covariance matrix $P_{k+1|k}$ are predicted using the current estimates $\hat{x}_{k|k}$, $P_{k|k}$ and the sigma points vectors $\chi_{i,q}, \chi_{i,p}$. It is clear that the UKF needs to be initialized with the initial state estimate $\hat{x}_p = E\{x_0\}$ and the initial covariance state matrix $P_0 = E\{(x_0 - \hat{x}_0)(x_0 - \hat{x}_0)^T\}$. Since the system states are on $\mathsf{TSE}(3)$, a retraction function $\varphi(\cdot) : \mathbb{R}^{2p} \to \mathsf{TSE}(3)$ is introduced [36,37], which is a smooth, arbitrarily-chosen function that encodes the mean and covariance noise on the Lie group and its tangent bundle. The retraction function is given as

$$\varphi(x, \chi_i) : \begin{cases} \varphi_g = g \exp(\chi_{g,i}^{\vee}) \\ \varphi_{\mathbb{V}} = \mathbb{V} + \chi_{\mathbb{V},i} \end{cases} \quad (23)$$

where $\chi_{g,i}$ indicates the first p elements of the sigma points vector χ_i, and $\chi_{\mathbb{V},i}$ the last p. Note that when $\chi_i = 0$ then $\varphi(x, 0) = x$. The inverse retraction function $\varphi^{-1} : \mathsf{TSE}(3) \to \mathbb{R}^{2p}$ makes use of the Lie algebra and is given as

$$\varphi^{-1}(\hat{x}, x) : \begin{cases} \varphi_g^{-1} = \log_{\mathsf{SE}(3)}(\hat{g}^{-1} g) \\ \varphi_{\mathbb{V}}^{-1} = \hat{\mathbb{V}} - \mathbb{V} \end{cases} \quad (24)$$

It is emphasized that the retraction function is used to encode the sigma points onto the manifold and its inverse is used to decode the sigma points from the manifold. Given the current optimal estimated state $\hat{x}_{k|k}$, the first set of sigma points are retracted into the manifold and then used to propagate the system dynamics starting from $\hat{x}_{k|k}$, i.e.

$$x_k(\chi_{p,i}) = f\left(\varphi\left(\hat{x}_{k|k}, \chi_{p,i}\right), \hat{u}_k, 0\right)$$
$$(i = 0, \ldots, 2p) \quad (25)$$

where the current input vector $\hat{u}_k \in \mathbb{R}^p$ is assumed not measurable, and hence it is estimated using the current state $\hat{x}_{k|k}$. The sigma points which represent the mean of the distribution, i.e. $\chi_{p,0}$, return the mean state which is used, along with the properties of the retraction function, to obtain the *a priori* state prediction, i.e.

$$\hat{x}_{k+1|k} = f(\varphi\left(\hat{x}_{k|k}, \chi_{p,0}\right), \hat{u}_k, 0)$$
$$= f(\hat{x}_{k|k}, \hat{u}_k, 0) \quad (26)$$

In order to compute the covariance matrix with respect to the state uncertainty, the obtained states are retracted back into $\mathbb{R}^{2p}$ with the inverse retraction function. The retracted sigma points matrix $\chi_p^r \in \mathbb{R}^{2p \times (4p+1)}$ is then obtained as

$$\chi_{p,i}^r = \varphi^{-1}(\hat{x}_{k+1|k}, x(\chi_{p,i})) \quad (i = 0, \ldots, 2p) \quad (27)$$

and since $x_{\chi_{p,0}} = \hat{x}_{k+1|k}$, the first column of the matrix is $\chi_{p,0}^r = 0$. The covariance matrix with

respect to the state uncertainty can then be computed as

$$P^{(1)}_{k+1|k} = \sum_{i=0}^{4p} W^{(c)}_{p,i}(\chi^r_p - \overline{\chi}^r_p)(\chi^r_p - \overline{\chi}^r_p)^T \tag{28}$$

where $\overline{\chi}^r_p \in \mathbb{R}^{2p}$ is the weighted mean of the retracted sigma points with $W^{(m)}_p$. This matrix needs to be corrected with the contribute which comes from the process noise. Hence, the second set of sigma points, $\chi_{q,i}$, is used similarly to the first one. The main important difference is that these points are not used as initial condition for the propagation, since they are not related to the state. Instead, they are introduced in the propagation as process noise, i.e.

$$x_{\chi_{q,i}} = f\left(\hat{x}_{k|k}, \hat{u}_k, \chi_{q,i}\right) \qquad (i = 0, \ldots, 2q) \tag{29}$$

It is clear that the first the sigma points which represents the mean of the distribution, $\chi_{q,0}$ returns $\hat{x}_{k+1|k}$, according to Eq. (26). The results are retracted back into $\mathbb{R}^{2q}$ with the inverse retraction function. The retracted sigma points matrix $\chi^r_q \in \mathbb{R}^{q\times(2q+1)}$ is then obtained as

$$\chi^r_{q,i} = \varphi^{-1}(\hat{x}_{k+1|k}, x_{\chi_{q,i}}) \qquad (i = 0, \ldots, 2q) \tag{30}$$

and since $x_{\chi_{q,0}} = \hat{x}_{k+1|k}$, the first column of the matrix is $\chi^r_{q,0} = 0$. The covariance matrix with respect to the noise can be finally computed as

$$P^{(2)}_{k+1|k} = \sum_{i=1}^{4q} W^{(c)}_{q,i}(\chi^r_q - \overline{\chi}^r_q)(\chi^r_q - \overline{\chi}^r_q)^T \tag{31}$$

where $\overline{\chi}^r_q \in \mathbb{R}^{2q}$ is the weighted mean of the retracted sigma points with $W^{(m)}_q$. Finally, the one-step-ahead state error covariance matrix is computed correcting Eq. (28) as

$$P_{k+1|k} = P^{(1)}_{k+1|k} + P^{(2)}_{k+1|k} \tag{32}$$

where $P^{(1)}_{k+1|k}$ and $P^{(2)}_{k+1|k}$ are given in Eqs. (28) and (31), respectively. Note that the second term, i.e. $P^{(2)}_{k+1|k}$, is weighted on the basis of the process noise covariance matrix Q, as can be seen in Eq. (21). If the knowledge of the true model is poor, then Q has large elements and then the *a priori* covariance state error matrix estimate has a large dispersion.

3.2.3 Measurement update step

Once $\hat{x}_{k+1|k}$ and $P_{k+1|k}$ are computed and the measurement $z_k \in \mathbb{R}^n$ is known, the correction can be performed. As mentioned, the third set of sigma points with the predicted state error covariance matrix are computed. The matrix $\chi_u \in \mathbb{R}^{2p\times(4p+1)}$ is formed according to

$$\begin{aligned}
\chi_{u,0} &= 0,\\
\chi_{u,i} &= \chi_{u,0} + \left(\sqrt{(p+\lambda_p)P_{k+1|k}}\right)_i \\
&\qquad (i = 1, \ldots, p)\\
\chi_{u,i} &= \chi_{u,0} - \left(\sqrt{(p+\lambda_p)P_{k+1|k}}\right)_{i-p} \\
&\qquad (i = p+1, \ldots, 2p)
\end{aligned} \tag{33}$$

Each point is retracted into the manifold and then passed through the measurement function. The matrix $z_{k+1} \in \mathbb{R}^{p\times(2p+1)}$ is constructed such that each column is in the form of

$$\begin{aligned}
z_{k+1,i} &= h(\varphi(\hat{x}_{k+1|k}, \chi_{u,i})),\\
&\qquad (i = 0, \ldots, 4p)
\end{aligned} \tag{34}$$

where the first column is $z_{k+1,0} = 0$ due to the retraction function properties. Since the ith measurement vector is part of $\mathbb{R}^{12}$ and not of TSE(3), there is no need to use the inverse of the retraction function. Therefore, the measurement covariance matrix $P_{zz,k+1}$ and the cross-covariance $P_{xz,k+1}$ can be obtained as

$$\begin{aligned}
P_{zz,k+1} &= \sum_{i=1}^{4p} W^{(c)}_{p,i}(z_{k+1} - \overline{z}_{k+1})(z_{k+1} - \overline{z}_{k+1})^T \\
&\quad + T\\
P_{xz,k+1} &= \sum_{i=1}^{4q} W^{(c)}_{p,i}\chi_u(z_{k+1} - \overline{z}_{k+1})^T
\end{aligned} \tag{35}$$

where $\overline{z}_{k+1}$ is the weighted mean with $W^{(m)}_{p,i}$. The Kalman gain is the factor which allows to minimize the state covariance matrix P and is computed by

$$K_{k+1} = P_{xz,k+1}P^{-1}_{zz,k+1} \tag{36}$$

Note that if a noisy sensor is used, the measurement covariance matrix has high elements and its inverse will produce a low Kalman gain. Finally, the *a posteriori* state estimate is

$$\hat{x}_{k+1|k+1} = \varphi(\hat{x}_{k+1|k}, K_{k+1}r_{k+1}) \tag{37}$$

where r is the residual, i.e. the discrepancy, between the estimated measurement $\overline{z}_{k+1}$ from the *a priori* predictions and the actual measurement z_{k+1}. It is clear that the Kalman gain K_{k+1} acts as a weighing factor for the residual. Particularly, when the measurement is corrupted and T assumes large values, then the Kalman gain and the residual weight are low. Therefore, this gain allows to have an optimal estimate weighting the received measurement on the basis of its reliability. This degree of reliability is achieved by comparing the covariance of the estimated measurement and the

covariance of the real measurement. Finally, the *a posteriori* error covariance matrix is computed as

$$P_{k+1|k+1}=P_{k+1|k} - K_{k+1}P_{zz,k+1}K_{k+1}^T \tag{38}$$

3.3 Tracking control design on Lie groups and their tangent bundles

In this section, two different control techniques are designed on $\mathsf{TSE}(3)$ to integrate with the navigation system: A MLBS control and a SMC.

3.3.1 Morse-Lyapunov Backstepping Control (MLBS)

In this section, a MLBS control is introduced to address tracking problem of reaching and maintaining a desired rotational and translational motion in the presence of stochastic processes. The control design in the $\mathsf{TSE}(3)$ framework enables one to treat both rotational and translational motions simultaneously. The feedback loop allows the computation of the difference between the desired and the measured configuration, which is affected by the measurements errors. The controller should be able to nullify the error between the actual and desired states. The desired states are computed by a guidance system, while the actual states are obtained from the navigation filter which filters out the measurement noise. Once the state configuration error is defined, the controller can command the rigid body translational and rotational motion through the actuators.

The guidance algorithm assigns the desired position r_{ref} in the inertial frame, velocity $\mathbb{V}_{\text{ref}}$ in the body frame, and attitude R_{ref} along with the actual states, to the control system. The UKF filter is used to obtain the estimated states $\hat{r}$, $\hat{\mathbb{V}}$ and $\hat{R}$ from noisy measurements. The tracking errors can then be computed as

$$\begin{aligned}\delta g_{\text{track}} &= g_{\text{ref}}^{-1}\hat{g} = \begin{bmatrix}\delta R_{\text{track}} & \delta r_{\text{track}}\\ 0 & 1\end{bmatrix}\\ &= \begin{bmatrix}R_{\text{ref}}^T(\Theta_{\text{ref}})\hat{R}(\hat{\Theta}) & R_{\text{ref}}^T(\Theta_{\text{ref}})\,(\hat{r}-r_{\text{ref}})\\ 0 & 1\end{bmatrix}\\ \delta\mathbb{V}_{\text{track}} &= \hat{\mathbb{V}} - \mathbb{V}_{\text{ref}}\end{aligned} \tag{39}$$

The error dynamics in terms of position and velocity should tend to zero, and the rotation matrix to the identity matrix. Since the state is on $\mathsf{TSE}(3)$ and the control input is in $\mathbb{R}^6$, different functions are introduced to allow the retraction from the manifold into Euclidean space. The nonlinear function of the velocity and configuration is defined as

$$\psi(\delta g_{\text{track}}, \delta\mathbb{V}_{\text{track}}) = \delta\mathbb{V}_{\text{track}} + K_1 l(\delta g_{\text{track}}) \tag{40}$$

where $K_1 = \text{blkdiag}(k_{11}, k_{12}) \in \mathbb{R}^{6\times 6}$ is a positive definite control gain matrix. The following vector function of the configuration is then introduced:

$$l(\delta g_{\text{track}}) = \left[s^T(\delta R_{\text{track}}), \delta r_{\text{track}}^T\right]^T \tag{41}$$

with its derivative

$$\dot{l}(\delta g_{\text{track}}) = \left[\dot{s}^T(\delta R_{\text{track}}), \delta v_{\text{track}}^T\right]^T \tag{42}$$

The $s(\cdot) : \text{SO}(3) \to \mathbb{R}^3$ and $\dot{s}(\cdot) : \text{SO}(3) \to \mathbb{R}^3$ are

$$\begin{aligned}s(\delta R_{\text{track}}) &= \sum_{i=1}^{3} a_i \left(\delta R_{\text{track}}^T e_i\right)^\times e_i\\ &= \sum_{i=1}^{3} \left(\delta R_{\text{track}}^T A^T e_i\right)^\times e_i\\ \dot{s}(\delta R_{\text{track}}, \delta\omega_{\text{track}}) &= (\text{tr}(A\delta R_{\text{track}})I_3 -\\ &\quad \delta R_{\text{track}}^T A)\delta\omega_{\text{track}}\end{aligned} \tag{43}$$

where e_i, $i = 1, 2, 3$, are the elements of the natural basis in $\mathbb{R}^3$, and $A = [\text{diag}\,(a_1, a_2, a_3)]$ with the scalars a_1, a_2, and a_3 selected such that $a_1 > a_2 > a_3 \geq 1$. The control law developed for rigid body regulation control on $\mathsf{TSE}(3)$ in [18] is revised here to account for a tracking problem:

$$\begin{aligned}u_c = &-\mathbb{I}K_1\dot{l} - \text{ad}^*_{\psi - K_1 l}\mathbb{I}\,(\psi - K_1 l) - \mathbb{I}K_2\psi\\ &-\mathbb{I}\kappa\left[0_{1\times 3}, \delta r_{\text{track}}^T\delta R_{\text{track}}^T\right]^T - u_e\end{aligned} \tag{44}$$

where $K_2 = \text{blkdiag}(k_{21}, k_{22}) \in \mathbb{R}^{6\times 6}$ is a positive definite control gain matrix, and k_{21} and k_{22} can be tuned suitably to adjust rotation and translation performance of the rigid body. Thus, the total augmented control input is $u_c = [F_c^T, M_c^T]^T$, as defined in Eq. (10).

The proof for almost global asymptotic stability of the tracking problem studied is similar to that given in [18] for the rigid body regulation problem using an attitude-dependent Morse- Lyapunov function and a backstepping state feedback control law of the form $\delta\mathbb{V}_{\text{track}} = -l(\delta g_{\text{track}})$. According to [52], the separation principle allows the design of the controller and the observer (filter algorithm) separately. Particularly, if the observer and the controller are both stable, then the closed-loop dynamics obtained using the augmented form is also stable. In many applications, this technique has proved to be a successful and stable design method. In order to highlight the different type of errors, the total error on each state can be rewritten as

$$\begin{aligned}\delta R &= R_{\text{ref}}^T(\Theta_{\text{ref}})\hat{R}(\hat{\Theta})\hat{R}^T(\hat{\Theta})R(\Theta) = \delta R_{\text{track}}\delta R_{\text{est}}\\ \delta r &= \hat{R}(\hat{\Theta})(r-\hat{r}) + R_{\text{ref}}^T(\Theta_{\text{ref}})(\hat{r} - r_{\text{ref}})\\ &= \delta r_{\text{est}} + \delta r_{\text{track}}\\ \delta\mathbb{V} &= \mathbb{V} - \hat{\mathbb{V}} + \hat{\mathbb{V}} - \mathbb{V}_{\text{ref}} = \delta\mathbb{V}_{\text{est}} + \delta\mathbb{V}_{\text{track}}\end{aligned} \tag{45}$$

where $\delta(\cdot)_{\text{est}}$ and $\delta(\cdot)_{\text{track}}$ denote the estimation error and the tracking error, respectively. According to Eq. (45), when the estimation error and tracking error go to zero, the total error goes to zero, meaning that both the estimator and controller are asymptotically stable (in addition, the controller is almost globally asymptotically stable [18]). The convergence of the controller results in a zero tracking error and the convergence of the filter results in a bounded estimation error with zero mean white noise. From Eq. (45), the coupling effect of the nonlinear dynamics is clear. The total position error is not able to converge to zero if the attitude total error does not converge.

Note that an alternative asset could be the implementation of a controller robust to the uncertainties, i.e. a stochastic robust controller analogous to that in [53] for robust pose control, without the use of a navigation system. However, for systems affected by different sources of high-magnitude noise, the states can easily diverge if the stochasticity is not filtered out unless the control inputs are selected to be large enough to compensate those stochasticities. The estimator-based controller proposed here is continuously updated with the system dynamics and, as a result, it avoids high control inputs.

3.3.2 Sliding Mode Control

In this section, an SMC is designed on TSE(3) to address some tracking control problem as in Section 3.3.1. In the SMC approach, a so-called sliding surface σ is defined, which is a subset of the state space on which the trajectory of the rigid body is desired to lie. A feedback law is realized such that this surface will be attractive and invariant, i.e. the rigid body trajectory evolves towards this surface and, once there, it stays close to it. The sliding surface σ is defined as a function of pose and velocity, i.e.

$$\sigma = c_1\, \delta\mathbb{V}_{\text{track}} + c_2\, l(\delta g_{\text{track}}) + c_3\, \lambda \;\in \mathbb{R}^6 \tag{46}$$

where $c_1 = \text{blkdiag}(c_{11} I_3, c_{12} I_3)$, $c_2 = \text{blkdiag}(c_{21} I_3, c_{22} I_3)$, $c_3 = \text{blkdiag}(c_{31} I_3, c_{32} I_3)$ are positive definite diagonal matrices, $l(\cdot)$ is defined Eq. (41), $\lambda = \int_0^t \psi(\delta g_{\text{track}},\, \delta\mathbb{V}_{\text{track}}) d\tau$, and $\psi(\cdot,\cdot)$ is defined in Eq. (40). The third integral term is added since it meaningfully reduces the steady state error. The addition of an integral action to define the sliding surface has been shown to lead to good results in literature [54–56]. The SMC control force and moment inputs are defined as

$$u_c = u_{eq} + u_d \tag{47a}$$

with

$$u_{eq} = -\text{ad}^*_{\delta\mathbb{V}_{\text{track}}} \mathbb{I}\delta\mathbb{V}_{\text{track}} - \mathbb{I}c_1^{-1} c_2\, \dot{l}(\delta g_{\text{track}}) - \mathbb{I}c_1^{-1} c_3\, \psi(\delta g_{\text{track}}, \delta\mathbb{V}_{\text{track}}) - u_e \tag{47b}$$

and

$$u_d = -K_\sigma \text{sgn}(\sigma) \tag{47c}$$

where $\text{sgn}(\cdot)$ denotes the vector sign function and $K_\sigma = \mathbb{I}c_1^{-1} c_4 = \text{blkdiag}(K_{\sigma,M} I_3, K_{\sigma,F} I_3)$ is a positive definite diagonal matrix which must be properly selected in order to have the sliding mode operate correctly while considering unmodeled dynamics. The first part (i.e. u_{eq}) is known as equivalent control and it represents the control function which needs to be applied to the system after reaching the sliding surface to ensure that the system trajectory thereafter stays on this surface. This feature is known as the invariant property and the control input guarantees the solution of the problem $\dot{\sigma} = 0$. The second part (i.e. u_d) is known as discontinuous control and it ensures that the system trajectory evolves towards the sliding surface. This feature is known as the attractive property and the switching control action allows the system trajectory to reach the surface. In order to achieve the asymptotic convergence of $l(\cdot)$ and $\psi(\cdot,\cdot)$ to zero (i.e. $\lim_{t\to\infty} l(\cdot) = 0$ and $\lim_{t\to\infty} \psi(\cdot,\cdot) = 0$) with a desired convergence rate and in the presence of bounded disturbance, the control input in Eq. (47) must drive the variable σ in Eq. (46) to zero within a finite time. This feature can be guaranteed to hold by applying the Lyapunov stability theory. The Lyapunov candidate function is selected as

$$\mathcal{V} = \frac{1}{2}\sigma^T \sigma \tag{48}$$

Taking the time derivative of the Lyapunov function above gives

$$\dot{\mathcal{V}} = \dot{\sigma}^T \sigma \tag{49}$$

Substituting Eq. (46) and its time derivative in Eq. (49), using the tracking-problem version of Eq. (10) (i.e. replacing g and $\mathbb{V}$ in that equation with δg_{track} and $\delta\mathbb{V}_{\text{track}}$, respectively), and simplification yields

$$\dot{\mathcal{V}} = -c_4\, \text{sgn}^T(\sigma)\, \sigma = -c_4\, \|\sigma\|_1 \tag{50}$$

Since $\dot{\mathcal{V}} < 0$ for $\sigma \neq 0$, the stability of the equilibria is proved. In Eq. (47a), $\|\cdot\|_1$ denotes the 1−norm of the sliding surface, i.e. $\|\sigma\|_1 = \sum_1^6 |\sigma_i|$. Note that this proof only guarantees the local stability of the equilibrium $(\delta g_{\text{track}}, \delta\mathbb{V}_{\text{track}}) = (I_4, 0)$ since, other than at equilibrium above, σ can also be zero for

some linear combination of $\delta\mathbb{V}_{\text{track}}$, $l(\cdot)$, and λ in Eq. (46).

Although, in contrast to the MLBS control, the SMC does not guarantee global asymptotic stability, it is independent of the knowledge of the mathematical model of the rigid body. However, the discontinuous nature of the control law might lead to a phenomenon called chattering, where high-frequency oscillations occur around the sliding surface. This phenomenon is undesirable in practical situations since it can cause high control activity and may excite high-frequency dynamics neglected in the model. One way to attenuate the chattering is to replace the discontinuous $\text{sgn}(\cdot)$ function in Eq. (47c) with an approximate smooth function such as a hyperbolic tangent function of the form $\tanh(b\,\sigma)$ or a sigmoid function of the form $\sigma/(\|\sigma\|+b)$ with the scalar b selected properly.

3.4 Variational integrator

In the numerical simulations provided in Section 5, the dynamics are propagated using a variational integrator in order to preserve geometric properties of the system. This integrator is applied directly on the nonlinear manifold $\mathsf{SE}(3)$, where the discretized Hamiltonian is used. The details of the variational integrator formalism are not shown here for brevity, but they can be found in [41, 57, 58], for instance.

4 Case Study: Dynamics of spacecraft hovering near small bodies

For proximity operations near small bodies, the asymmetric distribution of mass of those bodies becomes a more significant element in the dynamics than in their larger counterparts such as Earth, Jupiter, or their major moons. That in mind, the torque induced on a spacecraft modeled as a rigid body and caused by that asymmetry must be considered. The gravity force exerted by the asteroid on the spacecraft is described using a second degree and order spherical harmonic gravity field. Assuming the origin of the asteroid body-centered inertial frame (BCI) coincides with the center of mass of the body, the first degree and order gravity terms are $C_{11} = C_{10} = S_{11} = 0$. The asteroid is modeled as a constant density triaxial ellipsoid with major axes l_1, l_2, and l_3. This assumption makes the second degree and order terms C_{21}, S_{21}, S_{22} identically zero. The celestial body's gravity potential second degree and order terms are given in [59] and can be revisited as

$$U = \frac{\mu}{\|\rho\|}\left(1+\frac{1}{\|\rho\|^2}\left(C_{20}\left(-\frac{1}{2}+\frac{3}{2}(\hat{\rho}\cdot\hat{K})^2\right)+3C_{22}\left(1-(\hat{\rho}\cdot\hat{K})^2-2(\hat{\rho}\cdot\hat{J})^2\right)\right)\right)$$

where $\rho = \|\rho\|\hat{\rho} \in \mathbb{R}^3$ is the position vector of an arbitrary point on the spacecraft expressed in the BCI frame such that $r = \frac{1}{m}\int_{\mathcal{B}} \rho\, dm$, $(\hat{I}, \hat{J}, \hat{K})$ is the unit basis of the BCI frame, and the second degree and order coefficients are [60–62]

$$C_{20} = -J_2 = \frac{1}{5}(\gamma^2 - \frac{\alpha^2+\beta^2}{2}),$$
$$C_{22} = \frac{1}{20}(\alpha^2-\beta^2) \tag{51}$$

where $\alpha = 1$, $\beta = \frac{l_2}{l_1}$, and $\gamma = \frac{l_3}{l_1}$ are normalized axes of the ellipsoid. The presented gravitational potential is an effective way to study the orbit-attitude coupled spacecraft dynamics in proximity of small, irregular bodies]red [38]. By taking the partial derivative of the gravity potential U in Eq. (51) with respect to ρ, integrating over the body of the spacecraft, and keeping only the terms up to order $1/\rho^4$, the gravity gradient force applied to the spacecraft expressed in the spacecraft body fixed frame (SBF) can be approximated as

$$F_g = R^T \int_{\mathcal{B}} \frac{\partial U}{\partial \rho} dm = R^T\left(F_{g_1} + F_{g_2}\right) \tag{52}$$

where R is the rotation matrix from the SBF frame to the BCI frame,

$$F_{g_1} = -m\frac{\mu}{\|r\|^2}\left(1+\frac{3}{m\|r\|^2}\left[J+\frac{1}{2}\left(\text{tr}(J)-5\,\hat{r}^T R\,J\,R^T\,\hat{r}\right)I_3\right]\right)\hat{r} \tag{53}$$

$\hat{r} = r/\|r\|$, and

$$F_{g_2} = \frac{m\mu}{\|r\|^4}\left(\begin{bmatrix}\left(\frac{3}{2}C_{20}-9C_{22}\right)\left(\hat{r}\cdot\hat{I}\right)\\ \left(\frac{3}{2}C_{20}-21C_{22}\right)\left(\hat{r}\cdot\hat{J}\right)\\ \left(\frac{9}{2}C_{20}-15C_{22}\right)\left(\hat{r}\cdot\hat{K}\right)\end{bmatrix}\right. \tag{54}$$
$$\left.+\frac{15}{\|r\|}\left(\left(-\frac{C_{20}}{2}+C_{22}\right)\hat{r}\cdot\hat{K}+2C_{22}\hat{r}\cdot\hat{J}\right)\hat{r}\right)$$

which is an alternative representation to that given in [63]. The gravity gradient torque on the spacecraft due to the gravitational field of the central body is expressed in the SBF frame as

$$M_g = \frac{3\mu}{\|r\|^3}(R^T\hat{r})^{\times} J R^T\hat{r} \tag{55}$$

Therefore, the total augmented external effect in Eq. (10) is $u_e = [F_g^T, M_g^T]^T$, where the gravitational force and moment are given in Eqs. (52)-(55), respectively.

In this case study, the tracking orbit is chosen based on the mission timeline. Just before the

Table 1 Spacecraft and Bennu properties [63–67]

Parameter	Values
Spacecraft mass [kg]	$m = 850$
Spacecraft dimension [m]	$d_1 = 2.0,\ d_2, d_3 = 2.3$
Spacecraft inertia [kg m^2]	$J = \frac{m}{12}\text{diag}\,[d_1^2 + d_2^2,\ d_2^2 + d_3^2,\ d_3^2 + d_1^2]$
Bennu gravitational parameter [m^3 s^{-2}]	$\mu = 5.2060$
Bennu dimension [m]	$l_1 = 535,\ l_2 = 508,\ l_3 = 365$
Bennu coefficients	$C_{20} = -0.097070,\ C_{22} = 0.004919$
Bennu rotation period [hr]	$T_B = 4.297$

Table 2 Values used for the navigation and control systems

Parameter	Values
Measurement std [deg,m,deg,m/s]	$\sigma_{\zeta_\Theta} = 6,\ \sigma_{\zeta_r} = 100,\ \sigma_{\zeta_\omega} = 0.2,\ \sigma_{\zeta_v} = 2$
Measurement cov matrix	$T = \text{blkdiag}\left[\sigma^2_{\zeta_\Theta} I_3,\ \sigma^2_{\zeta_r} I_3,\ \sigma^2_{\zeta_\omega} I_3,\ \sigma^2_{\zeta_v}/10 I_3\right]$
Process cov matrix	$Q = \text{blkdiag}\,[10^{-10} I_3,\ 10^{-10} I_3,\ 10^{-10} I_3,\ 10^{-10} I_3]$
State cov matrix	$P_0 = \text{blkdiag}\,[10^{-10} I_3,\ 10^{-10} I_3,\ 10^{-10} I_3,\ 10^{-10} I_3]$
Control moment saturation per axis [N m]	$M_{c,i} = 24 \quad (i = 1,2,3)$
Control force saturation per axis [N]	$F_{c,i} = 366 \quad (i = 1,2,3)$
MLBS control gains:	
κ	1×10^{-6}
K_1	$\text{blkdiag}\,[5 \times 10^{-4} I_3,\ 1 \times 10^{-3} I_3]$
K_2	$\text{blkdiag}\,[2 \times 10^{-2} I_3,\ 1 \times 10^{-2} I_3]$
A	$[1.2,\ 1.1,\ 1]^T$
SMC gains:	
c_1	$\text{blkdiag}[1 \times 10^{-9} I_3, 0.002 I_3]$
c_2	$\text{blkdiag}[1 \times 10^{-11} I_3, 3 \times 10^{-5} I_3]$
c_3	$\text{blkdiag}[0_{3\times3}, 1 \times 10^{-10} I_3]$
K_σ	$\text{blkdiag}[100 I_3, 100 I_3]$

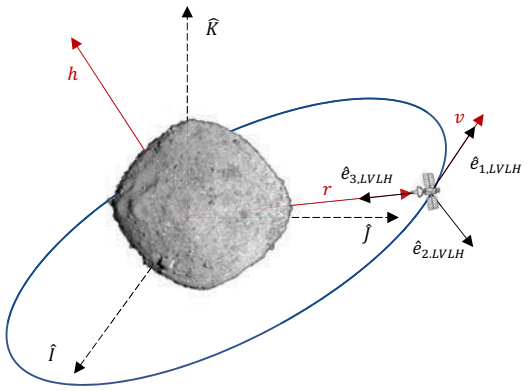

Fig. 1 LVLH and BCI reference frames representation

touch-and-go operation, the spacecraft navigates to a closed orbit with a radius of 1 km around Bennu. This phase is also important for the scientific return of the mission, since the spacecraft collects asteroid topography data to map its surface. For this reason, it is assumed to have a desired (reference) orbit that is circular with a nonzero inclination, and a nadir-pointing attitude such that a face of the satellite always points to the surface of the asteroid. The orbit is parameterized through trigonometric functions of time such that, at each time step, the reference position in BCI frame is

$$r_{\text{ref}}(t) = R_0\,[\rho_0 \sin(n_0\,t), \quad \rho_0 \cos(n_0\,t), \quad 0]^T \tag{56}$$

where ρ_0 denotes the radius of the desired circular orbit, n_0 is the orbital mean motion, R_0 represents the transformation matrix from the perifocal frame to the BCI frame, and the orbital mean motion is obtained from $n_0 = \frac{2\pi}{T_0}$, where the period of the orbit is computed with the third Kepler law $T_0 = 2\pi\sqrt{\frac{\rho_0^3}{\mu}}$. The reference translational velocity $v_{\text{ref}}(t)$ is obtained by taking the time derivative of the position vector in Eq. (56).

In order to discuss attitude in this case study, the local vertical local horizontal (LVLH) reference frame is introduced, whose representation is given in Fig. 1. Particularly, r represents the position vector from BCI to the satellite, v is the satellite's orbital velocity, and $h = r \times v$ the orbital angular momentum. The first axis is oriented in the $v_{\text{ref}}(t)$ direction, $\hat{e}_{1,\text{LVLH}}(t) = v_{\text{ref}}(t)/\|v_{\text{ref}}(t)\|$, the second axis is normal to the orbit plane in the opposite direction of angular momentum h, and the third axis is oriented in the $-r_{\text{ref}}(t)$ direction, $\hat{e}_{3,\text{LVLH}}(t) = -r_{\text{ref}}(t)/\|r_{\text{ref}}(t)\|$ such that the axes obey the right-hand rule. The reference angular velocity is simply defined as $\omega_{\text{ref}}(t) = -n_0\,\hat{e}_{2,\text{LVLH}}$ [68, 69]. The guidance system computes the reference attitude at each instant of time as

$$\Theta_{\text{ref}}(t) = \log_{\mathsf{SO(3)}}\left(R^T_{LVLH}(t)\right) \tag{57}$$

where R_{LVLH} is the rotation matrix from BCI to LVLH reference frame

$$R_{\text{LVLH}}(t)=\begin{bmatrix}\hat{e}_{1,\text{LVLH}}(t)\cdot\hat{I} & \hat{e}_{1,\text{LVLH}}(t)\cdot\hat{J} & \hat{e}_{1,\text{LVLH}}(t)\cdot\hat{K}\\ \hat{e}_{2,\text{LVLH}}(t)\cdot\hat{I} & \hat{e}_{2,\text{LVLH}}(t)\cdot\hat{J} & \hat{e}_{2,\text{LVLH}}(t)\cdot\hat{K}\\ \hat{e}_{3,\text{LVLH}}(t)\cdot\hat{I} & \hat{e}_{3,\text{LVLH}}(t)\cdot\hat{J} & \hat{e}_{3,\text{LVLH}}(t)\cdot\hat{K}\end{bmatrix} \tag{58}$$

with unit vectors $F_{BCI} = [\hat{I}, \hat{J}, \hat{K}]$ for the BCI frame and $F_{LVLH} = [\hat{e}_{1,LVLH}, \hat{e}_{2,LVLH}, \hat{e}_{3,LVLH}]$ for the LVLH frame.

5 Numerical Simulations and Discussion

In the numerical simulations presented here, the spacecraft initial conditions are chosen to be significantly different from the reference orbit and nadir-pointing attitude. All the states are selected randomly from Gaussian distributions with a standard deviations of 90 deg, 1000 m, 5 deg/s and 1 m/s for attitude, position, and velocities respectively. On the other hand, the UKF initial conditions are selected with an error of 10% for attitude and position and 20% for velocities, with respect to the spacecraft initial conditions.

5.1 Filter verification

In Eq. (57), the following values are chosen: $\rho_0 = 1$ km, $R_0 = R([0, \pi/4, 0])$. In order to investigate the performance of the proposed navigation and control system, a scenario with a high level of orbit-attitude coupling is studied here. The OSIRIS-REx mission is of specific interest as it involved visiting the small, irregular asteroid, Bennu. Publicly available data for this mission (Table 1) are used to define the properties of the spacecraft and the asteroid. The details of the spacecraft control system are used to define the saturation limits for the control moment and force. The control gains are tuned arbitrarily, but in such a way that the closed-loop dynamics become stable. The sensors employed in the navigation system are assumed to be characterized by worse statistics than one would expect to find in a real-world scenario, i.e., the standard deviations are assumed to be relatively large in order to verify the robustness of the proposed navigation and control system. The process noise covariance matrix is chosen with relatively small elements with respect to R, such that the UKF relies on the predictions and the noise can be efficiently filtered. The details of the navigation and control system can be found in Table 2.

The performance of the proposed UKF is compared to those of other state filters designed on $\mathsf{SE}(3)$ that can be found in literature. In particular, the algorithms selected for the comparison are i) the EKF on Lie group introduced in [27] (EKF), ii) the UKF on Lie group introduced in [31] (UKF), and iii) the discrete EKF on Lie group (DEKF) described in [29]. The performance analysis is conducted on the basis of position and attitude estimation results. The case study consists of the propagation of the open-loop spacecraft dynamics around the asteroid Bennu, where the data previously introduced are used. As in [30, 31], the results are shown in Fig. 2 in terms of the root mean square of the pose estimation error (RMSE). The first and second rows show the position and attitude RMSEs ϵ_r and ϵ_Θ, respectively, as a function of sample period Δt with $\zeta_r = 0.1$ km, $\zeta_\Theta = 0.1$ deg, $\chi_r = 0$ km, and $\chi_\Theta = 0$ km (left), initial condition inaccuracies χ_r and χ_Θ with $\zeta_r = 0.1$ km, $\zeta_\Theta = 0.1$ deg, and $\Delta t = 1$ s (center), and measurement noise standard deviations ζ_r km (with $\zeta_\Theta = 0.1$ deg) and ζ_Θ deg (with $\zeta_r = 0.1$ km), and $\Delta t = 1$ s (right).

In the left column of Fig. 2, the RMSE(s) for the position and attitude error are shown along with the sample period Δt from 0.1 to 20 seconds. It can be seen that the proposed filter (solid) and the UKF (dash) are more robust to changes in the sampling frequency than the EKF and DEKF. Particularly, the EKF (dot) and DEKF (dash-dot). For smaller time steps, the difference among different filters reduces. Then the UKF on $\mathsf{TSE}(3)$ and the UKF proposed in [31] behave almost the same, achieving an higher accuracy with respect to EKF and DEKF even for large Δt.

The center column of Fig. 2 shows the RMSE(s) for the position and attitude error along with the percentage of uncertainty on the filter initial pose estimate with respect to the true pose. Particularly, let the true values be r_0 and Θ_0, the filters initial guesses are parametrized as $r_0(1+\chi_r/100)$, $R(\Theta_0(1+\chi_\Theta/100))$. As expected, the best performance are achieved for small values of uncertainties. The UKF filters outperform the EKF filters for all the range of χ_r, χ_Θ since the EKF are particularly influenced by the initial condition accuracy.

Finally, in the right column of Fig. 2, the RMSE(s) are given as functions of the standard deviation of the measurement noise, for the position and attitude measurements. Note that the proposed UKF filter on $\mathsf{TSE}(3)$ achieves the lowest accuracy in terms of attitude $\mathrm{O}(10^{-1})$ deg even with the smallest noise standard deviation. This can be explained by the fact that the UKF on $\mathsf{TSE}(3)$ also estimates the velocities which are assumed to be provided by noisy sensors, while the

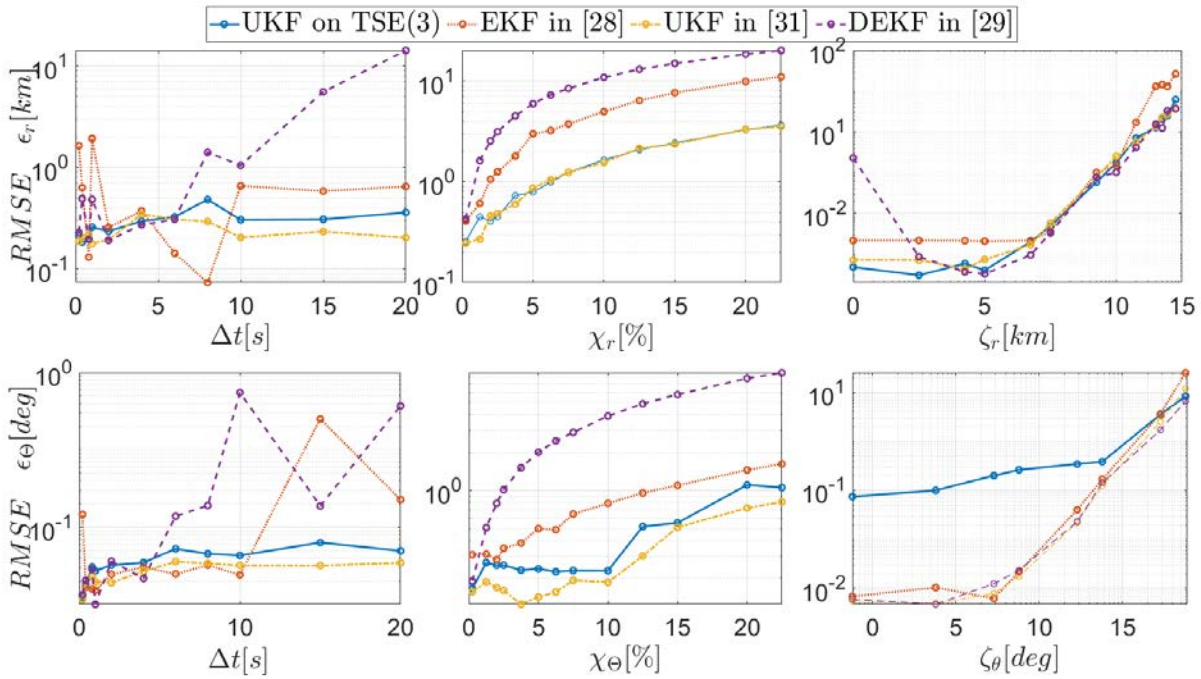

Fig. 2 Attitude and position RMSE as a function of sample period, initial condition inaccuracies and measurement noise standard deviations.

filter on SE(3) uses un-noisy velocities and only updates on position and attitude measurements.

As shown in the figure, the proposed UKF on TSE(3) and standard UKF generally perform better than others. Even if the DEKF seems to be robust to noisy measurements, it is dependent on the initial condition accuracy and sample frequency. According Fig. 2, the EKF on SE(3) [27] is able to achieve an higher accuracy of DEKF on SE(3) [29] and lower accuracy than the UKF on SE(3) [31] and the proposed UKF on TSE(3). The latter has proved to be particularly robust even with noisy measurements, inaccurate initial conditions, and low sampling frequency.

5.2 Performance of the closed-loop system

This section presents the results obtained via the implementation of the proposed TSE(3) filter and control designs in Section 3. In Figs. 3 and 4, the time histories of attitude, position and velocities in the BCI frame are provided. Particularly, three different quantities are analyzed: (i) The measured states which represent the state variables measured by noisy sensors, (ii) the estimated (filtered) states, which are the outputs of the navigation system, and (iii) the ideal states, which are the noise-free states obtained with ideal and perfect sensors. Moreover, for each state variable a magnified portion of the figure is also shown to provide the reader with an approximation of the convergence times. It can be seen that the estimated states start from a different point with respect to the measured and ideal states due to the different initial conditions in the UKF. However, the state filter is able to converge to the ideal states in less than a hundredth of the orbit period even when considering the saturation limits on the control input. It is worth noting that the navigation scheme is also able to handle an attitude variation from -180 deg to 180 deg with no issues.

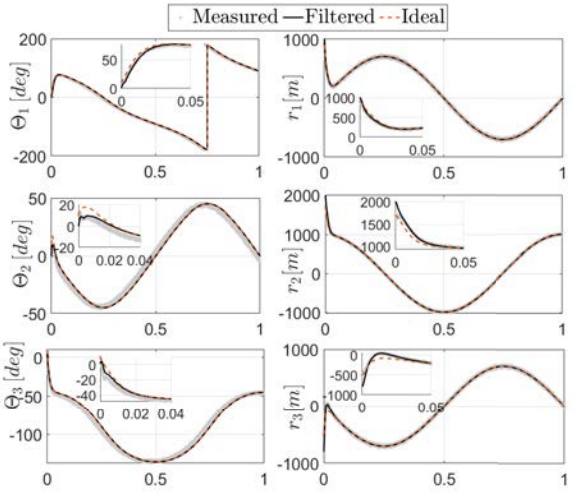

Fig. 3 Measured (grey), estimated (black), and ideal (red) states.

Figure 5 shows the trajectory of the spacecraft center of mass, the desired orbit, and the space-

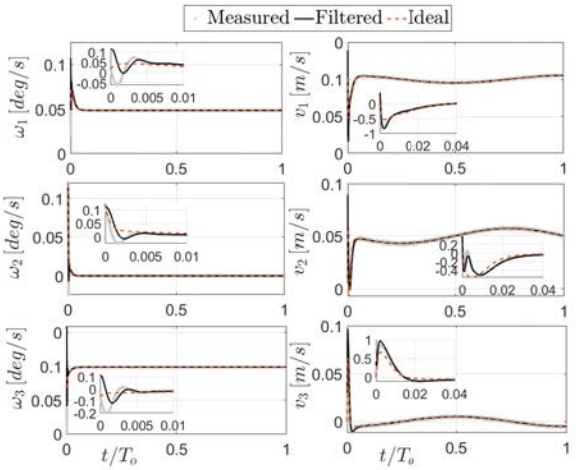

Fig. 4 Measured (grey), estimated (black), and ideal (red) states.

craft's position and attitude at different points in the orbit. The spacecraft starts with a completely different state relative to the desired, and is initially tumbling. The spacecraft transient response is highlighted in the magnified window in the right panel of Fig. 5. The convergence of the filter and controller proposed here result in the convergence of the estimated states (both trajectory and attitude) to the actual and desired state, as can be seen in the figure. It can be seen that as the spacecraft orbits around the asteroid, its attitude changes such that one side always faces Bennu.

In each panel of Fig. 6, the norms of the differences between the spacecraft estimated states and their corresponding desired states are shown, where the noisy measurements after initial convergence can be seen. The attitude error has a peak in correspondence of the Θ_1 discontinuity (Fig. 3) and a rapid convergence. The magnitude of the steady-state errors are acceptably small compared to the magnitude of the reference variables and large sources of noise. For instance, the proposed navigation and control system allows the simulation to reach a position error on the order of 1 m in an orbit with a 1000 m radius and with a position noise standard deviation of 100 m. The same rationale applies to the attitude, where an accuracy of 0.0001 deg is reached. The mean and the RMSE are reported for each state error. The results improve as the numerical values of mean and RMSE decrease, as also indicated in [70]. Note that both the mean and the RMSE would reduce with time, since the number of samples with small steady state error would increase. In fact, these two indices are influenced by the large state errors that exist before the convergence is achieved.

In Fig. 7, the estimated state error between the estimated and the ideal states are shown along

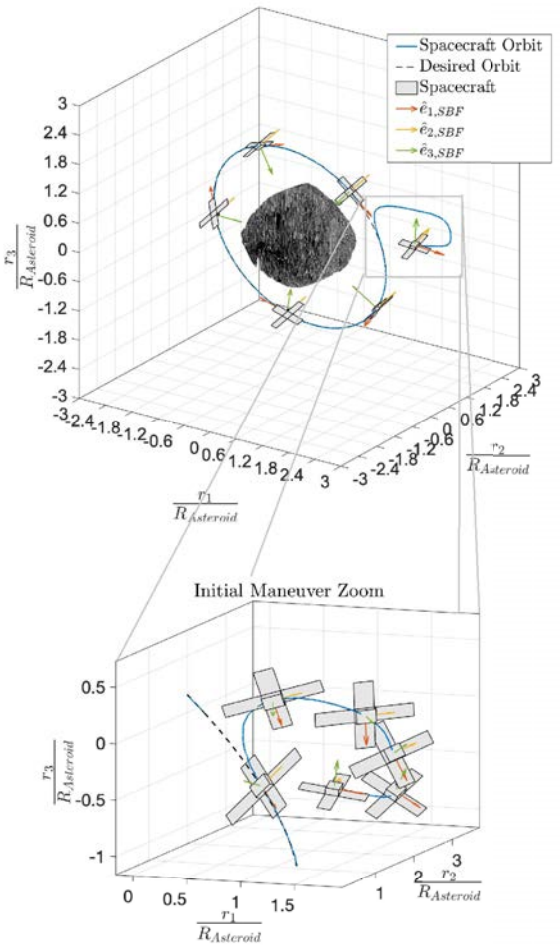

Fig. 5 SBF orientation, and spacecraft attitude and trajectory around Bennu in BCI frame obtained via the implementation of the navigation and control systems.

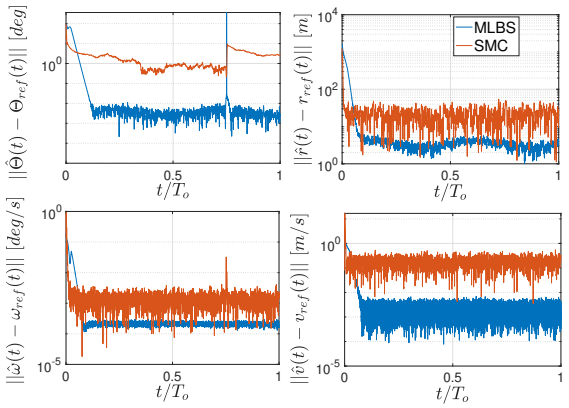

Fig. 6 Norm of the difference between the estimated states and reference states, for MLBS and SMC control systems. The spike near 0.75 is due to a singularity.

with the estimated confidence bounds of 3σ. The optimal performance of the estimator is generally indicated by the bounded estimation errors within the estimated standard deviation bounds [71, 72]. In other words, the UKF acts as an unbiased es-

timator, meaning that the expectation of the estimated state errors is zero [73]. From a statistical point of view, it is expected that about 99% of the samples remain bounded inside the two envelopes. Additionally, the performance of the UKF confirms the fact that the state errors are approximately zero mean white noise. Note that the attitude components exhibit a peak, which corresponds to the discontinuity of the Θ_1 when it goes from -180 deg to 180 deg, as shown in Fig. 3.

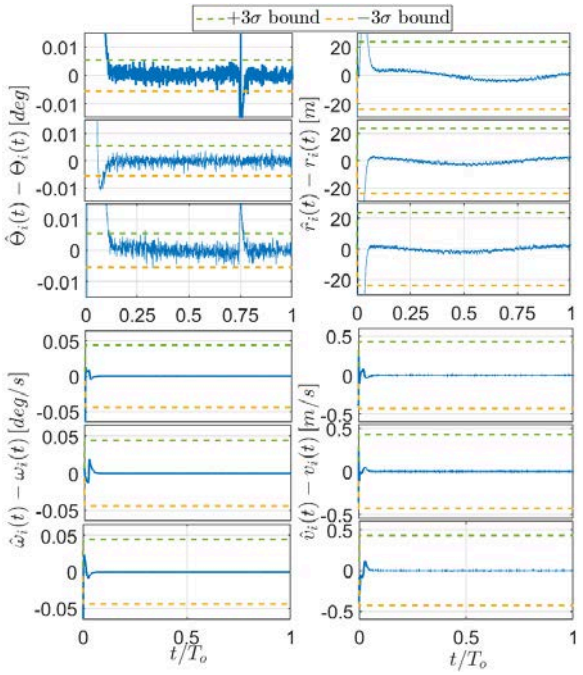

Fig. 7 State estimation error components between the estimated states and the ideal noise-free states.

The spacecraft can reach and maintain the desired orbit-attitude through the control system which produces the necessary control force and moment, that are shown in Fig. 8. In addition, the force control effort is quantified with the total integrated control force per unit mass that is computed as $\Delta V = \frac{1}{m}\int_0^t \|F_c(\tau)\| d\tau$. While the moment control effort is quantified with the integrated moment, i.e. $\Delta\tau = \int_0^t \|M_c(\tau)\| d\tau$. It can be seen that the proposed navigation and control system is able to guarantee the orbit and attitude tracking with a low amount of control moment and force, considering the initial conditions, the large saturation limits and noise statistics in Table 2. In fact, both F_c and M_c are well below the boundaries of 24 Nm and 366 N respectively. The total ΔV is less than those obtained in [74], where an adaptive controller was used for the orbital control. As a result of the UKF filtering action, they both appear without any residual noise, which would have introduced an extra control effort. Note that the control moment converges before the control force, in agreement with the magnified portions of Figs. 3 and 4. Moreover, as discussed in Section 3.3, since the orbit-attitude coupling is considered, the tracking position error can converge only if the tracking attitude error has converged. Therefore, the observed behavior is expected.

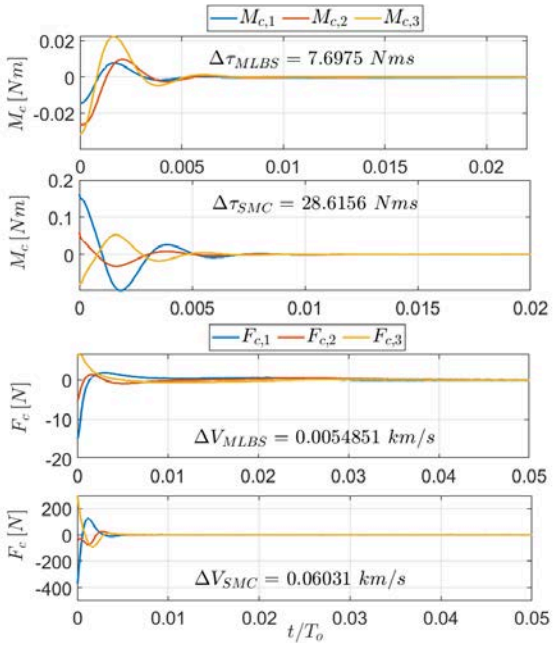

Fig. 8 Control inputs in terms of force and moment provided by the tracking controller, for MLBS and SMC control systems

6 Conclusions

In this paper, a novel rigid body navigation and control system has been introduced in the Lie group SE(3) and its tangent bundle in the presence of stochastic processes in the system. In the mathematical framework presented here, the geometrical characteristics of the system are well preserved and the translational and attitude motions are treated simultaneously. Hence, this formalism allows for the coupling between orbital and attitude motions of a rigid body to be considered in the control design. A special retraction function is used to allow the unscented Kalman filter (UKF) to encode the sigma points onto the manifold, and the inverse of that retraction function is used to decode the sigma points from the manifold. The performance achieved with the implementation of the proposed UKF on TSE(3) is compared in terms of robustness and accuracy to those of filters on SE(3) in the literature. In particular, the performance is studied under different sampling frequencies, ini-

tial condition uncertainty, and magnitude of measurement noise standard deviations. It is shown that the UKF on TSE(3) proposed in this work is in general a highly robust filter, while it also considers noise in the velocity measurement data (in addition to the noise in the pose data only, which is what is assumed in other filters).

Furthermore, the estimated states obtained using the proposed UKF on TSE(3) are used along with two different control techniques on TSE(3): A Morse-Lyapunov-based feedback tracking control with backstepping (MLBS) and a sliding mode-based control (SMC) for navigation and control of the system with noisy measurements. Finally, the robustness of the proposed stochastic navigation and control system is verified for the OSIRIS-REx mission parameters, where the results obtained by MLBS and SMC control techniques are compared, and various filters are implemented and weighed against the proposed UKF. It is shown that the the proposed UKF on TSE(3) is capable of directing the spacecraft towards a desired orbit while maintaining the principal axis of the spacecraft along the nadir direction, despite the presence of exaggerated noisy measurements. It is also shown that the MLBS controller on TSE(3) results in higher accuracy and less control input than its analogue SMC on TSE(3). Note that the orbit-attitude in scenarios such as spacecraft motion around irregular celestial bodies coupling cannot be neglected due to the highly perturbed environment.

Future work may consider further details in the modeling of the navigation system. Further accuracy in the model of the measurement sensors may be obtained via extending their noise characteristics to introduce biases, scale-factor errors, or mounting alignment errors. Also, realistic dynamics of the actuators can be considered in the design of the control system. The robustness of the proposed navigation and control system can also be verified in problems such as orbit transfers, and spacecraft rendezvous, proximity operations, and docking. In addition, the stochastic estimation and control scheme presented here can be extended to the problem of multibody dynamics and multiagent systems.

7 Declarations

7.1 Funding

Support from Faculty Innovative Research in Science and Technology (FIRST) is gratefully acknowledged.

7.2 Conflicts of interest/Competing interests

The authors have no relevant financial or non-financial interests to disclose.

7.3 Availability of data and material

Not Applicable

7.4 Code availability

This project was coded in Matlab using Simulink, and may be made available upon request.

7.5 Ethics approval

Not Applicable

7.6 Consent to participate

Not Applicable

7.7 Consent for publication

Not Applicable

References

1. K. R. Pollock, "An analysis of orbital propagators for Low Earth Orbit Rendezvous," *Naval Postgraduate School, Monterey, CA., Provided by the SAO/NASA Astrophysics Data System*, vol. OMB, no. 0704-0188, 1994.
2. S. P. Shuster, "A Survey and Performance Analysis of Orbit Propagators for LEO, GEO, and Highly Elliptical Orbits," *Utah State University*, vol. OMB, no. 0704-0188, 2017.
3. V. Vittaldev, E. Mooij, and M. C. Naeije, "Unified state model theory and application in Astrodynamics," *Celestial Mechanics and Dynamical Astronomy*, vol. 112, no. 3, pp. 253–282, 2012, doi: 10.1007/s10569-011-9396-5.
4. E. J. Lefferts, F. L. Markley, and M. D. Shuster, "Kalman filtering for spacecraft attitude estimation," *Journal of Guidance, Control and Dynamics*, vol. 5, no. 5, 1982, doi:10.2514/3.56190.
5. J. R. Carpenter and C. N. D'Souza, "Navigation Filter Best Practices," *NASA Technical Reports*, 2018, WBS: 869021.03.04.01.03.
6. C. G. Mayhew, R. G. Sanfelice, and A. R. Teel, "On quaternion-based attitude control and the unwinding phenomenon," in *Proceedings of the 2011 American Control Conference*, pp. 299–304, 2011, doi: 10.1109/ACC.2011.5991127.
7. J. Yang and E. Stoll, "Adaptive sliding mode control for spacecraft proximity operations based on dual quaternions," *Journal of Guidance, Control, and Dynamics*, vol. 42, no. 11, pp. 2356–2368, 2019, doi: 10.2514/1.G004435.

8. J. L. Crassidis and F. L. Markley, "Unscented filtering for spacecraft attitude estimation," *Journal of Guidance, Control, and Dynamics*, vol. 26, no. 4, pp. 536–542, 2003, doi: 10.2514/2.5102.
9. J. L. Crassidis, F. L. Markley, and Y. Cheng, "Survey of nonlinear attitude estimation methods," *Journal of Guidance, Control, and Dynamics*, vol. 30, no. 1, pp. 12–28, 2007, doi: 10.2514/1.22452.
10. J. T.-Y. Wen and K. Kreutz-Delgado, "The attitude control problem," *IEEE Transactions of Automatic Control*, vol. 36, no. 10, pp. 1148–1162, 1991, doi: 10.1109/9.90228.
11. S. P. Bhat and D. S. Bernstein, "A topological obstruction to continuous global stabilization of rotational motion and the unwinding phenomenon," *Systems & Control Letters*, vol. 39, no. 1, pp. 63–70, 2000, doi: 10.1016/S0167-6911(99)00090-0.
12. J. Bohn and A. K. Sanyal, "Almost global finite-time stabilization of rigid body attitude dynamics using rotation matrices," *International Journal on Robust and Nonlinear Control*, vol. 25, no. 4, 2015, doi: 10.1002/rnc.3399.
13. L. Sy, N. H. Lovell, and S. J. Redmond, "Estimating lower limb kinematics using a Lie group constrained EKF and a reduced wearable IMU count," in *8th IEEE RAS/EMBS International Conference for Biomedical Robotics and Biomechatronics (BioRob)*, pp. 310–315, 2020, doi: 10.1109/BioRob49111.2020.9224342.
14. B. P. Malladi, S. Di Cairano, and A. Weiss, "Nonlinear model predictive control of coupled rotational-translational spacecraft relative motion," in *2019 American Control Conference (ACC)*, pp. 3581–3586, 2019, doi: 10.23919/ACC.2019.8814345.
15. N. Filipe and P. Tsiotras, "Rigid body motion tracking without linear and angular velocity feedback using dual quaternions," in *2013 European Control Conference (ECC)*, pp. 329–334, 2013, doi: 10.23919/ECC.2013.6669564.
16. F. L. Markley and J. L. Junkins, "Fundamentals of spacecraft attitude determination and control," *Springer*, 2014.
17. D. Lee and G. Vukovich, "Robust adaptive terminal sliding mode control on se(3) for autonomous spacecraft rendezvous and docking," *Nonlinear Dynamics*, vol. 83, pp. 2263–2279, 2016, doi: 10.1007/s11071-015-2479-1.
18. M. Nazari, M. Maadani, E. A. Butcher, and T. Yucelen, "Morse-Lyapunov-based control of rigid body motion on TSE(3) via backstepping," *2018 AIAA Guidance, Navigation, and Control Conference*, 2018, doi: 10.2514/6.2018-0602.
19. D. Seo and M. Nazari, "Rigid body adaptive stabilization on the tangent bundle of the Lie groups," *AIAA Scitech 2019 Forum*, 2019, doi: 10.2514/6.2019-0653.
20. E. A. Butcher, J. Wang, and T. A. Lovell, "On Kalman filtering and observability in nonlinear sequential relative orbit estimation," *Journal of Guidance, Control, and Dynamics*, vol. 40, no. 9, 2017, doi: 10.2514/1.G002702.
21. C. A. Woolsey, "Reduced Hamiltonian dynamics for a rigid body coupled to a moving point mass," *Journal of Guidance, Control, and Dynamics*, vol. 28, no. 1, 2005, doi: 10.2514/1.54099.
22. Q. Lam, N. Stamatakos, C. Woodruff, and S. Ashton, *Gyro Modeling and Estimation of Its Random Noise Sources*.
23. K. Nirmal, A. G. Sreejith, J. Mathew, M. Sarpotdar, A. Suresh, A. Prakash, M. Safonova, and J. Murthy, "Noise modeling and analysis of an IMU-based attitude sensor: Improvement of performance by filtering and sensor fusion," in *Advances in Optical and Mechanical Technologies for Telescopes and Instrumentation II* (R. Navarro and J. H. Burge, eds.), vol. 9912, pp. 2138–2147, International Society for Optics and Photonics, SPIE, 2016, doi: 10.1117/12.2234255.
24. D. Lee, A. K. Sanyal, and E. A. Butcher, "Asymptotic tracking control for spacecraft formation flying with decentralized collision avoidance," *Journal of Guidance, Control, and Dynamics*, vol. 38, no. 4, pp. 587–600, 2015, doi: 10.2514/1.G000101.
25. D. Lee and G. Vukovich, "Robust adaptive terminal sliding mode control on SE(3) for autonomous spacecraft rendezvous and docking," *Nonlinear Dynamics*, 2016, doi: 10.1007/s11071-015-2479-1.
26. D. Lee, A. K. Sanyal, E. A. Butcher, and D. J. Scheeres, "Finite-time control for spacecraft body-fixed hovering over an asteroid," *IEEE Transactions on Aerospace and Electronic Systems*, vol. 51, no. 1, pp. 506–520, 2015, doi: 10.1109/TAES.2014.140197.
27. A. Sjøberg and O. Egeland, "An EKF for Lie groups with application to crane load dynamics," *Modeling, Identification and Control: A Norwegian Research Bulletin*, vol. 40, pp. 109–124, 04 2019, doi: 10.4173/mic.2019.2.3.
28. S. Heo and C. G. Park, "Consistent EKF-based visual-inertial odometry on matrix Lie group," *IEEE Sensors Journal*, vol. 18, no. 9, pp. 3780–3788, 2018, doi: 10.1109/JSEN.2018.2808330.
29. G. Bourmaud, R. Megret, A. Giremus, and Y. Berthoumieu, "Discrete extended Kalman filter on Lie groups," *21st European Signal Processing Conference*, 2013.
30. G. Bourmaud, R. Megret, M. Arnauden, and A. Giremus, "Continuous-discrete extended Kalman filter on matrix Lie groups using concentrated Gaussian distributions," *Journal of Mathematical Imaging and Vision*, vol. 51, pp. 209–228, 2015, doi: 10.1007/s10851-014-0517-0.
31. M. Brossard, S. Bonnabel, and J. Condomines, "Unscented Kalman filtering on Lie groups," *IEEE/RSJ International Conference on Intelligent Robots and Systems (IROS)*, 2017, doi: 10.1109/IROS.2017.8206066.
32. M. Brossard, S. Bonnabel, and A. Barrau, "Unscented Kalman filter on Lie groups for visual inertial odometry," *"IEEE/RSJ International Conference on Intelligent Robots and Systems (IROS)*, 2018, doi: 10.1109/IROS.2018.8593627.
33. G. Loianno, M. Watterson, and V. Kumar, "Visual inertial odometry for quadrotors on $\mathsf{SE}(3)$," *IEEE International Conference on Robotics and Automation (ICRA)*, 2016, doi: 10.1109/ICRA.2016.7487292.
34. E. A. Wan and R. Van Der Merwe, "The unscented Kalman filter for nonlinear estimation," *Proceedings of the IEEE 2000 Adaptive Systems for Signal Processing, Communications, and Control Symposium*, 2000, doi: 10.1109/ASSPCC.2000.882463.
35. T. D. Barfoot and P. T. Furgale, "Associating uncertainty with three-dimensional poses for use in estimation problems," *IEEE Transactions on Robotics*, vol. 30, no. 3, pp. 679–693, 2014, doi: 10.1109/TRO.2014.2298059.
36. P.-A. Absil, R. Mahony, and R. Sepulchre, *Optimization Algorithms on Matrix Manifolds*. Princeton University Press, 2008, isbn: 978-0-691-13298-3.
37. M. Brossard, A. Barrau, and S. Bonnabel, "A code for unscented Kalman filtering on manifolds (UKF-M)," *International Conference on Robotics and Automation (ICRA)*, 2020, arXiv:2002.00878.
38. G. Misra and A. K. Sanyal, "Analysis of orbit-attitude coupling of spacecraft near small solar system bodies," *AIAA Guidance, Navigation, and Control Conference*.

39. M. Wittal, G. Mangiacapra, A. Appakonam, M. Nazari, and E. Capello *AAS/AIAA Astrodynamics Specialist Conference*, pp. AAS 20–690, 2020, doi: 10.13140/RG.2.2.21502.82240.
40. A. Muller and Z. Terze, "The significance of the configuration space Lie group for the constraint satisfaction in numerical time integration of multi body systems," *Mechanism and Machine Theory*, vol. 82, pp. 173–202, 2014, doi: 10.1016/j.mechmachtheory.2014.06.014.
41. T. Lee, H. McClamroch, and M. Leok, "Optimal attitude control for a rigid body with symmetry," *Proceedings of the American Control Conference*, 2007, doi: 10.1109/ACC.2007.4282362.
42. J. Sola, J. Deray, and D. Atchuthan, "A micro Lie theory for state estimation in robotics," *2018 arXiv preprint*, 2018, arXiv: 1812.01537.
43. J. Gallier, "Basics of classical Lie groups: The exponential map, Lie groups, and Lie algebras," *Texts in Applied Mathematics, Geometric Methods and Applications*, vol. 38, pp. 367–414, 2001, doi: 10.1007/978-1-4613-0137-0_14.
44. R. M. Murray, Z. Li, and S. S. Sastry, *A Mathematical Introduction to Robotic Manipulation*. CRC Press, 1994.
45. M. Nazari, E. A. Butcher, T. Yucelen, and A. Sanyal, "Decentralized consensus control of a rigid-body spacecraft formation with communication delay," *Journal of Guidance, Control, and Dynamics*, 2016, doi: 10.2514/1.G001396.
46. H. Hajri, S. Said, and Y. Berthoumieu, "Maximum likelihood estimators on manifolds," in *Geometric Science of Information*, pp. 692–700, 2017, doi: 10.1007/978-3-319-68445-1_80.
47. P. T. Fletcher, S. Joshi, C. Lu, and S. Pizer, "Gaussian distributions on Lie groups and their application to statistical shape analysis," in *Information Processing in Medical Imaging*, pp. 450–462, 2003, doi: 10.1007/978-3-540-45087-0_38.
48. L. Falorsi, P. de Haan, T. R. Davidson, and P. Forré, "Reparameterizing distributions on Lie groups," in *Proceedings of the Twenty-Second International Conference on Artificial Intelligence and Statistics* (K. Chaudhuri and M. Sugiyama, ed.), vol. 89 of *Proceedings of Machine Learning Research*, pp. 3244–3253, 2019.
49. M. Vandyke, J. Schwartz, and C. Hall, "Unscented Kalman Filtering for spacecraft attitude state and parameter estimation," *Advances in the Astronautical Sciences*, vol. 119, 01 2004.
50. L. Perea, J. How, L. Breger, and P. Elosegui, *Nonlinearity in Sensor Fusion: Divergence Issues in EKF, Modified Truncated GSF, and UKF*.
51. M. Mohammed, H. Boussadia, A. Bellar, and A. Adnane, "Performance comparison of attitude determination, attitude estimation, and nonlinear observers algorithms," *Journal of Physics: Conference Series*, vol. 783, p. 012017, 01 2017, doi: 10.1088/1742-6596/783/1/012017.
52. K. K. Tønne, "Stability Analysis of EKF-Based Attitude Determination and Control," 2007.
53. E. Samiei, M. Nazari, E. A. Butcher, and A. K. Sanyal, "Robust stochastic stabilization of attitude motion," *International Journal of Dynamics and Control*, vol. 7, pp. 619–635, 2019, doi: 10.1007/s40435-018-0456-5.
54. K. Ghasemi, J. Ghaisari, and F. Abdollahi, "Robust formation control of multiagent systems on the Lie group SE(3)," *International Journal of Robust and Nonlinear Control*, vol. 30, pp. 1–33, 2019, doi: 10.1002/rnc.4806.
55. A. Chalanga, S. Kamal, L. M. Fridman, B. Bandyopadhyay, and J. A. Moreno, "Implementation of Super-Twisting Control: Super-Twisting and Higher Order Sliding-Mode Observer-Based Approaches," *IEEE Transactions on Industrial Electronics*, vol. 63, no. 6, pp. 3677–3685, 2016, doi: 10.1109/TIE.2016.2523913.
56. İ. Eker, "Sliding mode control with PID sliding surface and experimental application to an electromechanical plant," *ISA Transactions*, vol. 45, no. 1, pp. 109–118, 2006, doi: 10.1016/S0019-0578(07)60070-6.
57. T. Lee, M. Leok, and N. H. McClamroch, "Lie group variational integrators for the full body problem," *Computational Methods in Applied Mechanics and Engineering*, vol. 196, no. 8, 2005, doi: 10.1016/j.cma.2007.01.017.
58. C. Kane, J. Marsden, and M. Ortiz, "Symplectic-energy-momentum preserving variational integrators," *Journal of Mathematical Physics*, vol. 40, pp. 3353–3371, 1999, doi: 10.1063/1.532892.
59. D. J. Scheeres, *Orbital Motion in Strongly Perturbed Environments*. Springer, Berlin-Heidelberg, 2012.
60. W. M. Kaula, *Theory of Satellite Geodesy*. Blaisdell, Bosto, ISBN-13: 978-0486414652, ISBN-10: 0486414655, 1966.
61. D. J. Scheeres, S. J. Ostro, R. S. Hudson, E. M. DeJong, and S. Suzuki, "Dynamics of orbits close to asteroid 4179 Toutatis," *Icarus*, vol. 132, no. 1, pp. 53–79, 1998, doi: 10.1006/icar.1997.5870.
62. M. Nazari, R. Wauson, T. Critz, E. A. Butcher, and D. J. Scheeres, "Observer-based body-frame hovering control over a tumbling asteroid," *Acta Astronautica*, vol. 102, pp. 124–139, 2014, doi: 10.1016/j.actaastro.2014.05.016.
63. G. Misra, A. Sanyal, and D. J. Scheeres, "Coupled orbit-attitude dynamics and relative state estimation of spacecraft near small solar system bodies," *Advances in Space Research*, vol. 57, no. 8, pp. 1747–1761, 2015, doi: 10.1016/j.asr.2015.05.023.
64. E. B. Bierhaus *et al.*, "The OSIRIS-REx spacecraft and the touch-and-go sample acquisition mechanism (TAGSAM)," *Space Science Reviews*, vol. 214, no. 107, 2018, doi: 10.1007/s11214-018-0521-6.
65. E. Beshore *et al.*, "The OSIRIS-REx asteroid sample return mission," *IEEE Aerospace Conference Proceedings*, 2015, doi: 10.1109/AERO.2015.7118989.
66. P. Blau, *Spaceflight101.com*, 2020 (accessed January 12, 2021). `https://spaceflight101.com/osiris-rex/osiris-rex-spacecraft-overview/`.
67. L. M. Dani Hauf, *OSIRIS-REx, Discovering the Origins of the Solar System*, 2020 (accessed January 12, 2021). `https://www.lockheedmartin.com/en-us/products/osiris-rex.html`.
68. R. G. Melton, "Fundamentals of astrodynamics and applications," *Journal of Guidance, Control, and Dynamics*, vol. 21, no. 4, pp. 672–672, 1998, doi: 10.2514/2.4291.
69. B. Wie, *Space Vehicle Dynamics and Control*. American Institute of Aeronautics and Astronautics, 2 ed., 2008, isbn: 978-1-56347-953-3.
70. J. Havlík and O. Straka, "Performance evaluation of iterated extended Kalman filter with variable step-length," *Journal of Physics: Conference Series*, vol. 659, pp. 12–22, 2015, doi: 10.1088/1742-6596/659/1/012022.
71. I. Miletović, D. M. Pool, O. Stroosma, M. M. V. Paassen, and Q. Chu, "Improved Stewart platform state estimation using inertial and actuator position measurements," *Control Engineering Practice*, vol. 62, pp. 102–115, 2017, doi: 10.1016/j.conengprac.2017.03.006.

72. J. B. Moor and B. D. O. Anderson, *Optimal Filtering*. Prentice Hall Information and System Sciences Series, 1979.
73. F. L. Markley and J. L. Crassidis, *Correction to: Fundamentals of Spacecraft Attitude Determination and Control*. New York: Springer, 2014, isbn: 978-1-4939-0802-8.
74. K. W. Lee and S. N. Singh, "Adaptive and super-twisting adaptive spacecraft orbit control around asteroids," *Journal of Aerospace Engineering*, vol. 32, no. 4, p. 04019042, 2019, doi: 10.1061/(ASCE)AS.1943-5525.0001043.

Rebuttal
Click here to access/download;attachment to manuscript;MaWiCaNa21NoDy_submission_Rebuttal.pdf
Click here to view linked References

Rebuttal: Unscented Kalman Filter and Control on TSE(3) with Application to Spacecraft Dynamics

The authors would like to thank the reviewers for their very important feedback that helped improve the quality of the manuscript. The paper has been modified and updated according to the reviewers' comments and a point-by-point reply to these comments is included below. All other changes from the initial submission are indicated in red in the revised version of the manuscript. All of the equation numbers, figure numbers, and table numbers are based on the *revised* version. Note that if a figure, a table, or its caption is updated, only the caption is indicated in red.

Reviewer 2

A rigid-body spacecraft navigation and control architecture within the framework TSE(3) while considering stochastic processes in the system. This paper combines the ideas from several paper and have implemented to spacecraft dynamics. I appreciate the author's effort to bring all the ideas in a meticulous way for addressing the tracking problem of spacecraft near the asteroid Bennu. However, the same idea has been published as a conference paper titled "Stochastic Spacecraft Navigation And Control in Lie Group Se(3) Around Small Irregular Bodies" in AAS 20. I am not able to find any valuable research addition when compared to the conference paper. Hence, the article can be considered for publication as a good application oriented contribution with additional novel research addition.

The authors have improved the contribution of this manuscript, and have provided clarifications on how this manuscript is distinct from the conference paper by the authors. The contribution of this manuscript as compared to the author's conference paper in Ref. [39] follows:

a) A new subsection (Section 5.1) has already been included in the numerical simulations section in this manuscript to verify the performance of the proposed filter via providing a detailed comparison among the unscented Kalman filter (UKF) on tangent bundle of special Euclidean space $\mathsf{TSE}(3)$ proposed in this work and three other filters (extended Kalman filter on special Eulidean space $\mathsf{SE}(3)$ in Ref. [28], UKF on $\mathsf{SE}(3)$ in Ref. [31], and discrete EKF on $\mathsf{SE}(3)$ in Ref. [29]). According to the results provided in Fig. 2 of the manuscript and the discussion in that section, the controller on $\mathsf{TSE}(3)$ using a UKF proposed in this work is, in general, a highly robust filter. It also considers noise in the velocity measurement data (in addition to the noise in the pose data, which is what only what is assumed in other filters).

   Furthermore, and in order to improve the visibility, Fig. 2 has been expanded to span both columns, and the font size has been adjusted accordingly. For the convenience of the reviewer, that figure is also provided in this rebuttal.

b) A new section (Section 3.3.2) has been added in the revised version of the manuscript to study sliding mode control (SMC) on $\mathsf{TSE}(3)$, and to provide a tool for validating the Morse-Lyapunov backstepping (MLBS) control in $\mathsf{TSE}(3)$ used in this manuscript. For the reviewer's convenience, the contents of that new section are also provided below:

   "In this section, an SMC is designed on $\mathsf{TSE}(3)$ to address some tracking control problem as in Section 3.3.1. In the SMC approach, a so-called sliding surface σ is defined, which is a subset of the state space on which the trajectory of the rigid body is desired to lie. A feedback law is realized such

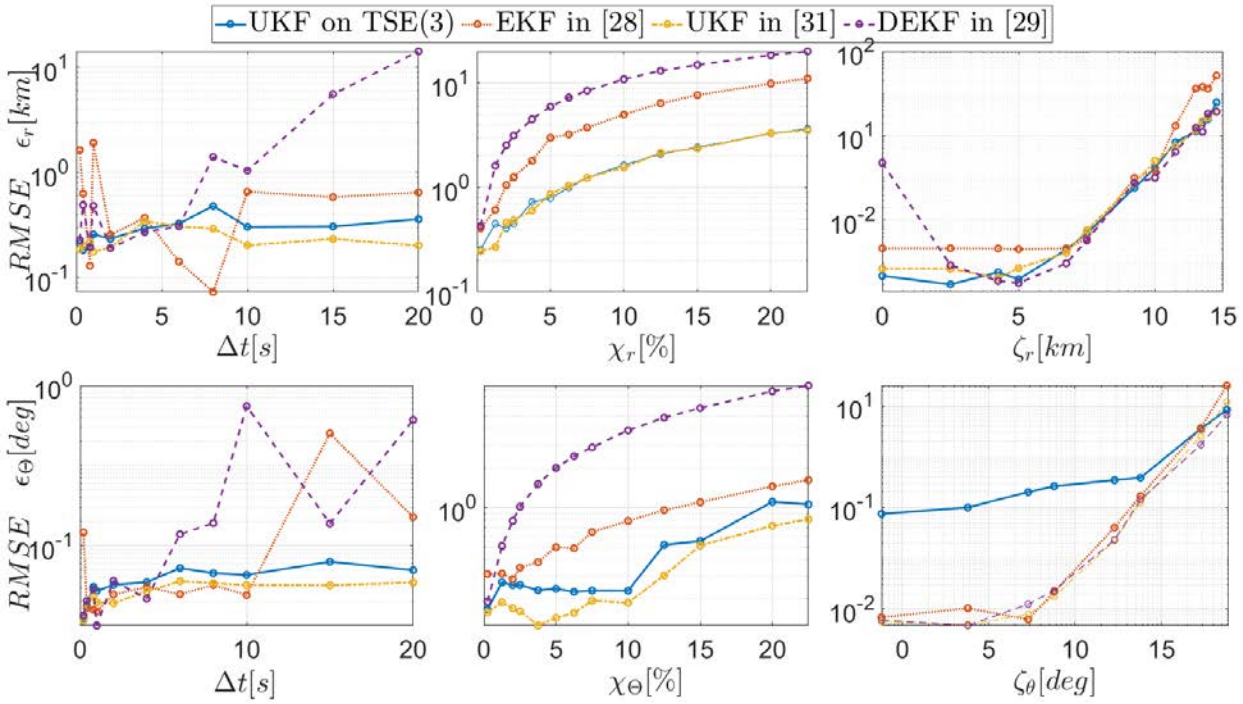

Figure 2: Attitude and position RMSE as a function of sample period, initial condition inaccuracies and measurement noise standard deviations.

that this surface will be attractive and invariant, i.e. the rigid body trajectory evolves towards this surface and, once there, it stays close to it. The sliding surface σ is defined as a function of pose and velocity, i.e.

$$\sigma = c_1\, \delta\mathbb{V}_{\text{track}} + c_2\, l(\delta g_{\text{track}}) + c_3\, \lambda \;\in \mathbb{R}^6 \tag{46}$$

where $c_1 = \text{blkdiag}(c_{11}I_3, c_{12}I_3)$, $c_2 = \text{blkdiag}(c_{21}I_3,\ c_{22}I_3)$, $c_3 = \text{blkdiag}(c_{31}I_3, c_{32}I_3)$ are positive definite diagonal matrices, $l(\cdot)$ is defined Eq. (41) $\lambda = \int_0^t \psi(\delta g_{\text{track}},\ \delta\mathbb{V}_{\text{track}})d\tau$, and $\psi(\cdot,\cdot)$ is defined in Eq. (40). The third integral term is added since it meaningfully reduces the steady state error. The addition of an integral action to define the sliding surface has been shown to lead to good results in literature [54-56]. The SMC control force and moment inputs are defined as

$$u_c = u_{eq} + u_d \tag{47a}$$

with

$$u_{eq} = -\text{ad}^*_{\delta\mathbb{V}_{\text{track}}}\mathbb{I}\delta\mathbb{V}_{\text{track}} - \mathbb{I}c_1^{-1}c_2\, \dot{l}(\delta g_{\text{track}}) - \mathbb{I}c_1^{-1}c_3\, \psi(\delta g_{\text{track}}, \delta\mathbb{V}_{\text{track}}) - u_e \tag{47b}$$

and

$$u_d = -K_\sigma \text{sgn}(\sigma) \tag{47c}$$

where $\text{sgn}(\cdot)$ denotes the vector sign function and $K_\sigma = \mathbb{I}c_1^{-1}c_4 = \text{blkdiag}(K_{\sigma,M}I_3, K_{\sigma,F}I_3)$ is a positive definite diagonal matrix which must be properly selected in order to have the sliding mode operate correctly while considering unmodeled dynamics. The first part (i.e. u_{eq}) is known as equivalent control and it represents the control function which needs to be applied to the system after reaching the sliding surface to ensure that the system trajectory thereafter stays on this surface. This feature is known as the invariant property and the control input guarantees the solution of the problem $\dot{\sigma} = 0$. The second part (i.e. u_d) is known as discontinuous control and it ensures that the system trajectory evolves towards the sliding surface. This feature is known as the attractive property and the switching control action allows the system trajectory to reach the surface. In order to achieve the asymptotic convergence of $l(\cdot)$ and $\psi(\cdot,\cdot)$ to zero (i.e. $\lim_{t\to\infty} l(\cdot) = 0$ and $\lim_{t\to\infty}\ \psi(\cdot,\cdot) = 0$) with a desired

convergence rate and in the presence of bounded disturbance, the control input in Eq. (47) must drive the variable σ in Eq. (46) to zero within a finite time. This feature can be guaranteed to hold by applying the Lyapunov stability theory. The Lyapunov candidate function is selected as

$$\mathcal{V} = \frac{1}{2}\sigma^T\sigma \tag{48}$$

Taking the time derivative of the Lyapunov function above gives

$$\dot{\mathcal{V}} = \dot{\sigma}^T\sigma \tag{49}$$

Substituting Eq. (46) and its time derivative in Eq. (49), using the tracking-problem version of Eq. (10) (i.e. replacing g and $\mathbb{V}$ in that equation with δg_{track} and $\delta\mathbb{V}_{\text{track}}$, respectively), and simplification yields

$$\dot{\mathcal{V}} = -c_4\,\text{sgn}^T(\sigma)\,\sigma = -c_4\,\|\sigma\|_1 \tag{50}$$

Since $\dot{\mathcal{V}} < 0$ for $\sigma \neq 0$, the stability of the equilibria is proved. In Eq. (47a), $\|\cdot\|_1$ denotes the $1-$norm of the sliding surface, i.e. $\|\sigma\|_1 = \sum_1^6 |\sigma_i|$. Note that this proof only guarantees the local stability of the equilibrium $(\delta g_{\text{track}}, \delta\mathbb{V}_{\text{track}}) = (I_4, 0)$ since, other than at equilibrium above, σ can also be zero for some linear combination of $\delta\mathbb{V}_{\text{track}}$, $l(\cdot)$, and λ in Eq. (46)."

"Although, in contrast to the MLBS control, the SMC does not guarantee global asymptotic stability, it is independent of the knowledge of the mathematical model of the rigid body. However, the discontinuous nature of the control law might lead to a phenomenon called chattering, where high-frequency oscillations occur around the sliding surface. This phenomenon is undesirable in practical situations since it can cause high control activity and may excite high-frequency dynamics neglected in the model. One way to attenuate the chattering is to replace the discontinuous sgn$(\cdot)$ function in Eq. (47c) with an approximate smooth function such as a hyperbolic tangent function of the form $\tanh(b\,\sigma)$ or a sigmoid function of the form $\sigma/(\|\sigma\| + b)$ with the scalar b selected properly."

Also, in order to support the discussion above, the following references have been added to the reference list in the revised version of the manuscript:

[54] K. Ghasemi, J. Ghaisari, and F. Abdollahi, "Robust formation control of multiagent systems on the Lie group SE(3)," International Journal of Robust and Nonlinear Control, vol. 30, pp. 1–33, 2019, doi: 10.1002/rnc.4806.

[55] A. Chalanga, S. Kamal, L. M. Fridman, B. Bandyopadhyay, and J. A. Moreno, "Implementation of Super-Twisting Control: Super-Twisting and Higher Order Sliding-Mode Observer-Based Approaches," IEEE Transactions on Industrial Electronics, vol. 63, no. 6, pp. 3677–3685, 2016, doi: 10.1109/TIE.2016.2523913.

[56] İ. Eker, "Sliding mode control with PID sliding surface and experimental application to an electromechanical plant," ISA Transactions, vol. 45, no. 1, pp. 109–118, 2006, doi: 10.1016/S0019-0578(07)60070-6.

Furthermore, a new discussion has been added in the numerical simulation section. Figure 6, included below for the convenience of the reviewer, has also been updated to include the results obtained using the SMC on $\mathsf{TSE}(3)$ and to provide a comparison between the two controllers (MLBS on $\mathsf{TSE}(3)$ and SMC on $\mathsf{TSE}(3)$) in terms of the normalized errors and control accelerations.

c) Revisions have been made throughout the entire manuscript, in terms of the discussions and notations used, to provide a clear understanding of the problem and to provide clear mathematical formulation conforming to standardized notation in the field, such as that used in [29, 32]. This includes the changes performed in Section 2 and 3 for further clarity.

d) Discussions of the contributions above have been added in the Abstract, the last paragraph of the Introduction (Section 1), and in different locations in the Conclusions (Section 6). For the convenience of the reviewer, those discussions are also provided in this rebuttal below:

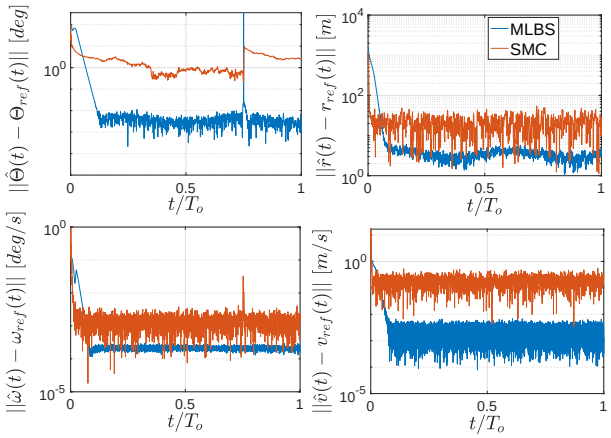

Figure 6: Norm of the difference between the estimated states and reference states, for MLBS and SMC control systems. The spike near 0.75 is due to a singularity.

i) in the Abstract:

"The navigation system is then integrated and evaluated with two different control techniques on $\mathsf{TSE}(3)$: An almost globally asymptotically stabilizing Morse-Lyapunov-based control system with backstepping and a robust sliding mode-based control system. Also, the performance of the UKF in $\mathsf{TSE}(3)$ proposed here is compared with similar filters in the literature to demonstrate the robustness and accuracy of the proposed filter in a realistic setting."

ii) in the last paragraph of the Introduction (Section 1):

"... by advancing the unscented transform (UT) based UKF introduced in [34] using retraction to address the fact that the system states are on $\mathsf{TSE}(3)$."

"The performance of the proposed filter is compared in terms of robustness and accuracy with three other Kalman filters on $\mathsf{SE}(3)$ in the literature. Furthermore, the regulation controller in [18] is extended to the case of tracking problem to design an almost globally asymptotically stable Morse-Lyapunov backstepping (MLBS) tracking control on $\mathsf{TSE}(3)$. In addition, a tracking sliding mode control (SMC) is designed on $\mathsf{TSE}(3)$ to verify the results of the MLBS tracking control."

"Note that the extensive contribution and revisions made in this paper as compared to the authors' previous work [39] including, but certainly not limited to, the tracking SMC and comparison of the filters provided here, makes this work distinct from the previous work."

iii) and in different locations in the Conclusions (Section 6):

"It is shown that the UKF on $\mathsf{TSE}(3)$ proposed in this work is in general a highly robust filter, while it also considers noise in the velocity measurement data (in addition to the noise in the pose data only, which is what is assumed in other filters)."

"Furthermore, the estimated states obtained using the proposed UKF on $\mathsf{TSE}(3)$ are used along with two different control techniques on $\mathsf{TSE}(3)$: A Morse-Lyapunov-based feedback tracking control with backstepping (MLBS) and a sliding mode-based control (SMC) for ..."

"... where the results obtained by MLBS and SMC control techniques are compared, and various filters are implemented and weighed against the proposed UKF. It is shown that the the proposed UKF on $\mathsf{TSE}(3)$ is capable of ..."

"... despite the presence of exaggerated noisy measurements. It is also shown that the MLBS controller on $\mathsf{TSE}(3)$ results in higher accuracy and less control input than its analogue SMC on $\mathsf{TSE}(3)$. Note that ..."

The authors believe that the contributions and revisions made in this manuscript including, but not limited to, SMC, comparison of filters, and revisions made to provide clear discussions and mathematical formulation, as mentioned above, make this work distinct from the authors' previous work.

Reviewer 3

The authors treat a control problem with noise for a space navigation and apply sophisticated methods to construct a reliable control regime. Unfortunately I cannot recommend the publication in its current state, due to the following reasons: For convenience of the reviewer, and in order to ensure all the reviewer's comments are addressed, the authors have split the reviewer's comments into different parts and provided a response for each part, as follows.

1. The explanation of the applied method, especially of the UKF for the nonlinear problem is quite hard to read: It contains fragments of Lie group theory, which are certainly well known to people working in that field, but might be hard to understand for others. It might improve the article, if the underlying mathematics would be elaborated more clearly.

   Revisions have been carried out throughout the entire manuscript to make the content easier to understand for the reader. In particular, the following changes have been made to address this comment:

   a) In order to address the reviewer's concern regarding the comprehensibility of Lie group theory, the following changes have been made in the revised version of the manuscript:

      i) Section 2 has been revised such that Lie group theory is discussed separately from the stochastic processes on Lie groups for the benefit of novices in the field. The first paragraph of Section 2.1 and the paragraph below Eq. (10) now contain clearer explanations of the definition of special Euclidean group $\mathsf{SE}(3)$, the states, and the control input:

      The first paragraph of Section 2.1: "The pose (configuration) of a rigid body, also known as the Denavit-Hartenberg representation within the robotics community ... i.e. $\mathsf{SE}(3) = \mathbb{R}^3 \ltimes \mathsf{SO}(3)$, $R \in \mathsf{SO}(3)$ is the rotation matrix from the body frame to the inertial frame such that $\det(R) = 1$ and $R^T R = I_3$ (I_3 is the 3×3 identity matrix), and ... The tangent space at the identity element of the group, i.e. $g = I_4$ (when $R = I_3$ and $r = [0, 0, 0]^T$), ..."

      The paragraph below Eq. (10): "$\mathbb{V} = [\omega^T, v^T]^T \in \mathbb{R}^6$ is the augmented velocity vector comprised of the angular velocity vector $\omega \in \mathbb{R}^3$ of the body and the translational velocity $v \in \mathbb{R}^3$ of the center of mass with respect to the inertial frame, expressed in the body frame. In Eq. (10), $u = u_e + u_c \in \mathbb{R}^6$ is the input, $u_e \in \mathbb{R}^6$ denotes the total external inputs (consisting of the external moments and external forces) and $u_c \in \mathbb{R}^6$ is the control input produced by the control system (consisting of the control moment and control force). Also, in Eq. (10), the inertia tensor is given as ..."

      Also, notations used in the wedge map in Eqs. (2) and (3) and the text describing them has been changed to be distinct from terms used elsewhere in the manuscript. The rigid body configuration on $\mathsf{SE}(3)$ following its definition in Eq. (10) has been reworded for further clarity. Some of the notations used in Section 3.1 have been edited to be consistent with those used in Section 3.2 and throughout the manuscript.

      ii) Changes have been made in Sections 3.1 and 3.2 including some of the notation used in the equations in those sections. Specifically, the noise contribution on $\mathsf{SE}(3)$ has been consistently shown as a post-multiplication operation, and noisy measurements are denoted with a hat throughout the revised version of the manuscript. The dimensions of noise vectors η and ζ have been clarified and made consistent with the covariance and sigma points throughout Section 3.

   b) In order to address the reviewer's comment about formulation legibility and clarity, the following changes have been made to the manuscript:

      i) The UKF formulation has likewise been simplified. The notation $x[k|k-1]$ has been changed to $x_{k|k-1}$, starting from the second paragraph of Section 3.2 and continuing to the end of Section 3.2.3, in order for it to be consistent with some of the notations used in the literature such as those in Refs. [29, 32]. All of the updated subscripts in that section are shown in red in the revised version of the manuscript.

      ii) The explicit time dependence for the sigma points in the revised version of the manuscript has been suppressed as it was deemed to be unnecessary. Note that although they are computed

at each time step, they are computed independently of one another and in no case does the sigma points of one time step depend on the sigma points of another. Thus, explicit notation such as $\chi_{p,0}[k]$ has been changed to simply $\chi_{p,0}$ and the assembled sigma points vectors $\chi_p[k]$ and $\chi_q[k]$ are now expressed as χ_p and χ_q, respectively (Section 3.2.2); see, for instance, Eq. (27) of the revised manuscript as compared to Eq. (37) of the previous version of the paper. All the changes have been shown in red in that section and subscripts have been revised.

iii) Eqs. (28), (31), (32), and (35) in Section 3.2.2 have been updated to include a summation to correctly reflect the operation being performed and to ensure consistent dimensionality.

$$P^{(1)}_{k+1|k} = \sum_{i=0}^{4p} W^{(c)}_{p,i}(\chi^r_p - \overline{\chi}^r_p)(\chi^r_p - \overline{\chi}^r_p)^T \tag{28}$$

$$P^{(2)}_{k+1|k} = \sum_{i=1}^{4q} W^{(c)}_{q,i}(\chi^r_q - \overline{\chi}^r_q)(\chi^r_q - \overline{\chi}^r_q)^T \tag{31}$$

$$P_{k+1|k} = P^{(1)}_{k+1|k} + P^{(2)}_{k+1|k} \tag{32}$$

$$\begin{aligned} P_{zz,k+1} &= \sum_{i=1}^{4p} W^{(c)}_{p,i}(z_{k+1} - \overline{z}_{k+1})(z_{k+1} - \overline{z}_{k+1})^T + T \\ P_{xz,k+1} &= \sum_{i=1}^{4q} W^{(c)}_{p,i}\chi_u(z_{k+1} - \overline{z}_{k+1})^T \end{aligned} \tag{35}$$

2. It should be made clear, in which spaces (in the algebra or in the group or in some larger tangent space) the different objects (noise input, observer noise, ...) live.

   All variables have been defined in terms of their dimensions and in which space they reside. Specifically, spaces have been defined in Eqs. (3), (9), (12-14), (16), (18), and (21), and throughout the text in Sections 3.1 and 3.2. Dimensions of many terms within the filter and sigma points section have likewise been revised or updated for clarity and consistency. This includes the clarifications about the dimensions of the sigma points, the fully assembled sigma point vector χ_q and χ_p, and the compiled weight matrices $W^{(m)}_p, W^{(c)}_p, W^{(m)}_q$, and $W^{(c)}_q$. Careful attention has been made to use consistent notation and dimensionality throughout the entire manuscript.

3. If there is a Gaussian distribution in the algebra, what is the corresponding distribution in the group? The maximum likelihood estimate for the group elements will not be the exponentials for the estimates in the algebra.

   A Gaussian distribution in the Lie algebra is mapped, through the wedge map, to the Lie group, and then through the exponential mapping to the Lie algebra. A generalized approach to determining the maximum likelihood estimates on manifolds was discussed in detail in Ref. [46], and specific approaches to Lie groups and the exponential-logarithm mapping of Gaussian distributions were explored in Refs. [47] and [48] demonstrated that any arbitrary Lie Group may have its distribution reparameterized to be optimized using standard stochastic gradient methods. This work does not explicitly discuss or use the maximum likelihood estimation (MLE), and thus the relationship between the MLE of group elements vs. that of the algebra is not explicitly defined. To address this, the following discussion has been added at the end of the second paragraph of Section 3.1 of the revised version of the manuscript:

   "... $Q_g \in \mathbb{R}^{p\times p}$. Note that the exponential mapping of η_g onto the estimated pose $\hat{g}$ is multiplicative, as shown in Eq. (14). Also note that calculation of the maximum likelihood estimate (MLE) should be performed within the Euclidean space in which the noise is defined, not in the Lie group or Lie algebra. The calculation of MLE is outside the scope of this paper, and thus the relationships among the MLE of group elements versus those of the algebra are not discussed here. For a generalized approach to determine the maximum likelihood estimates on manifolds, the reader is referred to [46]. Also, specific

approaches to Lie groups and the exponential-logarithm mappings of Gaussian distributions can be found in [47] and [48]."

Also, in order to support the discussion above, the following references have been added to the reference list in the revised version of the manuscript:

[46] H. Hajri, S. Said, and Y. Berthoumieu, "Maximum likelihood estimators on manifolds," in Geometric Science of Information, pp. 692–700, 2017, doi: 10.1007/978-3-319-68445-1_80.

[47] P. T. Fletcher, S. Joshi, C. Lu, and S. Pizer, "Gaussian distributions on Lie groups and their application to statistical shape analysis," in Information Processing in Medical Imaging, pp. 450–462, 2003, doi: 10.1007/978-3-540-45087-0_38.

[48] L. Falorsi, P. de Haan, T. R. Davidson, and P. Forré, "Reparameterizing distributions on Lie groups," in Proceedings of the Twenty-Second International Conference on Artificial Intelligence and Statistics (K. Chaudhuri and M. Sugiyama, ed.), vol. 89 of Proceedings of Machine Learning Research, pp. 3244–3253, 2019.

4. There exists also a proceedings contribution by quite the same authors on a very similar problem, which contains a lot of identical explanations and derivations. The authors must make clear how their new article differs from the other one, which scientific results are new. And they should avoid any self-plagiarism.

   The authors would like to refer the reviewer to the response provided to the comment of Reviewer 2, where the details of the contribution of this work as compared to the authors' conference paper in Ref. [39] are provided.

5. The article should also be carefully cross-read by a native speaker, it contains quite a lot of grammatical mistakes and typos.

   The manuscript has been thoroughly and carefully revisited by the authors, including a native English speaker, to improve the flow, grammar, and overall readability. All changes, both technical and grammatical, are shown in red within the revised version of the manuscript.

6. Also the tiny figures are sometimes hard to understand.

   To improve clarity and legibility of the figures, the following changes have been made in the revised manuscript: Figure 2 has been expanded to span both columns, and the font size has been adjusted accordingly. Also, the figure panels in Figs. 3 and 4 have been enlarged by adjusting those two figures from a 2×3 configuration to a 3×2 configuration, and font sizes have been adjusted for further clarity. Furthermore, Fig. 5 has been rearranged from a horizontal configuration to a vertical configuration with lines indicating the magnified portion for clarity. Finally, the figure panels in Fig. 7 have been enlarged by rearranging that figure from a 4×3 configuration to a 6×2 configuration. The revised versions of the figures above are also provided below (in this rebuttal) for the reviewer's convenience.

Additional actions taken by the authors for further clarity of the manuscript: In addition to the changes mentioned above, and for the sake of clarity and generality, the following changes have been made in the revised version of the manuscript:

i) The term "spacecraft" has been changed to "rigid body" in all parts of the revised manuscript except in Sections 4 and 5.

ii) Discussion and formulation associated with dynamics of spacecraft hovering near small bodies have been moved from Section 2.3 in the previous version to Section 4 of the revised version of the manuscript, as a case study, in order to make it clear that the formalism provided in this manuscript is generic and can be implemented in different applications.

iii) Reference [44] in the previous version of the manuscript has been removed from the revised version since the discussion related to that reference was not required in this paper. However, as mentioned before, Refs. [6, 46-48, 54-56] have been added to the reference list in the revised version of the manuscript to support the additional discussions (also see Part (b) of the authors' response to the comment of Reviewer 2 and the authors' response to Comment 3 of Reviewer 3).

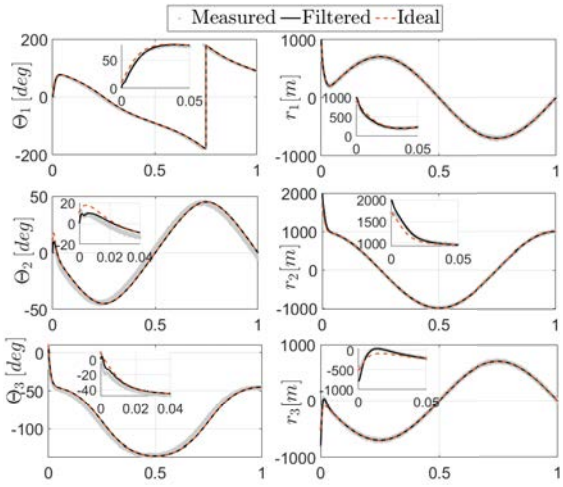

Figure 3: Measured (grey), estimated (black), and ideal (red) states.

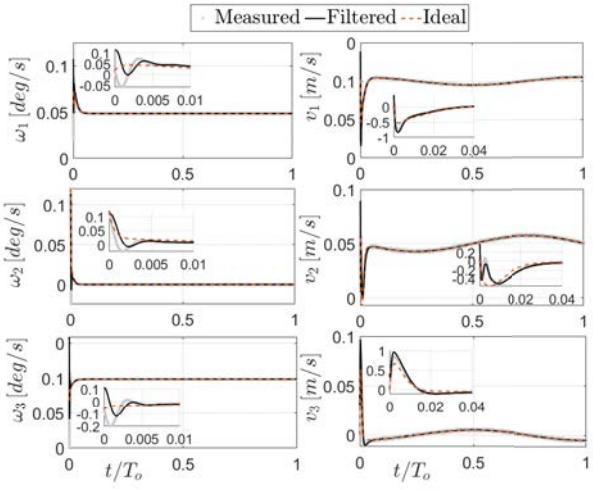

Figure 4: Measured (grey), estimated (black), and ideal (red) states.

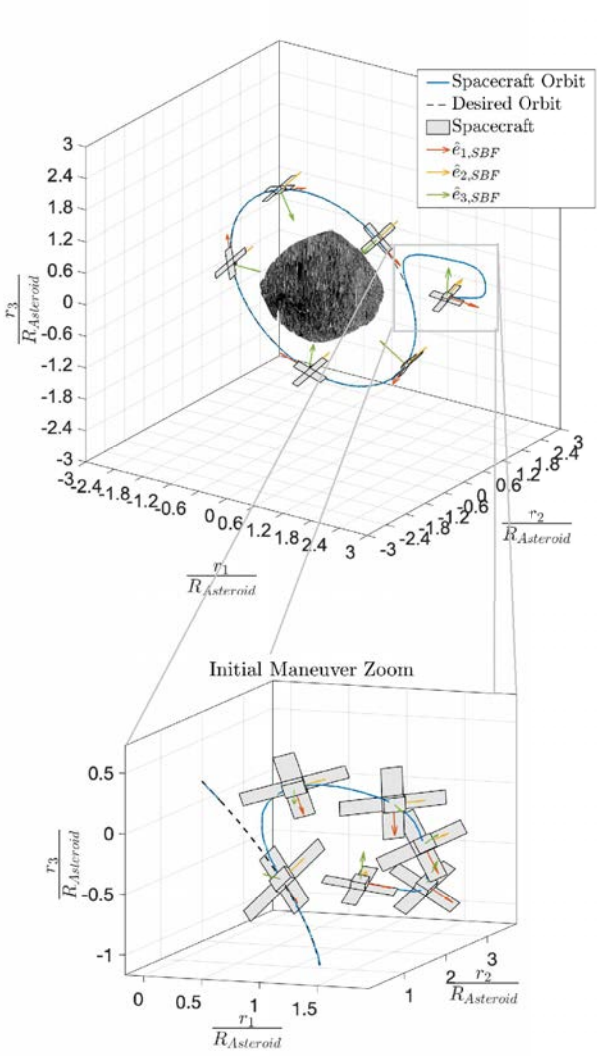

Figure 5: SBF orientation, and spacecraft attitude and trajectory around Bennu in BCI frame obtained via the implementation of the navigation and control systems.

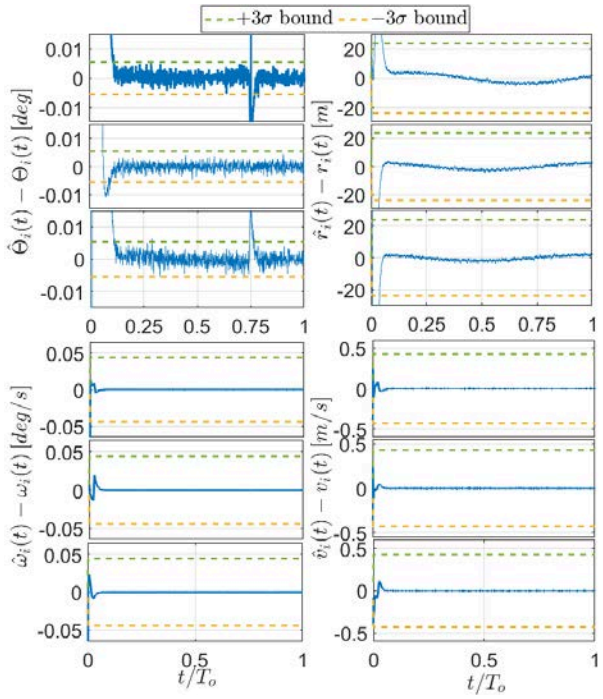

Figure 7: State estimation error components between the estimated states and the ideal noise-free states.

Original Manuscript of "Unscented Kalman Filter and Control in TSE(3) with Applications to Spacecraft Dynamics"
Click here to view linked References
Click here to access/download;attachment to manuscript;MaWiCaNa21NoDy_submission.pdf

Noname manuscript No.
(will be inserted by the editor)

Unscented Kalman Filter and Control on TSE(3) with Application to Spacecraft Dynamics

Gennaro Mangiacapra · Matthew M. Wittal · Elisa Capello · Morad Nazari

Abstract This paper presents a novel rigid-body spacecraft navigation and control architecture within the framework of special Euclidean group SE(3) and its tangent bundle TSE(3) while considering stochastic processes in the system. The proposed framework combines the orbit-attitude motions of the spacecraft into a single, compact set. The stochastic state filter is designed based on the unscented Kalman filter which uses a special retraction function to encode the sigma points onto the manifold. The navigation system is then integrated to an almost globally asymptotically stabilizing Morse-Lyapunov-based control system with backstepping. Numerical simulations are conducted to demonstrate the effectiveness of the proposed navigation filter for the full state estimation. In addition, the navigation and control system is tested in the nonlinear gravity field of a small celestial body with an irregular shape. In particular, the performance of the closed-loop system is studied in a tracking problem of spacecraft motion near the asteroid Bennu based on the OSIRIS-REx's mission data.

G. Mangiacapra
Politecnico di Torino, Torino 10129, Italy & Navigation System Engineer, Northrop Grumman Italia, Pomezia (RM), 00040, Italy; Email: gennaro.mangiacapra@outlook.it

M.M. Wittal
Embry-Riddle Aeronautical University, 1 Aerospace Blvd., Daytona Beach, FL 32114, USA & Scientist, NASA Kennedy Space Center, FL 32899, USA; Email: wittalm@my.erau.edu

E. Capello
Politecnico di Torino, CNR-IEIIT, Corso Duca degli Abruzzi 24, Torino, 10129, Italy; Email: elisa.capello@polito.it

M. Nazari
Embry-Riddle Aeronautical University, 1 Aerospace Blvd., Daytona Beach, FL 32114, USA; Email: nazarim@erau.edu

1 Introduction

Spacecraft translational motion can be formulated and propagated using several types of formulation such as Cowell, Encke, Clohessy-Wilthsire, equinoctial elements, or unified state model [1–3]. Spacecraft rotational kinematics are often modeled using attitude parameterization sets. Minimal parameterization sets (principal rotation, Euler angles, and classical and modified Rodrigues parameters) are defined in 3-dimensional Euclidean space $\mathbb{R}^3$ and can exhibit singularity. Quaternions are redundant and are defined on the 3-sphere S^3 [4, 5] and hence they do not have the singularity issue. However, due to the non-uniqueness of the quaternions, they can result in an undesired phenomenon called unwinding for large rotations, such as rigid body initial tumbling, although this can be avoided by using discontinuous feedback or nonlinear control laws [6]. The spacecraft attitude estimation has been performed using quaternions and a three-parameter set for the local error representation in the literature, including [7, 8]. Alternatively, rigid body attitude can be expressed using the rotation or direction cosine matrix defined on the special orthogonal group SO(3). Formalism of attitude using rotation matrices helps avoid the problems of singularity and non-uniqueness [9–12].

Conventionally, the analysis of the orbital and attitude dynamics of the spacecraft are conducted separately, resulting in separate control laws for attitude and translational motion. However, as clearly discussed in several references such as [13–15], the coupling between the translational and rotational dynamics of the spacecraft should be considered in spacecraft dynamics analysis and control design. The simultaneous modeling of spacecraft orbital-attitude dynamics using special Euclidean group SE(3) and their tangent bundle TSE(3) is especially advantageous due to its consideration of the

coupling between translational and rotational dynamics. Such coupling can be due to several effects such as nonlinear gravity fields or attitude-dependent forces due to drag and solar radiation pressure, and it occurs in missions such as spacecraft rendezvous, proximity operations and docking, or spacecraft hovering over small bodies. The consideration of this coupling results in accurate dynamic analysis and control design of the rigid body motion, as shown in [16–20], for example.

In real-world applications, the consideration of stochastic processes is a crucial part of any navigation and control system. The navigation system includes the sensors and the filter, while the control system is composed of the control algorithm and the actuators. The navigation filter enables the correct estimation of the states based on the sensor measurements. The on-board instruments, such as the inertial measurement unit, gyroscopes, accelerometers, and star trackers, have limited accuracy and are usually characterized by a degree of uncertainty. These uncertainties can arise not only due to the noise in the instruments, but also from electrical components, communication systems, or external disturbances, and result in inaccuracies and loss of precision in the measurements. In addition, some states might not be observable, as is the case with gyroscope biases. For the reasons mentioned above, there is a need for using state filters, such as the Kalman filters, that are capable of handling stochastic sources and can fuse the measurements from different sources optimally to estimate unobservable states [12, 21, 22].

Although the control problem on $\mathsf{TSE}(3)$ for space applications has been extensively studied [23–25], the navigation problem on $\mathsf{TSE}(3)$ still requires further research. State filter design on $\mathsf{SE}(3)$, with application to robotics, has been of growing interest in the literature. Extended Kalman filter (EKF) on $\mathsf{SE}(3)$ [26,27], discrete-EKF (D-EKF) on $\mathsf{SE}(3)$ [28, 29], and unscented Kalman filter (UKF) on $\mathsf{SE}(3)$ [30–32] are some examples. According to the literature, these estimators are more accurate than their counterparts designed in Euclidean space, although formulation development of the filter design on $\mathsf{SE}(3)$ is more complex than that in Euclidean space. The aforementioned work exploit the geometrical mechanics frameworks by using the associated maps and operators in the state update step, where the measurements are defined in the Lie algebra but the filter is designed on the Lie group $\mathsf{SE}(3)$.

In this paper, a novel spacecraft navigation and control system on Lie groups $\mathsf{SE}(3)$ and their tangent bundles $\mathsf{TSE}(3)$ is developed. The navigation filter is designed through a direct UKF based on the unscented transform (UT) described in [33], and the mathematical formalism in [34] is revised to describe the dynamic system characterized by stochastic processes in a compact form on $\mathsf{TSE}(3)$. The stochasticity is treated on $\mathsf{SE}(3)$ and its tangent bundle $\mathsf{TSE}(3)$ as discussed in [26, 30, 35] and a retraction function between the manifold and the Euclidean space [36, 37], the inverse of which is used to encode the UT sigma points onto the manifold and decode them from the manifold, respectively. The regulation controller in [17] is extended to design an almost globally asymptotically stable Morse-Lyapunov based tracking control algorithm. The integrated stochastic estimation and tracking control on Lie groups and their tangent bundles in this paper results in a precise, asymptotically stable navigation and control system that considers the orbit-attitude coupling in the presence of stochasticity. The efficacy of this navigation and control system is demonstrated in the problem of spacecraft motion around a small irregular central body which can be considered as a pre-landing phase that focuses on navigating to a specific point of interest. The properties of asteroid Bennu are used for the central body and the gravitational interaction between the rigid-body spacecraft and Bennu is modeled according to that in [38]. The accuracy of the estimator in the presence of stochasticity and stability and convergence of the closed loop are validated in the numerical simulation results.

2 Preliminaries and Problem Statement

2.1 Lie group $\mathsf{SE}(3)$ and its Lie algebra $\mathfrak{se}(3)$

The spacecraft configuration is defined by six degrees of freedom, three of which are related to the location of its center of mass and the other three are related to its attitude. According to [39, 40], the configuration space of a rigid-body spacecraft is a member of the Lie group $\mathsf{SE}(3)$ which is a smooth manifold obeying the group properties (closure under multiplication, identity, associativity, and invertability) and that the group operations are differentiable. The configuration of a rigid body can be expressed as

$$g = \begin{bmatrix} R & r \\ 0_{1\times 3} & 1 \end{bmatrix} \in \mathsf{SE}(3) \tag{1}$$

where $\mathsf{SE}(3)$ is defined as the semi-direct product of $\mathbb{R}^3$ and $\mathsf{SO}(3)$, i.e. $\mathsf{SE}(3) = \mathbb{R}^3 \times \mathsf{SO}(3)$, $R \in \mathsf{SO}(3)$ is the rotation matrix from the body frame to the inertial frame, $r \in \mathbb{R}^3$ is the position vector from the origin of the inertial frame to the center of mass of the rigid body expressed

in the inertial frame, and I_3 is the 3×3 identity matrix. The smoothness of the matrix Lie group implies the existence of a single tangent space at each point. The tangent space at the identity element of the group is referred to as Lie algebra [41] and is denoted as

$$\mathfrak{se}(3) = \left\{ \mathbb{V}^\vee = \begin{bmatrix} \omega^\times & v \\ 0_{1\times 3} & 0 \end{bmatrix},\ \omega^\times \in \mathfrak{so}(3),\ v \in \mathbb{R}^3 \right\} \tag{2}$$

where $(\cdot)^\vee$ indicates the wedge map, i.e. $(\cdot)^\vee : \mathbb{R}^6 \to \mathfrak{se}(3)$ applied to the vector $\mathbb{V} = [\omega^T, v^T]^T$ which is the augmented velocity vector, defined through the translational velocity $v \in \mathbb{R}^3$ and the angular velocity $\omega \in \mathbb{R}^3$; $\mathfrak{so}(3)$ is the set of 3 by 3 skew symmetric matrices such that $\omega^\times$ can be defined in terms of the components of the angular velocity vector. According to [42], given the vector $\omega = [\omega_1, \omega_2, \omega_3]^T$, the cross map $(\cdot)^\times : \mathbb{R}^3 \to \mathfrak{so}(3)$ is defined as

$$\omega^\times = \begin{bmatrix} 0 & -\omega_3 & \omega_2 \\ \omega_3 & 0 & -\omega_1 \\ -\omega_2 & \omega_1 & 0 \end{bmatrix} \tag{3}$$

From the definition of Lie group $\mathsf{SE}(3)$ and its Lie algebra $\mathfrak{se}(3)$, the geometric link between the two formulations can be understood. The Lie algebra can be considered as a linearization of the Lie group, near the identity element [43]. Due to the complexity of the nonlinear structure of the Lie group, it is difficult to study with conventional mathematical tools. The important feature of the Lie algebra is that it is a linear vector space and thus it can be studied using the tools developed in linear algebra. However, the extraction of the $\mathsf{SE}(3)$ properties from its Lie algebra opens the possibility to several scientific applications [44]. The exponential map $\exp : \mathfrak{se}(3) \to \mathsf{SE}(3)$ allows to transfer elements of the Lie algebra to the Lie group which, intuitively, can be interpreted as a wrapping operation, from the tangent plane onto the manifold. Formally, it is a local diffeomorphism from a neighborhood of zero in $\mathfrak{se}(3)$ onto a neighborhood of the identity element in $\mathsf{SE}(3)$ [42]. The exponential coordinates are defined as

$$\xi = \begin{bmatrix} \Theta \\ p \end{bmatrix} \in \mathbb{R}^6, \tag{4}$$

where $\Theta \in \mathbb{R}^3$ represents rotational vector. This is the product of eigenaxis (principal axis) and eigenangle (principal angle) of rotation, i.e. $\Theta = \theta e$, $\theta = \|\Theta\|$; $p \in \mathbb{R}^3$ represents the translational vector. Hence, the configuration g is obtained via exponential map $\exp : \mathfrak{se}(3) \to \mathsf{SE}(3)$ as

$$g = \exp(\xi^\vee) = \sum_{n=0}^{\infty} \frac{1}{n!} (\xi^\vee)^n, \tag{5}$$

which, according to [45], can be written as

$$g = \begin{bmatrix} R(\Theta) & S(\Theta)p \\ 0 & 1 \end{bmatrix} \in \mathsf{SE}(3), \tag{6}$$

where $R(\Theta) \in \mathsf{SO}(3)$ is the rotation matrix from body frame to the inertial frame. The rotation matrix is obtained via the Rodrigues formula as

$$R(\Theta) = \exp(\Theta^\times) = I + \frac{\sin\theta}{\theta}\Theta^\times + \frac{1-\cos\theta}{\theta^2}(\Theta^\times)^2, \tag{7}$$

and

$$S(\Theta) = I + \frac{1-\cos\theta}{\theta^2}\Theta^\times + \frac{\theta - \sin\theta}{\theta^3}(\Theta^\times)^2 \tag{8}$$

Note that the inverse of the exponential map is the logarithmic map $\log : \mathsf{SE}(3) \to \mathfrak{se}(3)$ which can be interpreted as an unwrapping operation. The exponential coordinates can be obtained via logarithmic map as

$$\xi^\vee = \log_{\mathsf{SE}(3)}(g) \tag{9}$$

2.2 Rigid body motion formulation on $\mathsf{SE}(3)$

The rigid body kinematic and kinetic equations of motion are given as

$$\begin{aligned} \dot{g} &= g\mathbb{V}^\vee, \\ \dot{\mathbb{V}} &= \mathbb{I}^{-1}\mathrm{ad}^*_{\mathbb{V}}\mathbb{I}\mathbb{V} + \mathbb{I}^{-1}\left(u_g + u_c\right), \end{aligned} \tag{10}$$

where $g \in \mathsf{SE}(3)$ represents the rigid body configuration as defined in Eq. (1), $\mathbb{V} = [\omega^T, v^T]^T$ denotes the rigid body augmented velocity vector expressed in the body frame, $u_g \in \mathbb{R}^6$ denotes the total external inputs due to gravitational effect, and $u_c \in \mathbb{R}^6$ is the control input produced by the control system (control moment and control force). The complete state is thus represented by $(g, \mathbb{V}) \in \mathsf{SE}(3) \times \mathbb{R}^6 = \mathsf{TSE}(3)$, the tangent bundle of $\mathsf{SE}(3)$. In this framework, both the attitude and the translational displacement are considered simultaneously. This allows to design an estimation algorithm and a control system in $\mathsf{TSE}(3)$, which is more versatile and more accurate than the standard decoupled procedures. In Eq. (10), the inertia tensor in $\mathsf{SE}(3)$ is given as

$$\mathbb{I} = \begin{bmatrix} J & 0_{3\times 3} \\ 0_{3\times 3} & mI_3 \end{bmatrix} \in \mathbb{R}^6 \tag{11}$$

where $J \in \mathbb{R}^{3\times 3}$ is the moment of inertia about the center of mass, and m is the mass of the system. Moreover, the co-adjoint operator is defined as

$$\mathrm{ad}^*_{\mathbb{V}} = \mathrm{ad}^T_{\mathbb{V}} = \begin{bmatrix} -\omega^\times & -v^\times \\ 0_{3\times 3} & -\omega^\times \end{bmatrix}, \tag{12}$$

where the adjoint operator $\mathrm{ad}_{\mathbb{V}}$ is

$$\mathrm{ad}_{\mathbb{V}} = \begin{bmatrix} \omega^{\times} & 0_{3\times 3} \\ -v^{\times} & -\omega^{\times} \end{bmatrix}. \tag{13}$$

From an intuitive point of view, this operator allows to transform a tangent vector from the tangent space around one element to the tangent space around another one.

2.3 Dynamics of spacecraft hovering near small bodies

For many small bodies, the asymmetric distribution of mass becomes a more significant element in the dynamics than in their larger counterparts such as Earth, Jupiter, or their major moons. For rigid body dynamics, the torque on the spacecraft body caused by the asymmetry must be considered. The gravity force exerted by the asteroid on the spacecraft is described using a second degree and order spherical harmonic gravity field. Assuming the origin of the asteroid body-centered inertial frame (BCI) coinciding with the center of mass of the body, the first degree and order gravity terms are $C_{11} = C_{10} = S_{11} = 0$. The asteroid is modeled as a constant density triaxial ellipsoid with major axes l_1, l_2, and l_3. This assumption makes the second degree and order terms C_{21}, S_{21}, S_{22} identically zero. The gravity potential of second degree and order of the celestial body given in [46] can be revisited as

$$\begin{aligned} U = \; & \frac{\mu}{\|\rho\|}\left(1 + \frac{1}{\|\rho\|^2}\left(C_{20}\left(-\frac{1}{2} + \frac{3}{2}(\hat{\rho}\cdot\hat{K})^2\right)\right.\right. \\ & \left.\left. +3C_{22}\left(1 - (\hat{\rho}\cdot\hat{K})^2 - 2(\hat{\rho}\cdot\hat{J})^2\right)\right)\right), \end{aligned}$$

where $\rho = \|\rho\|\hat{\rho} \in \mathbb{R}^3$ is the position vector of an arbitrary point on the spacecraft expressed in the BCI frame such that $r = \frac{1}{m}\int_{\mathcal{B}} \rho \, dm$, $(\hat{I}, \hat{J}, \hat{K})$ is the unit basis of the BCI frame, and the second degree and order coefficients are [47–49]

$$\begin{aligned} C_{20} &= -J_2 = \frac{1}{5}(\gamma^2 - \frac{\alpha^2 + \beta^2}{2}), \\ C_{22} &= \frac{1}{20}(\alpha^2 - \beta^2) \end{aligned} \tag{14}$$

where $\alpha = 1$, $\beta = \frac{l_2}{l_1}$, and $\gamma = \frac{l_3}{l_1}$ are normalized semi major axes of the ellipsoid. According to [38], the presented gravitational potential is effective to study the orbit-attitude coupled spacecraft dynamics in proximity of small irregular bodies. Taking the partial derivative of the gravity potential U in Eq. (14) with respect to ρ, integrating over the body of the spacecraft, and keeping only the terms up to order $1/\rho^4$, the gravity gradient force applied to the spacecraft expressed in spacecraft body fixed (SBF) coordinates is approximated as

$$F_g = R^T \int_{\mathcal{B}} \frac{\partial U}{\partial \rho} dm = R^T \left(F_{g_1} + F_{g_2}\right), \tag{15}$$

where R is the rotation matrix from the SBF frame to the BCI frame,

$$\begin{aligned} F_{g_1} = \; & -m\frac{\mu}{\|r\|^2}\left(1 + \frac{3}{m\|r\|^2}\left[J + \frac{1}{2}\left(\mathrm{tr}(J)\right.\right.\right. \\ & \left.\left.\left. -5\,\hat{r}^T R\, J\, R^T\,\hat{r}\right) I_3\right]\right)\hat{r}, \end{aligned} \tag{16}$$

$\hat{r} = r/\|r\|$, and

$$\begin{aligned} F_{g_2} = \; & \frac{m\mu}{\|r\|^4}\left(\begin{bmatrix} \left(\frac{3}{2}C_{20} - 9C_{22}\right)\left(\hat{r}\cdot\hat{I}\right) \\ \left(\frac{3}{2}C_{20} - 21C_{22}\right)\left(\hat{r}\cdot\hat{J}\right) \\ \left(\frac{9}{2}C_{20} - 15C_{22}\right)\left(\hat{r}\cdot\hat{K}\right) \end{bmatrix}\right. \\ & \left. + \frac{15}{\|r\|}\left(\left(-\frac{C_{20}}{2} + C_{22}\right)\hat{r}\cdot\hat{K} + 2C_{22}\hat{r}\cdot\hat{J}\right)\hat{r}\right) \end{aligned} \tag{17}$$

which is an alternative representation to that given in [50]. The gravity gradient torque on the rigid-body spacecraft due to the gravitational field of the central body is expressed in the SBF frame as

$$M_g = \frac{3\mu}{\|r\|^3}(R^T\hat{r})^{\times} J R^T \hat{r} \tag{18}$$

Therefore, the total augmented external effect in Eq. (10) is $u_g = [F_g^T, M_g^T]^T$, where the gravitational force and moment are given in Eqs. (15)-(18), respectively.

3 Stochastic Processes, Filter, and Control Design on Lie Group and its Tangent Bundle

3.1 Stochastic processes on Lie groups and system formulation

The mathematical model employed for the control and state estimation is usually developed in Euclidean space, which is an affine space and, by definition, is a geometric structure based on the vectorial space [41]. When the mathematical modeling is performed in Euclidean space, it is common to deal with uncertainties simply by using an additive approach. Basically, an additive white Gaussian noise can be considered as representative of the many random processes that occur in nature. However, when the model is developed in $\mathsf{SE}(3)$ and its tangent bundle $\mathsf{TSE}(3)$, uncertainties and stochastic processes cannot be formulated using the conventional mathematical models that are commonly used in the Euclidean space. This is due to the fact that $\mathsf{SE}(3)$ is a nonlinear manifold

and not a vectorial space [35]. In this paper, the formulation covered in [26,30] is used to accommodate a stochastic process in the model. Since the source of noise is assumed to be in vector space, the exponential map $\exp(\cdot)$ is used to map it into $\mathsf{SE}(3)$ as

$$\chi_\eta = \bar{\chi}_\eta \exp(\eta^\vee) \quad \eta \sim \mathcal{N}(0, N) \tag{19}$$

where χ_η is the noise in $\mathsf{SE}(3)$ and $\mathcal{N}(0, N)$ denotes the Gaussian distribution in Euclidean space with zero mean and covariance matrix $N \in \mathbb{R}^{6\times6}$. In Eq. (19), pre multiplication by $\bar{\chi}_\eta \in \mathsf{SE}(3)$ causes the original Gaussian $\eta \in \mathbb{R}^6$ of the Lie algebra to center at $\bar{\chi}_\eta \in \mathsf{SE}(3)$. The symbols χ_η and $\bar{\chi}_\eta$ represent a small perturbation with covariance P and a large source of noise, respectively.

The stochastic system formulation which best accommodates the application of Kalman filter theory considers an additive approach for both the process and the measurement noise. The process noise is added to the state derivative equation and the measurement noise is added to the system output equation. In this work, the aforementioned approach cannot be adopted, because the state of the system $x = (g, \mathbb{V})$ is on $\mathsf{TSE}(3)$. Although the velocity, expressed in $\mathbb{R}^6$, allows the simple addition of the noise, the pose requires the notation given in Eq. (19), since it is defined on $\mathsf{SE}(3)$. Despite the fact that different estimation techniques can be found in the literature, none of them account for a state vector that is defined on $\mathsf{TSE}(3)$. Therefore, a novel, augmented formulation is introduced.

It is assumed that the spacecraft pose and velocity are measurable and the output of the system, $z \in \mathbb{R}^{12}$, consists of the principal angles of rotation Θ, the translational vector components r, the angular velocity ω, and the translational velocity v. It must be emphasized that principal rotation angles are only used to represent the attitude in the simulation results, while they are obtained based on the rotation matrix. Instead Θ is just used to represent the rotation matrix as output of the system. In addition, using the principal angle of rotation allows us to take advantage of the $\mathsf{SE}(3)$ maps and operator previously defined, thus having a compact stochastic system formulation. Particularly, the stochastic system can be written on $\mathsf{TSE}(3)$ as

$$\dot{x}(t) : \begin{cases} \dot{g} = \chi_{\eta_g}\, g\mathbb{V}^\vee \\ \dot{\mathbb{V}} = \mathbb{I}^{-1}\mathrm{ad}^*_{\mathbb{V}+\frac{1}{2}\eta_\mathbb{V}}\mathbb{I}(\mathbb{V}+\eta_\mathbb{V}) + \mathbb{I}^{-1}u \end{cases} \tag{20}$$

$$z(t) = [(\log_{\mathsf{SE}(3)}(\chi_{\zeta_g} g)^\vert)^T,\ \mathbb{V}^T + \zeta_\mathbb{V}^T]^T \tag{21}$$

where $(\cdot)^\vert$ is the inverse of the wedge map. The dependence on time is omitted in the right sides for the readability of the equations. The measurement noise $\zeta = [\zeta_g^T, \zeta_\mathbb{V}^T]^T \in \mathbb{R}^{12}$ and the process noise $\eta = [\eta_g^T, \eta_\mathbb{V}^T]^T \in \mathbb{R}^{12}$ are assumed to be Gaussian white-noise processes. In addition, they are assumed to be uncorrelated and thus the second order joint central moment, i.e. the covariance, is zero. The aforementioned assumption yields

$$\begin{aligned} &E\{\eta(t)\} = B_\eta \\ &E\left\{\eta(t)\,\eta(t)^T(t+\tau)\right\} = Q \\ &\eta \sim \mathcal{N}(B_\eta, Q) \end{aligned} \tag{22}$$

$$\begin{aligned} &E\{\zeta(t)\} = B_\zeta \\ &E\left\{\zeta(t)\,\zeta^T(t+\tau)\right\} = T \\ &\zeta \sim \mathcal{N}(0, T) \end{aligned} \tag{23}$$

$$E\left\{\zeta(t)\eta^T(t+\tau)\right\} = 0 \tag{24}$$

where $Q \in \mathbb{R}^{12\times12}$ is the process noise covariance matrix, $T \in \mathbb{R}^{12\times12}$ is the measurement noise covariance matrix and $B_\eta \in \mathbb{R}^{12\times12}$ contain the measurement noise biases. The process noise is zero mean since the bias is encoded through the post multiplication in $\mathsf{SE}(3)$. In fact, the pose state equation can be revised as

$$\dot{g} = \bar{\chi}_{\eta_g} \exp(\eta_g^\vee) g\mathbb{V}^\vee \tag{25}$$

where the noise biases are represented by $\hat{\chi}_{\zeta_g} \in \mathsf{SE}(3)$. The stochastic system formulation in Eq. (20)-(21) is written in the following compact form, which will be employed in the description of the UKF steps described in the subsequent section:

$$\begin{aligned} \dot{x}(t) &= f(x(t), u(t), \eta(t)) \\ z(t) &= h(x(t), \zeta(t)) \end{aligned} \tag{26}$$

where $f(\cdot) \in \mathsf{TSE}(3)$ represents the nonlinear state function, which depends on the state, input, process noise, and time and $h(\cdot) \in \mathbb{R}^{12}$ represents the measurement function which depends on the state, the measurement noise, and time. Note that the time dependence is omitted.

3.2 Unscented Kalman filter design on Lie group and its tangent bundle

Starting from the stochastic system formulation introduced in with Eq. (20)-(21), the state estimation is performed using a UKF, which was selected from among the different Kalman filters because it is a reliable solution for nonlinear systems. This type of Kalman filter belongs to the family of sigma-point Kalman filters or linear regression

Kalman filters, which use the a statistical linearization technique. In general, in the EKF-based approaches, the state distribution is propagated analytically through the first-order linearization of the nonlinear system. This procedure can lead to large errors or corrupted estimates [32]. The UKF, instead, handles the problem with a deterministic sampling approach. The Gaussian state distribution is represented by a set of sample points that completely capture the mean and covariance of the distribution. These points are known as sigma points and are propagated through the nonlinear dynamics with the purpose of capturing the *a posteriori* mean and covariance with high accuracy [37]. As opposed to the UKF method, the EKF approach is only capable of achieving a first-order accuracy due to the linearization [33]. The UKF is based on the leading intuition that it is harder to approximate an arbitrary nonlinear function than to approximate a probability distribution [51]. This idea results in a filter which is able to achieve good performances even with pronounced nonlinearities or non-Gaussian distributions [52]. However, this algorithm has a higher computational cost than conventional EKF filters, even if the computation of the Jacobian is spared [53]. The UKF algorithm is sub optimal, as are nonlinear filters in general.

Generally, the Kalman filter techniques consists of two main steps: 1) The prediction step where the state and its error covariance are predicted on the basis of the system mathematical model. Usually this phase takes the name of *a priori* estimate of the system and leads to the estimated state and state error covariance $\hat{x}\,[k+1|k]$, $P\,[k+1|k]$. 2) the measurement update step where the *a priori* state is corrected with an external measure. This procedure allows to obtain a better state estimate, defined as *a posteriori* estimate of the system, $\hat{x}\,[k+1|k+1]\,, P\,[k+1|k+1]$. The UKF has an additional preliminary step, which consists in the UT and hence the computation of the sigma points.

3.2.1 Sigma points selection step

The number of the sigma points clearly depends on the number of dimensions in the system. From now on, the letter p will indicate the number of dimensions in the state and the quantities related to it, and the letter q will refer to the process noise. Given the current state covariance matrix $P[k|k]$ and process noise matrix Q, two different sets of sigma points are computed. The UT requires $2p+1$ points for the first set and $2q+1$ for the second one, where the additional point refers to the mean of the distribution. Therefore, $2p+1$ sigma points in χ_p are related to the state error covariance matrix and $2q+1$ sigma points in χ_q are related to the process noise matrix are defined. The matrix $\boldsymbol{\chi}_p[k] \in \mathbb{R}^{p\times 2p+1}$ of $2p$ sigma column vectors $\chi_{p,i}[k]$ is formed according to

$$\begin{aligned}
&\chi_{p,0}[k] = 0\\
&\chi_{p,i}[k] = \chi_{p,0}[k] + \left(\sqrt{(p+\lambda_p)P[k|k]}\right)_i\\
&\qquad (i = 1,\cdots,p)\\
&\chi_{p,i}[k] = \chi_{p,0}[k] - \left(\sqrt{(p+\lambda_p)P[k|k]}\right)_{i-p}\\
&\qquad (i = p+1,\cdots,2p)
\end{aligned} \tag{27}$$

where $\chi_{p,0}[k]$ represents the mean of the distribution, and the other $2p$ points the dispersion around it. $[k]$ indicates the current kth step and $\lambda_p = (\alpha^2-1)p$ is a scaling parameter. The constants α determines the spread of the sigma points around their mean and is usually set to a small positive value, e.g. $10^{-4} \leq \alpha \leq 1$. $(\sqrt{(p+\lambda_p)P[k|k]}\,)_i$ is the ith column of the matrix square root (e.g. lower triangular Cholesky factorization). Moreover the sigma points are defined along with their weights

$$\begin{aligned}
&W_{p,0}^{(m)} = \frac{\lambda_p}{\lambda_p+p},\;\; W_{p,0}^{(c)} = \frac{\lambda_p}{\lambda_p+p} + (1-\alpha^2+\beta)\\
&W_{p,i}^{(m)} = W_{p,i}^{(c)} = \frac{1}{2(d+\lambda_d)} \quad (i = 1,...,2p)
\end{aligned} \tag{28}$$

where the superscripts (c) and (m) refer to the covariance and the mean, respectively. The first ones will be used to compute the sigma points mean after they are passed through the nonlinear system, while the latter ones are used for the computation of the sigma points covariances. In addition the subscript 0 refers to the mean of the distribution. The constant β is used to incorporate prior knowledge of the distribution of the state. The value $\beta = 2$ is optimal for Gaussian distribution and is commonly selected as value. In other words, the matrix $\boldsymbol{\chi}_p[k]$ and its weights are constructed as

$$\begin{aligned}
\boldsymbol{\chi}_p[k] = \;&\Big[\chi_{p,0}[k],\; \chi_{p,0}[k] + \sqrt{(p+\lambda_p)P[k|k]},\\
&\chi_{p,0}[k] - \sqrt{(p+\lambda_p)P[k|k]}\Big]
\end{aligned} \tag{29}$$

$$\begin{aligned}
W_p^{(m)} &= \Big[W_{p,0}^{(m)}\; W_{p,1}^{(m)}\; \cdots\; W_{2p,1}^{(m)}\Big]\\
W_p^{(c)} &= \Big[W_{p,0}^{(c)}\; W_{p,1}^{(c)}\; \cdots\; W_{2p,1}^{(c)}\Big]
\end{aligned} \tag{30}$$

The same procedure applies to the set $\boldsymbol{\chi}_q[k]$ related to the process noise matrix. In particular the matrix $\boldsymbol{\chi}_q[k] \in \mathbb{R}^{q\times(2q+1)}$ of $2q$ sigma column vectors

$\chi_{q,i}[k]$ is formed according to

$$\begin{aligned}
&\chi_{q,0}[k] = 0,\\
&\chi_{q,i}[k] = \chi_{q,0}[k] + \left(\sqrt{(q+\lambda_q)Q}\right)_i \\
&\qquad\qquad (i = 1,\dots,q)\\
&\chi_{q,i}[k] = \chi_{q,0}[k] - \left(\sqrt{(q+\lambda_q)Q}\right)_{i-q} \\
&\qquad\qquad (i = q+1,\dots,2q)
\end{aligned} \tag{31}$$

and their weights

$$\begin{aligned}
&W_{q,0}^{(m)} = \frac{\lambda_q}{q+\lambda_q},\ W_{q,0}^{(c)} = \frac{\lambda_q}{q+\lambda_p} + (1-\alpha^2+\beta)\\
&W_{q,i}^{(m)} = W_{q,i}^{(c)} = \frac{1}{2(q+\lambda_q)} \quad (i = 1,...,2q)
\end{aligned} \tag{32}$$

In other words, the matrix $\boldsymbol{\chi}_q[k]$ and the weights $W_q^{(m)}$ and $W_q^{(c)}$ can be defined. In the update step, a third set of sigma points $\boldsymbol{\chi}_u$[k] will be generated with the one-step-ahead state prediction $\hat{x}[k+1|k]$. In principle a third set of weights may be defined, however the same of the $\boldsymbol{\chi}_p$[k] set will be used.

3.2.2 Prediction step

The *a priori* state estimate $x[k+1|k]$ and the state error state covariance matrix $P[k+1|k]$ are predicted using the current estimates $\hat{x}[k|k]$, $P[k|k]$ and the sigma points vectors $\chi_{i,q}, \chi_{i,p}$. It is clear that the UKF needs to be initialized with the initial state estimate $\hat{x}_0 = E\{x_0\}$ and the initial covariance state matrix $P_0 = E\{(x_0 - \hat{x}_0)(x_0 - \hat{x}_0)^T\}$. Since the system states are on $\mathsf{TSE(3)}$, a retraction function $\varphi(\cdot) : \mathbb{R}^{12} \to \mathsf{TSE(3)}$ is introduced [36,37], which is a smooth, arbitrarily-chosen function that encodes the mean and covariance noise on the Lie group and its tangent bundle. The retraction function is

$$\varphi(x, \chi_i) : \begin{cases} \varphi_g = g\exp(\chi_{g,i}^{\vee})) \\ \varphi_{\mathbb{V}} = \mathbb{V} + \chi_{\mathbb{V},i} \end{cases} \tag{33}$$

where $\chi_{g,i}$ indicates the first $p/2$ elements of the sigma points vector χ_i, and $\chi_{\mathbb{V},i}$ the latest $p/2$. Note that when $\chi_i = 0$ then $\varphi(x,0) = x$. The inverse retraction function $\varphi^{-1} : \mathsf{TSE(3)} \to \mathbb{R}^{12}$ makes use of the Lie algebra and is

$$\varphi^{-1}(\hat{x}, x) : \begin{cases} \varphi_g^{-1} = \log_{\mathsf{SE(3)}}(\hat{g}^{-1}g) \\ \varphi_{\mathbb{V}}^{-1} = \hat{\mathbb{V}} - \mathbb{V} \end{cases} \tag{34}$$

where $\hat{x} = (\hat{g}, \hat{\mathbb{V}})$ and $x = (g, \mathbb{V})$. It is emphasized that the retraction function is used to encode the sigma points onto the manifold and its inverse is used to decode the sigma points from the manifold. Given the current optimal estimated state $\hat{x}[k|k]$, the first set of sigma points are retracted into the manifold and then used to propagate the system dynamics starting from $\hat{x}[k|k]$

$$\begin{aligned}
x_{\chi_{p,i}}[k] &= f\left(\varphi\left(\hat{x}[k|k], \chi_{p,i}[k]\right), \hat{u}[k], 0\right)\\
&\qquad (i = 0,\dots,2p)
\end{aligned} \tag{35}$$

where the current input vector $\hat{u}[k]$ is assumed not measurable, and hence it is estimated using the current state $\hat{x}[k|k]$. The sigma points which represents the mean of the distribution, $\chi_{p,0}[k]$ returns the mean state which is used as one-step-ahead state prediction

$$\begin{aligned}
\hat{x}[k+1|k] &= f(\varphi\left(\hat{x}[k|k], \chi_{p,0}[k]\right), \hat{u}[k], 0)\\
&= f(\hat{x}[k|k], \hat{u}[k], 0)
\end{aligned} \tag{36}$$

using the properties of the retraction function.

In order to compute the covariance matrix with respect to the state uncertainty, the obtained states are retracted back into $\mathbb{R}^{12}$ with the inverse retraction function. The retracted sigma points matrix $\boldsymbol{\chi}_p^r[k] \in \mathbb{R}^{p\times(2p+1)}$ is then obtained as

$$\chi_{p,i}^r[k] = \varphi^{-1}(\hat{x}[k+1|k], x_{\chi_{p,i}}[k]) \quad (i = 0,\dots,2p) \tag{37}$$

and since $x_{\chi_{p,0}}[k] = \hat{x}[k+1|k]$, the first column of the matrix is $\chi_{p,0}^r[k] = 0$. The covariance matrix with respect to the state uncertainty can be finally computed as

$$P[k+1|k] = W_p^{(c)}(\boldsymbol{\chi}_p^r[k] - \overline{\chi}_p^r[k])(\boldsymbol{\chi}_p^r[k] - \overline{\chi}_p^r[k])^T \tag{38}$$

where $\overline{\chi}_p^r[k] \in \mathbb{R}^{2p}$ is the weighted mean of the retracted sigma points with $W_p^{(m)}$. This matrix needs to be corrected with the contribute which comes from the process noise. Hence, the second set of sigma points, $\chi_{q,i}[k]$, is used similarly to the first one. The main important difference is that these points are not used as initial condition for the propagation, since they are not related to the state. Instead, they are introduced in the propagation as process noise

$$x_{\chi_{q,i}}[k] = f\left(\hat{x}[k|k], \hat{u}[k], \chi_{q,i}[k]\right) \qquad (i = 0,\dots,2q) \tag{39}$$

It is clear that the first the sigma points which represents the mean of the distribution, $\chi_{q,0}[k]$ returns $\hat{x}[k+1|k]$, according to Eq. (36). The obtained states are retracted back into $\mathbb{R}^{12}$ with the inverse retraction function. The retracted sigma points matrix $\boldsymbol{\chi}_q^r[k] \in \mathbb{R}^{q\times(2q+1)}$ is then obtained as

$$\chi_{q,i}^r[k] = \varphi^{-1}(\hat{x}[k+1|k], x_{\chi_{q,i}}[k]) \qquad (i = 0,\dots,2q)$$

(40)

and since $x_{\chi_{q,0}}[k] = \hat{x}[k+1|k]$, the first column of the matrix is $\chi^r_{q,0}[k] = 0$. The covariance matrix with respect to the noise can be finally computed as

$$Q[k+1|k] = W_q^{(c)}(\boldsymbol{\chi}^r_q[k] - \overline{\chi}^r_q[k])(\boldsymbol{\chi}^r_q[k] - \overline{\chi}^r_q[k])^T \tag{41}$$

where $\overline{\chi}^r_q[k] \in \mathbb{R}^{2q}$ is the weighted mean of the retracted sigma points with $W_q^{(m)}$. Finally, the one-step-ahead state error covariance matrix is computed correcting Eq. (38) as

$$\begin{aligned} P[k+1|k] &= P[k+1|k] + Q[k+1|k] \\ &= W_p^{(c)}(\boldsymbol{\chi}^r_p[k] - \overline{\chi}^r_p[k])(\boldsymbol{\chi}^r_p[k] - \overline{\chi}^r_p[k])^T \\ &+ W_q^{(c)}(\boldsymbol{\chi}^r_q[k] - \overline{\chi}^r_q[k])(\boldsymbol{\chi}^r_q[k] - \overline{\chi}^r_q[k])^T \end{aligned} \tag{42}$$

Note that the second contribute is weighted on the basis of the process noise covariance matrix Q. If the knowledge of the true model is poor, then Q has large elements and then the *a priori* covariance state error matrix estimate has a large dispersion.

3.2.3 Measurement update step

Once $\hat{x}[k+1|k]$ and $P[k+1|k]$ are computed and the measurement $z[k]$ is known, the correction can be performed. As mentioned, the third set of sigma points with the predicted state error covariance matrix are computed. The matrix $\boldsymbol{\chi}_u[k] \in \mathbb{R}^{p\times(2p+1)}$ of $2p$ sigma column vectors $\chi_{u,i}[k]$ is formed according to

$$\begin{aligned} &\chi_{u,0}[k+1]=0, \\ &\chi_{u,i}[k+1]=\chi_{u,0}[k+1]+\Big(\sqrt{(p+\lambda_d)P[k+1|k]}\Big)_i \\ &\qquad (i=1,\dots,p) \\ &\chi_{u,i}[k+1]=\chi_{u,0}[k+1]-\Big(\sqrt{(p+\lambda_d)P[k+1|k]}\Big)_{i-p} \\ &\qquad (i=p+1,\dots,2p) \end{aligned} \tag{43}$$

or equivalently expressed through $\boldsymbol{\chi}_u[k+1]$. Each point is retracted into the manifold and then passed through the measurement function. The matrix $z_u \in \mathbb{R}^{p\times(2p+1)}$ is constructed such that each column is

$$\begin{aligned} z_{u,i}[k+1] = h(\varphi(\hat{x}[k+1|k], \chi_{u,i}[k+1])), \\ (i=0,\dots,2p) \end{aligned} \tag{44}$$

where the first column is $z_{u,0}[k] = 0$ due to the retraction function properties. Since the ith measurement vector is part of $\mathbb{R}^{12}$ and not of $\mathsf{TSE}(3)$, there is no need to use the inverse of the retraction function. Therefore, the measurement covariance matrix $P_{zz}[k+1]$ and the cross-covariance $P_{xz}[k+1]$ can then be obtained

$$\begin{aligned} P_{zz}[k+1] = \; & W_p^{(c)}(z_u[k+1] - \overline{z}[k+1])(z_u[k+1] \\ & -\overline{z}[k+1])^T + T \end{aligned} \tag{45}$$

$$P_{xz}[k+1] = \; W_p^{(c)}\boldsymbol{\chi}_u[k+1](z_u[k+1] - \overline{z}[k+1])^T \tag{46}$$

where $\overline{z}[k+1]$ is the weighted mean with $W_{p,i}^{(m)}$. The Kalman gain is the factor which allows to minimize the state covariance matrix P and is computed by

$$K[k+1] = P_{xz}[k+1]P_{zz}[k+1]^{-1} \tag{47}$$

Note that if a noisy sensor is used, the measurement covariance matrix has high elements and its inverse will produce a low Kalman gain. Finally, the *a posteriori* state estimate is

$$\hat{x}[k+1|k+1] = \varphi(\hat{x}[k+1|k], K[k+1]r[k+1]) \tag{48}$$

where r is the residual, i.e. the discrepancy, between the estimated measurement $\overline{z}[k+1]$ from the *a priori* predictions and the actual measurement $z[k+1]$. It is clear that the Kalman gain $K[k+1]$ acts as a weighing factor for the residual. Particularly, when the measurement is corrupted and T assumes large values, then the Kalman gain and the residual weight are low. Therefore, this gain allows to have an optimal estimate weighting the received measurement on the basis of its reliability. This degree of reliability is achieved by comparing the covariance of the estimated measurement and the covariance of the real measurement. Finally, the *a posteriori* state error covariance matrix is computed as

$$P[k+1|k+1]=P[k+1|k]-K[k+1]P_{zz}[k+1]K[k+1]^T \tag{49}$$

3.3 Tracking control design on Lie groups and their tangent bundles

The control design in the $\mathsf{TSE}(3)$ framework enables one to treat both rotational and translational motions simultaneously. The feedback loop allows the computation of the difference between the desired and the measured configuration, which is affected by the measurements errors. The controller should be able to nullify the error between the actual and desired state. The latter is computed by a guidance system, while the actual states are obtained from the navigation filter which filters out

the measurement noise. Once the state configuration error is defined, the controller can command the spacecraft translational and rotational motion through the actuators.

Here, the tracking problem of reaching and maintaining a desired orbit around a small body is considered. The guidance algorithm assigns the desired position r_{ref} in BCI frame, velocity $\mathbb{V}_{\text{ref}}$ in SBF frame, and attitude Θ_{ref} in combination with the actual states, to the control system. The UKF filter is used to obtain the estimated states $\hat{r}$, $\hat{\mathbb{V}}$ and $\hat{\Theta}$ from noisy measurements. Finally, the tracking errors can then be computed as

$$\begin{aligned}\delta g_{\text{track}} &= g_{\text{ref}}^{-1}\hat{g} = \begin{bmatrix}\delta R_{\text{track}} & \delta r_{\text{track}}\\ 0 & 1\end{bmatrix}\\ &= \begin{bmatrix}R_{\text{ref}}^T(\Theta_{\text{ref}})R(\hat{\Theta}) & R_{\text{ref}}^T(\Theta_{\text{ref}})\,(\hat{r}-r_{\text{ref}})\\ 0 & 1\end{bmatrix}\\ \delta\mathbb{V}_{\text{track}} &= \hat{\mathbb{V}} - \mathbb{V}_{\text{ref}}\end{aligned} \tag{50}$$

The error dynamics in terms of position and velocity should tend to zero, and the rotation matrix to the identity matrix. Since the state is on $\mathsf{TSE}(3)$ and the control input is in $\mathbb{R}^6$, different functions are introduced to allow the retraction from the manifold into Euclidean space. The nonlinear function of the velocity and configuration is defined as

$$\psi(\delta g_{\text{track}}, \delta\mathbb{V}_{\text{track}}) = \delta\mathbb{V}_{\text{track}} + K_1 l(\delta g_{\text{track}}) \tag{51}$$

where $K_1 = \text{blkdiag}(k_{11}, k_{12}) \in \mathbb{R}^{6\times 6}$ is a positive definite control gain matrix. The following vector function of the configuration is then introduced:

$$l(\delta g_{\text{track}}) = \left[s^T(\delta R_{\text{track}}), \delta r_{\text{track}}^T\right]^T \tag{52}$$

with its derivative

$$\dot{l}(\delta g_{\text{track}}) = \left[\dot{s}^T(\delta R_{\text{track}}), \delta v_{\text{track}}^T\right]^T \tag{53}$$

The $s(\cdot) : \text{SO}(3) \to \mathbb{R}^3$ and $\dot{s}(\cdot) : \text{SO}(3) \to \mathbb{R}^3$ are

$$\begin{aligned}s(\delta R_{\text{track}}) &= \sum_{i=1}^{3} a_i \left(\delta R_{\text{track}}^T e_i\right)^\times e_i\\ &= \sum_{i=1}^{3} \left(\delta R_{\text{track}}^T A^T e_i\right)^\times e_i\\ \dot{s}(\delta R_{\text{track}}, \delta\omega_{\text{track}}) &= (\text{tr}(A\delta R_{\text{track}})I_3 -\\ &\quad \delta R_{\text{track}}^T A)\delta\omega_{\text{track}}\end{aligned} \tag{54}$$

where e_i, $i = 1, 2, 3$, are the elements of the natural basis in $\mathbb{R}^3$, and $A = [\text{diag}\,(a_1, a_2, a_3)]$ with the scalars a_1, a_2, and a_3 selected such that $a_1 > a_2 > a_3 \geq 1$. The control law developed for rigid body regulation control on $\mathsf{TSE}(3)$ in [17] is revised here to account for a tracking problem as

$$\begin{aligned}u_c = &-\mathbb{I}K_1\dot{l} - \text{ad}^*_{\psi - K_1 l}\,\mathbb{I}\,(\psi - K_1 l) - \mathbb{I}K_2\psi\\ &-\mathbb{I}\kappa\left[0_{1\times 3}, \delta r_{\text{track}}^T \delta R_{\text{track}}^T\right]^T\end{aligned} \tag{55}$$

where $K_2 = \text{blkdiag}(k_{21}, k_{22}) \in \mathbb{R}^{6\times 6}$ is a positive definite control gain matrix, and k_{21} and k_{22} can be tuned suitably to adjust rotation and translation performance of the spacecraft. Thus, the total augmented control input is $u_c = [F_c^T, M_c^T]^T$, as defined in Eq. (10).

The proof for almost global asymptotic stability of the tracking problem studied is similar to that given in [17] for the rigid body regulation problem using an attitude-dependent Morse-Lyapunov function and a backstepping state feedback control law of the form

$$\delta\mathbb{V}_{\text{track}} = -l(\delta g_{\text{track}})$$

According to [54], the separation principle allows the design of the controller and the observer (filter algorithm) separately. Particularly, if the observer and the controller are both stable, then the closed-loop dynamics obtained using the augmented form is also stable. In many applications, this technique has proved to be a successful and stable design method. In order to highlight the different type of errors, the total error on each state can be rewritten as

$$\begin{aligned}\delta R &= R_{\text{ref}}^T(\Theta_{\text{ref}})\hat{R}(\hat{\Theta})\hat{R}^T(\hat{\Theta})R(\Theta) = \delta R_{\text{track}}\delta R_{\text{est}}\\ \delta r &= \hat{R}(\hat{\Theta})(r-\hat{r}) + R_{\text{ref}}^T(\Theta_{\text{ref}})(\hat{r} - r_{\text{ref}})\\ &\quad = \delta r_{\text{est}} + \delta r_{\text{track}}\\ \delta\mathbb{V} &= \mathbb{V} - \hat{\mathbb{V}} + \hat{\mathbb{V}} - \mathbb{V}_{\text{ref}} = \delta\mathbb{V}_{\text{est}} + \delta\mathbb{V}_{\text{track}}\end{aligned} \tag{56}$$

where $\delta(\cdot)_{\text{est}}$ and $\delta(\cdot)_{\text{track}}$ denote the estimation error and the tracking error, respectively. According to Eq. (56), when the estimation error and tracking error go to zero, the total error goes to zero, meaning that both the estimator and controller are asymptotically stable (in addition, the controller is almost globally asymptotically stable [17]). The convergence of the controller results in a zero tracking error and the convergence of the filter results in a bounded estimation error with zero mean white noise. From Eq. (56), the coupling effect of the nonlinear dynamics is clear. The total position error is not able to converge to zero if the attitude total error does not converge.

Note that an alternative asset could be the implementation of a controller robust to the uncertainties, i.e. a stochastic robust controller analogous to that in [55] for robust pose control, without the use of a navigation system. However, for systems affected by different sources of high-magnitude noise, the states can easily diverge if the stochasticity is not filtered out unless the control inputs are selected to be large enough to compensate those stochasticities. The estimator-based controller proposed in this manuscript is continuously updated with the system dynamics which, as a result, avoids high control inputs.

3.4 Variational integrator

In the numerical simulations provided in Section 4, the dynamics are propagated using a variational integrator in order to preserve geometric properties of the system. This integrator is applied directly on the nonlinear manifold $\mathsf{SE}(3)$, where the discretized Hamiltonian is used. The details of the variational integrator formalism are not shown here for brevity, but they can be found in [40, 56, 57], for instance.

4 Numerical Simulations and Discussion

In order to investigate the performance of the proposed navigation and control system, a scenario with high orbit-attitude coupling is studied here. Particularly, the NASA's asteroid-study and sample-return mission, OSIRIS-REx, is considered. The publicly available data of this mission (Table 1) are used to define the properties of the spacecraft and the small irregular asteroid Bennu.

The details of the spacecraft control system are used to define the saturation limits for the control moment and force. The control gains are tuned arbitrarily but such that they satisfy stability of the closed-loop dynamics. The sensors employed in the navigation system are assumed to be characterized by a worse statistics than the real-world scenario; i.e., the standard deviations are assumed to be relatively large in order to verify the robustness of the proposed navigation and control system. The process noise covariance matrix is chosen with relatively small element with respect to R, such that the UKF relies on the predictions and the noise can be efficiently filtered. The details of navigation and control systems are reported in Table 2.

The tracking orbit is chosen based on the mission timeline. Just before the touch and go operation, the spacecraft flies a closed orbit with a radius of 0.6 miles (1 km) around Bennu. This phase is also important for the scientific return of the mission, since the spacecraft collects asteroid's data to map its surface. For this reason, it is assumed a desired (reference) circular orbit with a nonzero inclination, and a nadir-pointing attitude such that a face of the satellite always points to the surface of the asteroid. The orbit is parameterized through trigonometric functions of time such that, at each time step, the reference position in BCI frame is

$$r_{\text{ref}}(t) = R_o \left[\rho_o \sin\left(n_o\, t\right), \quad \rho \cos\left(n_o\, t\right), \quad 0\right]^T \tag{57}$$

where ρ_o denotes the radius of the desired circular orbit, n_o is the orbital mean motion, and R_o represents the transformation matrix from the perifocal frame to the BCI frame. The orbital mean motion is obtained from Kepler's third law. The reference translational velocity $v_{\text{ref}}(t)$ is obtained by taking the time derivative of the position vector in Eq. (57). The following values are chosen: $\rho_o = 1$ km, $R_o = R([0,\, \pi/4,\, 0])$, $n_o = \frac{2\pi}{T_o}$, where the period of the orbit is computed with the third Kepler law $T_o = 2\pi\sqrt{\frac{\rho^3}{\mu}}$. In order to guarantee the nadir pointing attitude, the local vertical local horizontal (LVLH) reference frame is introduced, whose representation is given in Fig. 1. Particularly, r represents the position vector from BCI to the satellite, v the satellite's orbital velocity and $h = r \times v$ the orbital angular momentum. The first axis is oriented in the $v_{\text{ref}}(t)$ direction, $\hat{e}_{1,\text{LVLH}}(t) = v_{\text{ref}}(t)/\|v_{\text{ref}}(t)\|$; the third axis is is oriented in the $-r_{\text{ref}}(t)$ direction, $\hat{e}_{3,\text{LVLH}}(t) = -r_{\text{ref}}(t)/\|r_{\text{ref}}(t)\|$; the second axis is normal to the orbit plane and in the direction of angular momentum h with opposite sign, $\hat{e}_{2,\text{LVLH}}(t) = \hat{e}_{2,\text{LVLH}}(t) \times \hat{e}_{1,\text{LVLH}}(t)$. The reference angular velocity is simply defined as $\omega_{\text{ref}}(t) = -n_o\, \hat{e}_{2,\text{LVLH}}$ [62,63]. The guidance system computes the reference attitude at each instant of time as

$$\Theta_{\text{ref}}(t) = \log_{\mathsf{SO(3)}}\left(R_{LVLH}^T(t)\right) \tag{58}$$

where R_{LVLH} is the rotation matrix from BCI to LVLH reference frame

$$R_{\text{LVLH}}(t) = \begin{bmatrix} \hat{e}_{1,\text{LVLH}}(t)\cdot\hat{I} & \hat{e}_{1,\text{LVLH}}(t)\cdot\hat{J} & \hat{e}_{1,\text{LVLH}}(t)\cdot\hat{K} \\ \hat{e}_{2,\text{LVLH}}(t)\cdot\hat{I} & \hat{e}_{2,\text{LVLH}}(t)\cdot\hat{J} & \hat{e}_{2,\text{LVLH}}(t)\cdot\hat{K} \\ \hat{e}_{3,\text{LVLH}}(t)\cdot\hat{I} & \hat{e}_{3,\text{LVLH}}(t)\cdot\hat{J} & \hat{e}_{3,\text{LVLH}}(t)\cdot\hat{K} \end{bmatrix} \tag{59}$$

with unit vectors $F_{BCI} = [\hat{I}, \hat{J}, \hat{K}]$ for the BCI frame and $F_{LVLH} = [\hat{e}_{1,LVLH}, \hat{e}_{2,LVLH}, \hat{e}_{3,LVLH}]$ for the LVLH frame. The spacecraft initial conditions are chosen reasonably different from the desired ones, i.e. the reference orbit and nadir-pointing attitude. All the states are selected randomly from Gaussian distributions with a standard deviations of 90 deg, 1000 m, 5 deg/s and 1 m/s for attitude, position, and velocities respectively. On the other hand, the UKF initial conditions are selected with an error of 10% for attitude and position and 20% for velocities, with respect to the spacecraft initial conditions.

4.1 Filter verification

The performance of the proposed UKF is compared to those of other state filters designed on $\mathsf{SE}(3)$ that can be found in literature. In particular, the algorithms selected for the comparison are i)

Table 1 Spacecraft and Bennu properties [50, 58, 59].

Parameter	Values
Spacecraft mass [kg]	$m = 850$
Spacecraft dimension [m]	$d_1 = 2.0$, $d_2, d_3 = 2.3$
Spacecraft inertia [kg m^2]	$J = \frac{m}{12}\text{diag}\left[(d_1^2 + d_2^2),\, (d_2^2 + d_3^2),\, (d_1^2 + d_2^2)\right]$
Bennu gravitational parameter [m^3 s^{-2}]	$\mu = 5.2060$
Bennu dimension [m]	$l_1 = 535$, $l_2 = 508$, $l_3 = 365$
Bennu coefficients	$C_{20} = -0.097070$, $C_{22} = 0.004919$
Bennu rotation period [hr]	$T_B = 4.297$

Table 2 Values used for the navigation and control systems [60, 61].

Parameter	Values
Measurement std [deg,m,deg,m/s]	$\sigma_{\zeta_\Theta} = 6$, $\sigma_{\zeta_r} = 100$, $\sigma_{\zeta_\omega} = 0.2$, $\sigma_{\zeta_v} = 2$
Measurement cov matrix [deg,m,deg,m/s]	$T = \text{blkdiag}\left[\sigma^2_{\zeta_\Theta} I_3,\, \sigma^2_{\zeta_r} I_3,\, \sigma^2_{\zeta_\omega} I_3,\, \sigma^2_{\zeta_v}/10 I_3\right]$
Process cov matrix [deg,m,deg,m/s]	$Q = \text{blkdiag}\left[10^{-10} I_3,\, 10^{-10} I_3,\, 10^{-10} I_3,\, 10^{-10} I_3\right]$
State cov matrix [deg,m,deg,m/s]	$P_0 = \text{blkdiag}\left[10^{-10} I_3,\, 10^{-10} I_3,\, 10^{-10} I_3,\, 10^{-10} I_3\right]$
Control Moment Saturation per axis [N m]	$M_{c,i} = 24$
Control Force Saturation per axis [N]	$F_{c,i} = 366$
κ [km s^{-2}]	1×10^{-6}
K_1 [s^{-1}]	$\text{blkdiag}\left[5 \times 10^{-4} I_3,\, 1 \times 10^{-3} I_3\right]$
K_2 [s^{-1}]	$\text{blkdiag}\left[2 \times 10^{-2} I_3,\, 1 \times 10^{-2} I_3\right]$
a	$[1.2,\, 1.1,\, 1.0]^T$

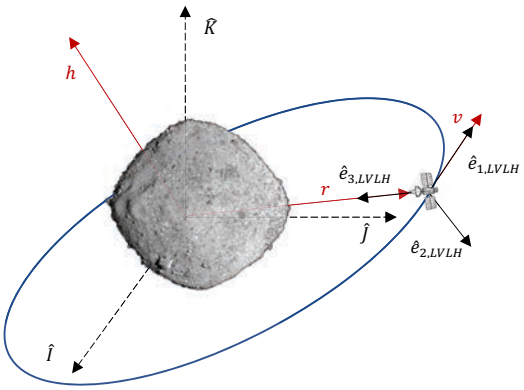

Fig. 1 Local vertical local horizontal (LVLH) and body-centered inertial (BCI) reference frames representation.

the EKF on Lie group introduced in [26] (EKF), ii) the UKF on Lie group introduced in [30] (UKF), and iii) the discrete EKF on Lie group (DEKF) described in [28]. The performance analysis is conducted on the basis of position and attitude estimation results. The case study consists of the propagation of the open loop spacecraft dynamics around the asteroid Bennu, where the data previously introduced are used. As in [29, 30], the results are shown in Fig. 2 in terms of the root mean square of the pose estimation error (RMSE). The first and second rows show the position and attitude RMSEs, respectively, as a function of sample period Δt (left) with $\zeta_r = 10^{-1}$ km, $\zeta_\Theta = 10^{-1}$ deg, and $\chi_r = 0$ km, $\chi_\Theta = 0$ km (left); initial condition inaccuracies χ_r, χ_Θ with $\zeta_r = 10^{-1}$ km, $\zeta_\Theta = 10^{-1}$ deg, and $\Delta t = 1$ s (center); and measurement noise standard deviations ζ_r km, $\zeta\Theta$ deg with $\zeta_r = 10^{-1}$ km, $\zeta_\Theta = 10^{-1}$ deg, and $\Delta t = 1$ s (right).

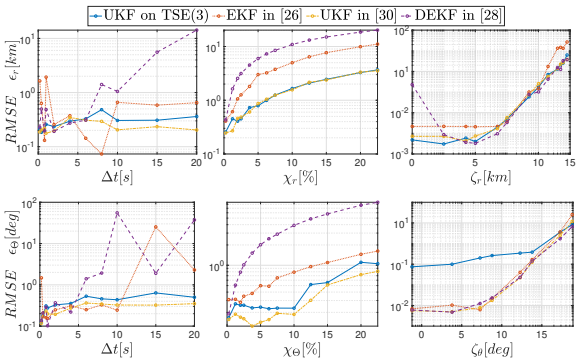

Fig. 2 Attitude and position RMSE as a function of sample period, initial condition inaccuracies and measurement noise standard deviations.

In the left column of Fig. 2, the RMSE(s) for the position and attitude error are shown along with the sample period Δt from 0.1 to 20 seconds. It can be seen that the proposed filter (solid) and the UKF (dash) are more robust to changes in the sampling frequency than the EKF and DEKF. Particularly, the EKF (dot) and DEKF (dash-dot). For smaller time steps, the difference among different filters reduces. Then the UKF on TSE(3) and the UKF proposed in [30] behave almost the same, achieving an higher accuracy with respect to EKF and DEKF even for large Δt.

The center column of Fig. 2 shows the RMSE(s) for the position and attitude error along with the percentage of uncertainty on the filter initial pose estimate with respect to the true pose. Particu-

larly, let the true values be r_0 and Θ_0, the filters initial guesses are parametrized as $r_0(1+\chi_r/100)$, $R(\Theta_0(1+\chi_\Theta/100))$. As expected, the best performance are achieved for small values of uncertainties. The UKF filters outperform the EKF filters for all the range of χ_r, χ_Θ since the EKF are particularly influenced by the initial condition accuracy.

Finally, in the right column of Fig. 2, the RMSE(s) are given as functions of the standard deviation of the measurement noise, for the position and attitude measurements. Note that the proposed UKF filter on $\mathsf{TSE}(3)$ achieves the lowest accuracy in terms of attitude $\mathrm{O}(10^{-1})$ deg even with the smallest noise standard deviation. It can be explained by the fact that the UKF on $\mathsf{TSE}(3)$ also estimates the velocities which are assumed to be provided by noisy sensors, while the filter on $\mathsf{SE}(3)$ uses un-noisy velocities and only updates on position and attitude measurements.

Generally, as shown in the figure, the proposed UKF on $\mathsf{TSE}(3)$ and standard UKF perform better than others. Even if the DEKF seems to be robust to noisy measurements, it is dependent on the initial condition accuracy and sample frequency. According Fig. 2, the EKF on $\mathsf{SE}(3)$ [26] is able to achieve an higher accuracy of DEKF on $\mathsf{SE}(3)$ [28] and lower accuracy than the UKF on $\mathsf{SE}(3)$ [30] and the proposed UKF on $\mathsf{TSE}(3)$. The latter one has proved to be particularly robust even with noisy measurements, inaccurate initial conditions, and low sampling frequency.

4.2 Performance of the closed-loop system

This section presents the results obtained via the implementation of the proposed $\mathsf{TSE}(3)$ filter and control designs in Section 3. In Figs. 3-4 the time histories of attitude, position and velocities in the BCI frame are provided. Particularly, three different quantities are analyzed: (i) The measured states which represent the state variables measured by sensors and hence are affected by noise, (ii) the estimated (filtered) states, which are the outputs of the navigation system, and (iii) the ideal states, which are the noise-free states obtained with ideal and perfect sensors. Moreover, for each state variable, a magnified portion of the figure is also shown to provide an approximation of the convergence times. It can be seen in the figures that the estimated states start from a different point with respect to the measured and ideal states, due to the different UKF initial conditions. However, the state filter is able to converge to the ideal states in less than a hundredth of the orbit period. Also, note that the attitude varies from -180 deg to 180 deg and the navigation scheme is able to handle this large variation with no issues.

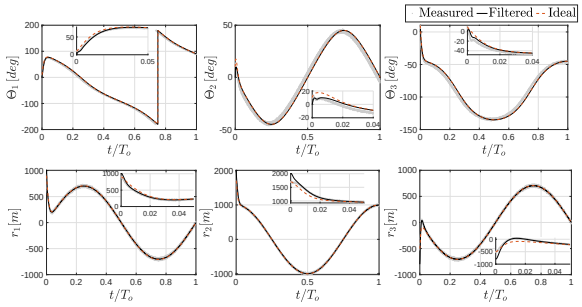

Fig. 3 Measured (grey), estimated (black), and ideal (red) states.

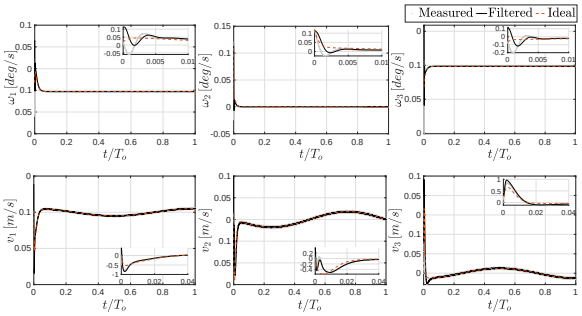

Fig. 4 Measured (grey), estimated (black), and ideal (red) states.

Figure 5 shows the trajectory of the spacecraft center of mass, the desired orbit, and the spacecraft's position and attitude at different points in the orbit. The spacecraft starts with a completely different attitude with respect to the desired ones, and in addition has an initial tumbling. The spacecraft transient response is highlighted in the magnified window in the right panel of Fig. 5. The convergence of the filter and controller proposed here results in the convergence of the estimated states (including trajectory and attitude) to the actual states and desired states, as can be seen in the figure. It can be seen that as the spacecraft orbits around the asteroid, its attitude changes such that its bottom always faces towards Bennu.

In each panel of Fig. 6, the norms of the differences between the spacecraft estimated states and their corresponding desired states are shown, where a noisy behavior of the aforementioned errors after the initial convergence can be seen. The attitude error has a peak in correspondence of the Θ_1 discontinuity (Fig. 3) and a rapid convergence. The order of magnitude of the stead state errors are satisfactorily small compared to the order of magnitude of the reference variables and the large

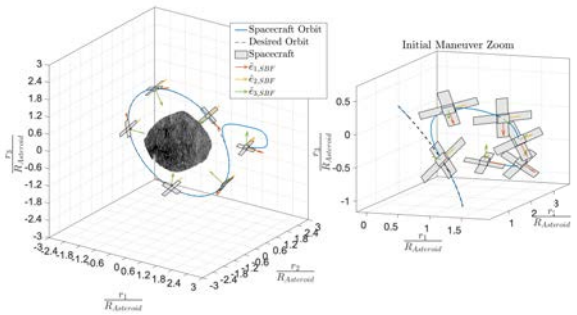

Fig. 5 SBF orientation, and spacecraft attitude and trajectory around Bennu in BCI frame obtained via the implementation of the navigation and control systems.

sources of noise. For instance, the proposed navigation and control system allows to reach a position error in the order of 1 m in the orbit with 1000 m of radius and with a position noise standard deviation of 100 m. The same rationale applies to the attitude, where an accuracy of 0.0001 deg is reached. The mean and the RMSE are reported for each state error. The results improve as the numerical values of mean and RMSE decrease, as also indicated in [64]. Note that both the mean and the RMSE would reduce with time, since the number of samples with small steady state error would increase. In fact, these two indices are influenced by the large state errors that exist before the convergence is achieved.

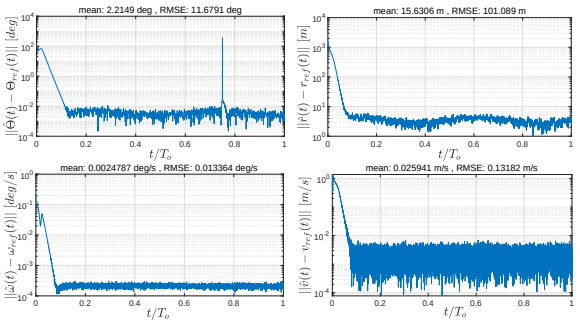

Fig. 6 Norm of the difference between the estimated states and reference states

In Fig. 7, the estimated state error between the estimated and the ideal states are shown along with the estimated confidence bounds of 3σ. The optimal performance of the estimator is generally indicated by the bounded estimation errors within the estimated standard deviation bounds [65, 66]. In other words, the UKF acts as an unbiased estimator, meaning that the expectation of the estimated state errors is zero [67]. From a statistical point of view, it is expected that about 99% of the samples remain bounded inside the two envelopes. Additionally, the performance of the UKF confirms the fact that the state errors are approximately zero mean white noise. Note that the attitude components are characterized by a peak, which corresponds to the discontinuity of the Θ_1 when it goes from -180 deg to 180 deg, as shown in Fig. 3.

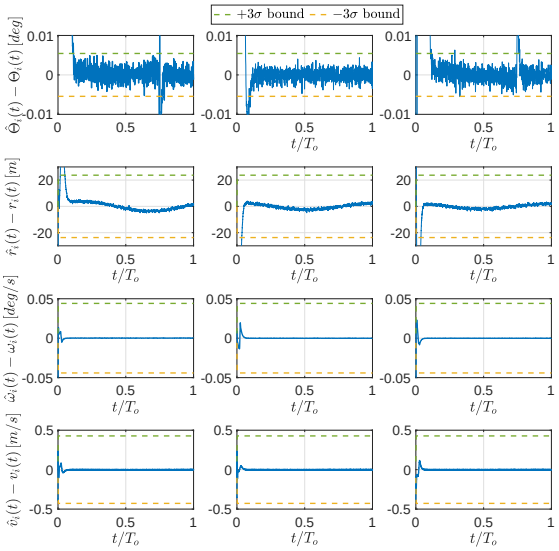

Fig. 7 State estimation error components between the estimated states and the ideal noise-free states.

The spacecraft can reach and maintain the desired orbit-attitude through the control system which produces the necessary control force and moment, that are shown in Fig. 8. In addition, the force control effort in quantified with the total integrated control force per unit mass that is computed as $\Delta V = \frac{1}{m}\int_0^t \|F_c(\tau)\| d\tau$. While the moment control effort is quantified with the integrated moment, i.e. $\Delta\tau = \int_0^t \|M_c(\tau)\| d\tau$. It can be seen that the proposed navigation and control system is able to guarantee the orbit and attitude tracking with a low amount of control moment and force, considering the initial conditions, the large saturation limits and noise statistics in Tab. 2. In fact, both F_c and M_c are well below the boundaries of 24 Nm and 366 N respectively. The total ΔV is less than those obtained in [68], where an adaptive controller was used for the orbital control. As a result of the UKF filtering action, they both appear without any residual noise, which would have introduced an extra control effort. Note that the control moment converges before the control force, in agreement with the magnified portions of Fig. 3-4. Moreover, as discussed in Section 3.3, since the orbit-attitude coupling is considered, the tracking position error can converge only if the tracking attitude error has converged. Therefore, the observed behavior is expected. It is emphasized that the gain selection is

the results of a compromise between convergence time, steady state accuracy and control effort.

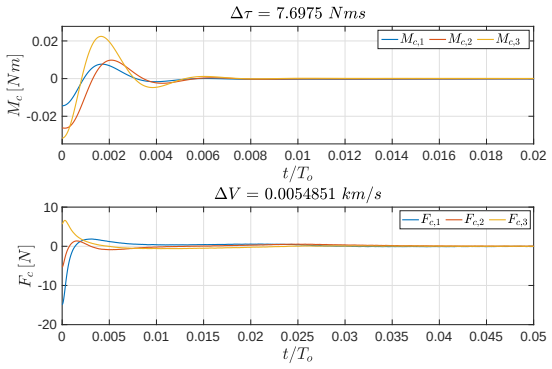

Fig. 8 Control inputs in terms of force and moment provided by the tracking controller

5 Conclusions

In this paper, a novel spacecraft navigation and control system has been introduced in the Lie group $\mathsf{SE}(3)$ and its tangent bundle in the presence of stochastic processes in the system. In the mathematical framework presented here, the geometrical characteristics of the system are well preserved and the translational and attitude motions are treated simultaneously. Hence, this formalism allows for the coupling between orbital and attitude motions of the spacecraft to be considered in the control design. The orbit-attitude coupling cannot be neglected in scenarios such as spacecraft motion around irregular celestial bodies due to their highly perturbed environments. The estimated states obtained using the proposed unscented Kalman filter (UKF) on $\mathsf{TSE}(3)$ are used along with a Lyapunov-Morse-based feedback tracking control with backstepping for navigation and control of the system with noisy measurements. A special retraction function is used to allow the UKF to encode the sigma points onto the manifold, and the inverse of that retraction function is used to decode the sigma points from the manifold. The performance achieved with the implementation of the proposed UKF on $\mathsf{TSE}(3)$ is compared to that of filters on $\mathsf{SE}(3)$ in the literature. In particular, the performance is studied under different sampling frequencies, initial condition uncertainty, and magnitude of measurement noise standard deviations. Finally, the robustness of the proposed stochastic navigation and control system is verified for the OSIRIS-REx mission parameters, where it is shown that it is capable of directing the spacecraft towards a desired orbit while maintaining the principal axis of the spacecraft along the nadir direction, despite the noisy measurements.

Future work may consider further details in the modeling of the navigation system. Further accuracy in the model of the measurement sensors may be obtained via extending their noise characteristics to introduce biases, scale-factor errors, or mounting alignment errors. Also, realistic dynamics of the actuators can be considered in the design of the control system. The robustness of the proposed navigation and control system can also be verified in problems such as orbit transfers, and spacecraft rendezvous, proximity operations, and docking. In addition, the stochastic estimation and control scheme presented here can be extended to the problem of multibody dynamics and multiagent systems.

6 Declarations

6.1 Funding

Support from Faculty Innovative Research in Science and Technology (FIRST) is gratefully acknowledged.

6.2 Conflicts of interest/Competing interests

The authors have no relevant financial or non-financial interests to disclose.

6.3 Availability of data and material

Not Applicable

6.4 Code availability

This project was coded in Matlab using Simulink, and may be made available upon request.

6.5 Ethics approval

Not Applicable

6.6 Consent to participate

Not Applicable

6.7 Consent for publication

Not Applicable

References

1. K. R. Pollock, "An analysis of orbital propagators for Low Earth Orbit Rendezvous," *Naval Postgraduate School, Monterey, CA., Provided by the SAO/NASA Astrophysics Data System*, vol. OMB, no. 0704-0188, 1994.
2. S. P. Shuster, "A Survey and Performance Analysis of Orbit Propagators for LEO, GEO, and Highly Elliptical Orbits," *Utah State University*, vol. OMB, no. 0704-0188, 2017.
3. V. Vittaldev, E. Mooij, and M. C. Naeije, "Unified state model theory and application in Astrodynamics," *Celestial Mechanics and Dynamical Astronomy*, vol. 112, no. 3, pp. 253–282, 2012, doi: 10.1007/s10569-011-9396-5.
4. E. J. Lefferts, F. L. Markley, and M. D. Shuster, "Kalman filtering for spacecraft attitude estimation," *Journal of Guidance, Control and Dynamics*, vol. 5, no. 5, 1982, doi:10.2514/3.56190.
5. J. R. Carpenter and C. N. D'Souza, "Navigation Filter Best Practices," *NASA Technical Reports*, 2018, WBS: 869021.03.04.01.03.
6. J. Yang and E. Stoll, "Adaptive sliding mode control for spacecraft proximity operations based on dual quaternions," *Journal of Guidance, Control, and Dynamics*, vol. 42, no. 11, pp. 2356–2368, 2019, doi: 10.2514/1.G004435.
7. J. L. Crassidis and F. L. Markley, "Unscented filtering for spacecraft attitude estimation," *Journal of Guidance, Control, and Dynamics*, vol. 26, no. 4, pp. 536–542, 2003, doi: 10.2514/2.5102.
8. J. L. Crassidis, F. L. Markley, and Y. Cheng, "Survey of nonlinear attitude estimation methods," *Journal of Guidance, Control, and Dynamics*, vol. 30, no. 1, pp. 12–28, 2007, doi: 10.2514/1.22452.
9. J. T.-Y. Wen and K. Kreutz-Delgado, "The attitude control problem," *IEEE Transactions of Automatic Control*, vol. 36, no. 10, pp. 1148–1162, 1991, doi: 10.1109/9.90228.
10. S. P. Bhat and D. S. Bernstein, "A topological obstruction to continuous global stabilization of rotational motion and the unwinding phenomenon," *Systems & Control Letters*, vol. 39, no. 1, pp. 63–70, 2000, doi: 10.1016/S0167-6911(99)00090-0.
11. J. Bohn and A. K. Sanyal, "Almost global finite-time stabilization of rigid body attitude dynamics using rotation matrices," *International Journal on Robust and Nonlinear Control*, vol. 25, no. 4, 2015, doi: 10.1002/rnc.3399.
12. L. Sy, N. H. Lovell, and S. J. Redmond, "Estimating lower limb kinematics using a Lie group constrained EKF and a reduced wearable IMU count," in *8th IEEE RAS/EMBS International Conference for Biomedical Robotics and Biomechatronics (BioRob)*, pp. 310–315, 2020, doi: 10.1109/BioRob49111.2020.9224342.
13. B. P. Malladi, S. Di Cairano, and A. Weiss, "Nonlinear model predictive control of coupled rotational-translational spacecraft relative motion," in *2019 American Control Conference (ACC)*, pp. 3581–3586, 2019, doi: 10.23919/ACC.2019.8814345.
14. N. Filipe and P. Tsiotras, "Rigid body motion tracking without linear and angular velocity feedback using dual quaternions," in *2013 European Control Conference (ECC)*, pp. 329–334, 2013, doi: 10.23919/ECC.2013.6669564.
15. F. L. Markley and J. L. Junkins, "Fundamentals of spacecraft attitude determination and control," *Springer*, 2014.
16. D. Lee and G. Vukovich, "Robust adaptive terminal sliding mode control on se(3) for autonomous spacecraft rendezvous and docking," *Nonlinear Dynamics*, vol. 83, pp. 2263–2279, 2016, doi: 10.1007/s11071-015-2479-1.
17. M. Nazari, M. Maadani, E. A. Butcher, and T. Yucelen, "Morse-Lyapunov-based control of rigid body motion on TSE(3) via backstepping," *2018 AIAA Guidance, Navigation, and Control Conference*, 2018, doi: 10.2514/6.2018-0602.
18. D. Seo and M. Nazari, "Rigid body adaptive stabilization on the tangent bundle of the Lie groups," *AIAA Scitech 2019 Forum*, 2019, doi: 10.2514/6.2019-0653.
19. E. A. Butcher, J. Wang, and T. A. Lovell, "On Kalman filtering and observability in nonlinear sequential relative orbit estimation," *Journal of Guidance, Control, and Dynamics*, vol. 40, no. 9, 2017, doi: 10.2514/1.G002702.
20. C. A. Woolsey, "Reduced Hamiltonian dynamics for a rigid body coupled to a moving point mass," *Journal of Guidance, Control, and Dynamics*, vol. 28, no. 1, 2005, doi: 10.2514/1.54099.
21. Q. Lam, N. Stamatakos, C. Woodruff, and S. Ashton, *Gyro Modeling and Estimation of Its Random Noise Sources*.
22. K. Nirmal, A. G. Sreejith, J. Mathew, M. Sarpotdar, A. Suresh, A. Prakash, M. Safonova, and J. Murthy, "Noise modeling and analysis of an IMU-based attitude sensor: Improvement of performance by filtering and sensor fusion," in *Advances in Optical and Mechanical Technologies for Telescopes and Instrumentation II* (R. Navarro and J. H. Burge, eds.), vol. 9912, pp. 2138–2147, International Society for Optics and Photonics, SPIE, 2016, doi: 10.1117/12.2234255.
23. D. Lee, A. K. Sanyal, and E. A. Butcher, "Asymptotic tracking control for spacecraft formation flying with decentralized collision avoidance," *Journal of Guidance, Control, and Dynamics*, vol. 38, no. 4, pp. 587–600, 2015, doi: 10.2514/1.G000101.
24. D. Lee and G. Vukovich, "Robust adaptive terminal sliding mode control on SE(3) for autonomous spacecraft rendezvous and docking," *Nonlinear Dynamics*, 2016, doi: 10.1007/s11071-015-2479-1.
25. D. Lee, A. K. Sanyal, E. A. Butcher, and D. J. Scheeres, "Finite-time control for spacecraft body-fixed hovering over an asteroid," *IEEE Transactions on Aerospace and Electronic Systems*, vol. 51, no. 1, pp. 506–520, 2015, doi: 10.1109/TAES.2014.140197.
26. A. Sjøberg and O. Egeland, "An EKF for Lie groups with application to crane load dynamics," *Modeling, Identification and Control: A Norwegian Research Bulletin*, vol. 40, pp. 109–124, 04 2019, doi: 10.4173/mic.2019.2.3.
27. S. Heo and C. G. Park, "Consistent EKF-based visual-inertial odometry on matrix Lie group," *IEEE Sensors Journal*, vol. 18, no. 9, pp. 3780–3788, 2018, doi: 10.1109/JSEN.2018.2808330.
28. G. Bourmaud, R. Megret, A. Giremus, and Y. Berthoumieu, "Discrete extended Kalman filter on Lie groups," *21st European Signal Processing Conference*, 2013.
29. G. Bourmaud, R. Megret, M. Arnauden, and A. Giremus, "Continuous-discrete extended Kalman filter on matrix Lie groups using concentrated Gaussian distributions," *Journal of Mathematical Imaging and Vision*, vol. 51, pp. 209–228, 2015, doi: 10.1007/s10851-014-0517-0.
30. M. Brossard, S. Bonnabel, and J. Condomines, "Unscented Kalman filtering on Lie groups," *IEEE/RSJ International Conference on Intelligent Robots and Systems (IROS)*, 2017, doi: 10.1109/IROS.2017.8206066.

31. M. Brossard, S. Bonnabel, and A. Barrau, "Unscented Kalman filter on Lie groups for visual inertial odometry," *"IEEE/RSJ International Conference on Intelligent Robots and Systems (IROS)*, 2018, doi: 10.1109/IROS.2018.8593627.
32. G. Loianno, M. Watterson, and V. Kumar, "Visual inertial odometry for quadrotors on $\mathsf{SE}(3)$," *IEEE International Conference on Robotics and Automation (ICRA)*, 2016, doi: 10.1109/ICRA.2016.7487292.
33. E. A. Wan and R. Van Der Merwe, "The unscented Kalman filter for nonlinear estimation," *Proceedings of the IEEE 2000 Adaptive Systems for Signal Processing, Communications, and Control Symposium*, 2000, doi: 10.1109/ASSPCC.2000.882463.
34. M. Wittal, G. Mangiacapra, A. Appakonam, M. Nazari, and E. Capello, *Stochastic spacecraft navigation and control in Lie group SE(3) around small irregular bodies*, pp. AAS 20–690. 2020, doi: 10.13140/RG.2.2.21502.82240.
35. T. D. Barfoot and P. T. Furgale, "Associating uncertainty with three-dimensional poses for use in estimation problems," *IEEE Transactions on Robotics*, vol. 30, no. 3, pp. 679–693, 2014, doi: 10.1109/TRO.2014.2298059.
36. P.-A. Absil, R. Mahony, and R. Sepulchre, *Optimization Algorithms on Matrix Manifolds*. Princeton University Press, 2008, isbn: 978-0-691-13298-3.
37. M. Brossard, A. Barrau, and S. Bonnabel, "A code for unscented Kalman filtering on manifolds (UKF-M)," *International Conference on Robotics and Automation (ICRA)*, 2020, arXiv:2002.00878.
38. G. Misra and A. K. Sanyal, "Analysis of orbit-attitude coupling of spacecraft near small solar system bodies," *AIAA Guidance, Navigation, and Control Conference*.
39. A. Muller and Z. Terze, "The significance of the configuration space Lie group for the constraint satisfaction in numerical time integration of multi body systems," *Mechanism and Machine Theory*, vol. 82, pp. 173–202, 2014, doi: 10.1016/j.mechmachtheory.2014.06.014.
40. T. Lee, H. McClamroch, and M. Leok, "Optimal attitude control for a rigid body with symmetry," *Proceedings of the American Control Conference*, 2007, doi: 10.1109/ACC.2007.4282362.
41. J. Sola, J. Deray, and D. Atchuthan, "A micro Lie theory for state estimation in robotics," *2018 arXiv preprint*, 2018, arXiv: 1812.01537.
42. R. M. Murray, Z. Li, and S. S. Sastry, *A Mathematical Introduction to Robotic Manipulation*. CRC Press, 1994.
43. J. Gallier, "Basics of classical Lie groups: The exponential map, Lie groups, and Lie algebras," *Texts in Applied Mathematics, Geometric Methods and Applications*, vol. 38, pp. 367–414, 2001, doi: 10.1007/978-1-4613-0137-0_14.
44. M.-A. A. H. Ahmed, "On extracting properties of Lie groups from their Lie algebras," *American Journal of Computational and Applied Mathematics*, vol. 6, no. 5, pp. 182–186, 2016, doi: 10.5923/j.ajcam.20160605.02.
45. M. Nazari, E. A. Butcher, T. Yucelen, and A. Sanyal, "Decentralized consensus control of a rigid-body spacecraft formation with communication delay," *Journal of Guidance, Control, and Dynamics*, 2016, doi: 10.2514/1.G001396.
46. D. J. Scheeres, *Orbital Motion in Strongly Perturbed Environments*. Springer, Berlin-Heidelberg, 2012.
47. W. M. Kaula, *Theory of Satellite Geodesy*. Blaisdell, Bosto, ISBN-13: 978-0486414652, ISBN-10: 0486414655, 1966.
48. D. J. Scheeres, S. J. Ostro, R. S. Hudson, E. M. DeJong, and S. Suzuki, "Dynamics of orbits close to asteroid 4179 Toutatis," *Icarus*, vol. 132, no. 1, pp. 53–79, 1998, doi: 10.1006/icar.1997.5870.
49. M. Nazari, R. Wauson, T. Critz, E. A. Butcher, and D. J. Scheeres, "Observer-based body-frame hovering control over a tumbling asteroid," *Acta Astronautica*, vol. 102, pp. 124–139, 2014, doi: 10.1016/j.actaastro.2014.05.016.
50. G. Misra, A. Sanyal, and D. J. Scheeres, "Coupled orbit-attitude dynamics and relative state estimation of spacecraft near small solar system bodies," *Advances in Space Research*, vol. 57, no. 8, pp. 1747–1761, 2015, doi: 10.1016/j.asr.2015.05.023.
51. M. Vandyke, J. Schwartz, and C. Hall, "Unscented Kalman Filtering for spacecraft attitude state and parameter estimation," *Advances in the Astronautical Sciences*, vol. 119, 01 2004.
52. L. Perea, J. How, L. Breger, and P. Elosegui, *Nonlinearity in Sensor Fusion: Divergence Issues in EKF, Modified Truncated GSF, and UKF*.
53. M. Mohammed, H. Boussadia, A. Bellar, and A. Adnane, "Performance comparison of attitude determination, attitude estimation, and nonlinear observers algorithms," *Journal of Physics: Conference Series*, vol. 783, p. 012017, 01 2017, doi: 10.1088/1742-6596/783/1/012017.
54. K. K. Tønne, "Stability Analysis of EKF-Based Attitude Determination and Control," 2007.
55. E. Samiei, M. Nazari, E. A. Butcher, and A. K. Sanyal, "Robust stochastic stabilization of attitude motion," *International Journal of Dynamics and Control*, vol. 7, pp. 619–635, 2019, doi: 10.1007/s40435-018-0456-5.
56. T. Lee, M. Leok, and N. H. McClamroch, "Lie group variational integrators for the full body problem," *Computational Methods in Applied Mechanics and Engineering*, vol. 196, no. 8, 2005, doi: 10.1016/j.cma.2007.01.017.
57. C. Kane, J. Marsden, and M. Ortiz, "Symplectic-energy-momentum preserving variational integrators," *Journal of Mathematical Physics*, vol. 40, pp. 3353–3371, 1999, doi: 10.1063/1.532892.
58. E. B. Bierhaus *et al.*, "The OSIRIS-REx spacecraft and the touch-and-go sample acquisition mechanism (TAGSAM)," *Space Science Reviews*, vol. 214, no. 107, 2018, doi: 10.1007/s11214-018-0521-6.
59. E. Beshore *et al.*, "The OSIRIS-REx asteroid sample return mission," *IEEE Aerospace Conference Proceedings*, 2015, doi: 10.1109/AERO.2015.7118989.
60. P. Blau, *Spaceflight101.com*, 2020 (accessed January 12, 2021). `https://spaceflight101.com/osiris-rex/osiris-rex-spacecraft-overview/`.
61. L. M. Dani Hauf, *OSIRIS-REx, Discovering the Origins of the Solar System*, 2020 (accessed January 12, 2021). `https://www.lockheedmartin.com/en-us/products/osiris-rex.html`.
62. R. G. Melton, "Fundamentals of astrodynamics and applications," *Journal of Guidance, Control, and Dynamics*, vol. 21, no. 4, pp. 672–672, 1998, doi: 10.2514/2.4291.
63. B. Wie, *Space Vehicle Dynamics and Control*. American Institute of Aeronautics and Astronautics, 2 ed., 2008, isbn: 978-1-56347-953-3.
64. J. Havlík and O. Straka, "Performance evaluation of iterated extended Kalman filter with variable step-length," *Journal of Physics: Conference Series*, vol. 659, pp. 12–22, 2015, doi: 10.1088/1742-6596/659/1/012022.
65. I. Miletović, D. M. Pool, O. Stroosma, M. M. V. Paassen, and Q. Chu, "Improved Stewart platform state estimation using inertial and actuator position measurements," *Control Engineer-*

ing Practice, vol. 62, pp. 102–115, 2017, doi: 10.1016/j.conengprac.2017.03.006.

66. J. B. Moor and B. D. O. Anderson, *Optimal Filtering*. Prentice Hall Information and System Sciences Series, 1979.
67. F. L. Markley and J. L. Crassidis, *Correction to: Fundamentals of Spacecraft Attitude Determination and Control*. New York: Springer, 2014, isbn: 978-1-4939-0802-8.
68. K. W. Lee and S. N. Singh, "Adaptive and super-twisting adaptive spacecraft orbit control around asteroids," *Journal of Aerospace Engineering*, vol. 32, no. 4, p. 04019042, 2019, doi: 10.1061/(ASCE)AS.1943-5525.0001043.

Cover Letter for "Unscented Kalman Filter and Control in TSE(3) with Applications to Spacecraft Dynamics"
Click here to view linked References
Click here to access/download;attachment to manuscript;Journal Cover Letter_NoDy.pdf

Dear Journal Editor,

Please find enclosed our manuscript, “Unscented Kalman Filter and Control on TSE(3) with Applications to Spacecraft Dynamics” by G. Mangiacapra, M. Wittal, E. Capello, and M. Nazari which we would like to submit for publication in the Nonlinear Dynamics Journal.

In this paper, we present a novel rigid-body spacecraft navigation and control architecture within the framework of special Euclidean group SE(3) and its tangent bundle TSE(3) while considering stochastic processes in the system. The proposed framework combines the orbit-attitude motions of the spacecraft into a single, compact set. The stochastic state filter is designed based on the unscented Kalman filter which uses a special retraction function to encode the sigma points onto the manifold. The navigation system is then integrated to an almost globally asymptotically stabilizing Morse-Lyapunov-based control system with backstepping. Numerical simulations are conducted to demonstrate the effectiveness of the proposed navigation filter for the full state estimation. In addition, the navigation and control system is tested in the nonlinear gravity field of a small celestial body with an irregular shape. In particular, the performance of the closed-loop system is studied in a tracking problem of spacecraft motion near the asteroid Bennu based on the OSIRIS-REx’s mission data. We believe our findings would appeal to the readership of the Nonlinear Dynamics Journal.

All authors have approved the manuscript and agree with its submission to the Nonlinear Dynamics Journal. We also confirm that this manuscript is not under consideration by another journal. Please address all correspondence to Matthew Wittal, email: wittalm@my.erau.edu .

We look forward to hearing from you at your earliest convenience.

Thank you,

Matthew M. Wittal

Click here to access/download;Authorship change form;MaWiCaNa_2021_AuthorshipChangeForm.pdf

Adis | Bohn Stafleu van Loghum | palgrave macmillan | Springer

Change of authorship request form (pre-acceptance)

Please read the important information on page 4 before you begin

This form should be used by authors to request any change in authorship including changes in corresponding authors. Please fully complete all sections. Use black ink and block capitals and provide each author's full name with the given name first followed by the family name.

Please note: In author collaborations where there is formal agreement for representing the collaboration, it is sufficient for the representative or legal guarantor (usually the corresponding author) to complete and sign the Authorship Change Form on behalf of all authors.

Section 1: Please provide the current title of manuscript
(For journals: Please provide the manuscript ID, title and/or DOI if available.)
(For books: Please provide the title, ISBN and/or DOI if available.)

Manuscript ID no. in case of unpublished manuscript:	NODY-D-21-01189R1
DOI in case of published manuscript:	
ISBN (for books):	

Title: Unscented Kalman Filter and Control on TSE(3) with Application to Spacecraft Dynamics

Section 2: Please provide the previous authorship, in the order shown on the manuscript before the changes were introduced. Please indicate the corresponding author by adding (CA) behind the name.

	First name(s)	Family name	ORCID or SCOPUS id, if available
1st author	Matthew	Withal (CA)	0000-0002-2127-2318
2nd author	Gennaro	Mangiacapra	
3rd author	Morad	Nazari	0000-0001-8556-4355
4th author	Elisa	Capello	0000-0001-9364-5817
5th author			
6th author			
7th author			

Please use an additional sheet if there are more than 7 authors.

SPRINGER NATURE Springer Nature is one of the world's leading global research, educational and professional publishers, created in May 2015 through the combination of Nature Publishing Group, Palgrave Macmillan, Macmillan Education and Springer Science+Business Media.

Adis Bohn Stafleu van Loghum palgrave macmillan Springer

Change of authorship request form (pre-acceptance)

Section 3: Please provide a justification for change. Please use this section to explain your reasons for changing the authorship of your manuscript, e.g. what necessitated the change in authorship? Please refer to the (journal) policy pages for more information about authorship. Please explain why omitted authors were not originally included and/or why authors were removed on the submitted manuscript.

Author name order on online form only was adjusted to reflect the name order on the manuscript, which has not changed between the previous and revised version.
No new authors were added nor were any authors removed.

Section 4: Proposed new authorship. Please provide your new authorship list in the order you would like it to appear on the manuscript. Please indicate the corresponding author by adding (CA) behind the name. If the corresponding author has changed, please indicate the reason under section 3.

	First name(s)	Family name (this name will appear in full on the final publication and will be searchable in various abstract and indexing databases)
1st author	Gennaro	Mangiacapra
2nd author	Matthew	Wittal (CA)
3rd author	Elisa	Capello
4th author	Morad	Nazari
5th author		
6th author		
7th author		

Please use an additional sheet if there are more than 7 authors.

SPRINGER NATURE Springer Nature is one of the world's leading global research, educational and professional publishers, created in May 2015 through the combination of Nature Publishing Group, Palgrave Macmillan, Macmillan Education and Springer Science+Business Media.

Adis | Bohn Stafleu van Loghum | palgrave macmillan | Springer

Change of authorship request form (pre-acceptance)

Section 5: Author contribution, Acknowledgement and Disclosures. Please use this section to provide a new disclosure statement and, if appropriate, acknowledge any contributors who have been removed as authors and ensure you state what contribution any new authors made (if applicable per the journal or book (series) policy). Please ensure these are updated in your manuscript - after approval of the change(s) - as our production department will not transfer the information in this form to your manuscript.

New acknowledgements:

None

New Disclosures (financial and non-financial interests, funding):

None

New Author Contributions statement (if applicable per the journal policy):

None

State 'Not applicable' if there are no new authors.

SPRINGER NATURE Springer Nature is one of the world's leading global research, educational and professional publishers, created in May 2015 through the combination of Nature Publishing Group, Palgrave Macmillan, Macmillan Education and Springer Science+Business Media.

Adis Bohn Stafleu van Loghum palgrave macmillan Springer

Change of authorship request form (pre-acceptance)

Section 6: Declaration of agreement. *All* authors, unchanged, new and removed *must* sign this declaration.
(NB: Please print the form, sign and return a scanned copy. Please note that signatures that have been inserted as an image file are acceptable as long as it is handwritten. Typed names in the signature box are unacceptable.) *** Please delete as appropriate. Delete all of the bold if you were on the original authorship list and are remaining as an author.**

	First name	Family name		Signature	Affiliated institute	Date
1st author	Gennaro	Mangiacapra	I agree to the proposed new authorship shown in section 4 ,		Politecnico di Torino	07/12/2021
2nd author	Matthew	Wittal	I agree to the proposed new authorship shown in section 4	Matthew Wittal Digitally signed by Matthew Wittal Date: 2021.12.07 10:11:36 -05'00'	Embry-Riddle Aeronautical Univ. & NASA	12-07-2021
3rd author	Elisa	Capello	I agree to the proposed new authorship shown in section 4 ,	Elisa Capello Firmato digitalmente da Elisa Capello ND: cn=Elisa Capello, o=Politecnico di Torino, ou=CNR-IEIIT, email=elsia.capello@polito.it, c=IT Data: 2021.12.07 18:15:22 +01'00'		
4th authors	Morad	Nazari	I agree to the proposed new authorship shown in section 4 ,		Embry-Riddle Aeronautical Univ.	12-08-2021
5th author			I agree to the proposed new authorship shown in section 4 **/and the addition/removal*of my name to the authorship list.**			
6th author			I agree to the proposed new authorship shown in section 4 **/and the addition/removal*of my name to the authorship list.**			
7th author			I agree to the proposed new authorship shown in section 4 **/and the addition/removal*of my name to the authorship list.**			

Please use an additional sheet if there are more than 7 authors.

SPRINGER NATURE Springer Nature is one of the world's leading global research, educational and professional publishers, created in May 2015 through the combination of Nature Publishing Group, Palgrave Macmillan, Macmillan Education and Springer Science+Business Media.

Adis Bohn Stafleu van Loghum palgrave macmillan Springer

Change of authorship request form (pre-acceptance)

Important information. Please read.

- Please return this form, fully completed, to Springer Nature. We will consider the information you have provided to decide whether to approve the proposed change in authorship. We may choose to contact your institution for more information or undertake a further investigation, if appropriate, before making a final decision.
- By signing this declaration, all authors guarantee that the order of the authors are in accordance with their scientific contribution, if applicable as different conventions apply per discipline, and that only authors have been added who made a meaningful contribution to the work.
- Please note, we cannot investigate or mediate any authorship disputes. If you are unable to obtained agreement from all authors (including those who you wish to be removed) you must refer the matter to your institution(s) for investigation. Please inform us if you need to do this.
- If you are not able to return a fully completed form within **30 days** of the date that it was sent to the author requesting the change, we may have to withdraw your manuscript. We cannot publish manuscripts where authorship has not been agreed by all authors (including those who have been removed).
- Incomplete forms will be rejected.

SPRINGER NATURE Springer Nature is one of the world's leading global research, educational and professional publishers, created in May 2015 through the combination of Nature Publishing Group, Palgrave Macmillan, Macmillan Education and Springer Science+Business Media.